Physics – Uspekhi **60** (11) 1087 – 1120 (2017)

REVIEWS OF TOPICAL PROBLEMS

PACS numbers: **32.80.–t**, **42.50.–p**, **42.65.–k**, **78.20.–e**

IN MEMORY OF LEONID VENIAMINOVICH KELDYSH

Keldysh photoionization theory: through the barriers

A M Zheltikov

DOI: https://doi.org/10.3367/UFNe.2017.08.038198

Contents

Abstract. The Keldysh photoionization theory is a conceptual cornerstone and a universal framework for the description of a broad class of fundamental effects in light–matter interaction. Here, we provide an overview of the Keldysh theory as a significant milestone in the development of modern optical physics and offer a historical perspective on the fundamental role of this theory, from the early pioneering work on quantum tunneling to the latest breakthroughs in laser optics, attosecond technologies, and ultrafast optics of high-intensity laser pulses.

A M Zheltikov Lomonosov Moscow State University, Faculty of Physics, Leninskie gory 1, str. 2, 119991 Moscow, Russian Federation;
Texas A&M University, Department of Physics and Astronomy, College Station, Texas 77843, USA;
Lomonosov Moscow State University, International Laser Center, Leninskie gory 1, str. 62, 119991 Moscow, Russian Federation;
International Center for Quantum Optics and Quantum Technologies (Russian Quantum Center), ul. Novaya 100a, 143025 Skolkovo, Moscow, Russian Federation;
National Research Centre 'Kurchatov Institute', pl. Kurchatova 1, 123182 Moscow, Russian Federation;
Kazan Quantum Center, Kazan National Research Technical University named after A N Tupolev, ul. Chetaeva 18a, 420126 Kazan, Russian Federation
E-mail: zheltikov@physics.msu.ru

Received 15 June 2017, revised 8 August 2017
Uspekhi Fizicheskikh Nauk **187** (11) 1169 – 1204 (2017)
DOI: https://doi.org/10.3367/UFNr.2017.08.038198
Translated by A M Zheltikov

Keywords: Keldysh theory of photoionization, light–matter interaction, ultrafast optics

1. Introduction

For over more than half a century, the Keldysh theory of photoionization [1] has served as a conceptual foundation for the description of laser–matter interactions. A closed form equation for the rate of photionization provided by this theory is the key parameter for the analysis of a broad class of phenomena observed in laser experiments, including laser breakdown [2–4], high-order harmonic generation (HHG) [5, 6], laser-induced filamentation [7, 8], and the generation of ultrashort pulses of electric current in solids [9, 10]. The Keldysh γ parameter is a fundamental characteristic that controls the regime of laser–matter interaction. This para-

meter simultaneously defines the borderline between the weak- and strong-field regimes of light–matter interactions and provides a measure for the adiabaticity of photoionization, as well as for the adiabaticity of a broad class of nonlinear-optical phenomena accompanying the interaction of intense electromagnetic radiation with matter.

The Keldysh photoionization theory offers a universal framework for the analysis of the key effects underlying the interaction of electromagnetic radiation with matter, including field-induced ionization in gases, solids, liquids, and biological tissues. As one of its central results, this theory offers a fundamental insight into multiphoton and tunneling ionization as two limiting regimes of the same physical phenomenon – ionization induced by an ac electromagnetic radiation field. The Keldysh formalism is the first theory that provides a unified quantitative description of multiphoton and tunneling ionization as two pathways that dominate laser-induced ionization in the weak- and strong-field regimes, respectively.

In the limiting case of large values of the Keldysh parameter, $\gamma \gg 1$, the closed-form equations for the photoionization rate derived within the framework of the Keldysh theory are reduced to well-known weak-field perturbation-theory expressions for the rate of multiphoton ionization. In the opposite limiting case, $\gamma \ll 1$, the Keldysh formula for the photoionization probability yields the celebrated quantum-tunneling exponential. In the low-frequency limit, this expression is reduced to the formula for the probability of tunneling through a potential barrier formed by the potential of an ionic core and an external field. In the pre-Keldysh-theory epoch, the vast parameter space between these two limiting regimes was a *Hic sunt dracones* land. Without the Keldysh parameter, even the borderlines of this land remained unknown. As we now know, beyond these borderlines is found a landscape of incredible variety. We know this land as modern ultrafast optics and high-field optical physics. This is the land where ultrafast processes can be detected on the attosecond time scale [11], a semiconductor can be switched to the conducting state and back within a tiny fraction of the field cycle [10], high-power laser beams can be transmitted in new regimes [7, 8, 12], and flashes of electromagnetic radiation of unprecedented brevity can be generated within an extraordinarily broad range of spectrum — from the X-ray to the terahertz region [5].

Photoionization is one of the key processes in laser–matter interaction. Remarkable properties of ionization phenomena induced by ultrashort light pulses are interesting from a fundamental point of view, as well as in the context of spectral–temporal transformation and transmission of ultrashort laser pulses and material microprocessing. Optical nonlinearities of ionized gas media provide efficient spectral broadening of ultrashort laser pulses [7, 8], enabling the generation of broadband radiation (supercontinuum) [14] in the visible, infrared (IR), and ultraviolet (UV) ranges [15], revealing new regimes of optical harmonic generation [16, 17] and offering new methods of laser material processing [18] and temporal compression of ultrashort pulses to few-cycle pulse widths [19, 20]. Understanding the physics and the main tendencies in the ionization of liquid-phase materials is central to defining the optimal regimes in a broad class of laser–biotissue interactions, including those occurring in laser surgery and laser transfection [21–23]. The Keldysh photoionization theory — an extraordinary example of outstanding scientific vision and researcher's courage — is the key to understanding diversified physical phenomena at the heart of modern ultrafast optics.

The Keldysh photoionization theory with all its methodological aspects and numerous applications has been a subject of several in-depth, illuminating reviews [24–27]. The purpose of this paper is to discuss, avoiding repetition whenever possible, the significance of the Keldysh theory as an important milestone in the development of modern optical physics and to highlight the cornerstone role of this theory in the historical perspective, starting with the pioneering studies of quantum tunneling in the early days of quantum mechanics all the way to the latest breakthroughs in laser science, attosecond technologies, and ultrafast high-intensity laser–matter interaction optical physics.

2. Photons and barriers

2.1 I^N or $\exp(-E_0/E)$?

In the pre-Keldysh-theory epoch, quantum tunneling and multiphoton ionization were considered as independent phenomena. In view of diversified manifestations of quantum tunneling and its special role in the development of quantum physics, such a perspective was in every respect natural. Long before the advent of lasers, quantum tunneling was studied in the context of molecular spectra, field-induced ionization of atoms, electron emission from metal surfaces, alpha decay of nuclei, electric breakdown of dielectrics, and interband transitions in semiconductor devices.

The theory of various multiphoton processes — two-photon absorption in the first place — was also developed in the pre-laser era. However, systematic experimental studies of multiphoton phenomena became possible only with the advent of lasers. The early days of the laser epoch have witnessed the first experiments on multiphoton ionization of atoms, as well as the development of a consistent theory of, first, two-photon and then multiphoton ionization.

The Keldysh formalism is the first theory that provides a universal framework for a consistent quantitative description of multiphoton ionization and quantum tunneling as two limiting cases of the same physical phenomenon — ionization induced by an ac electromagnetic radiation field. Below in this section, we provide a brief historical review of the main concepts and approaches used in the analysis of quantum tunneling and multiphoton ionization and discuss the significance of the Keldysh photoionization theory as a unifying theory, which treats quantum tunneling and multiphoton ionization as two pathways and two limiting regimes of laser-induced ionization and defines, for the first time, a clear criterion, setting a borderline between these two regimes.

2.2 Tunneling effect: welcome to the quantum world

The realization that a quantum particle can penetrate through a potential barrier is closely related to the development of the key concepts of quantum mechanics in the 1920s. Within a remarkably short span of time of just a few months — from November 1926 until late July 1928 — several seminal studies dealing with different manifestations of quantum tunneling [28] were submitted to various journals. These studies laid the foundations for the theory of quantum tunneling. The key ideas and approaches discussed in these papers are reproduced almost in their original form in many textbooks on quantum mechanics to date. Since the theory of quantum

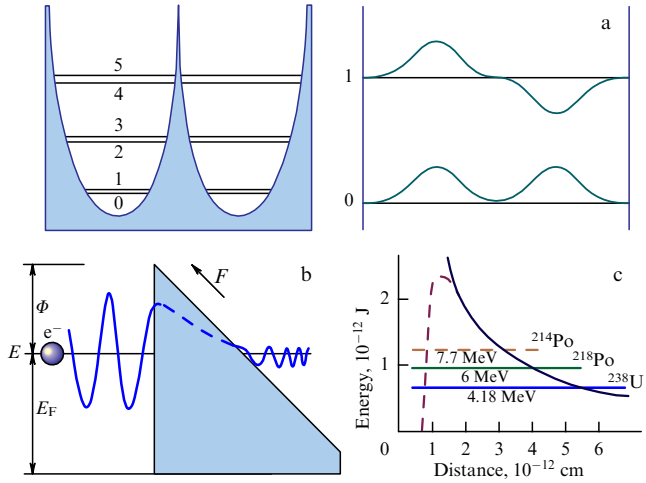

Figure 1. (Color online.) (a) Molecular potential in Hund's problem (left) and its even and odd first excited states (right). (b) Electron tunneling from metal surface in the presence of a dc electric field F (Fowler–Nordheim tunneling): E_F is the electron Fermi energy in the conduction band of the metal; $\Phi = V - E_F$ is the work function, with V being the potential barrier on the metal surface. (c) Tunneling in alpha decay. Horizontal lines correspond to the alpha decay of uranium-238 (4.18 MeV), polonium-218 (6.00 MeV), and polonium-214 (7.69 MeV).

tunneling developed in 1926 – 1928 offers important physical insights into laser-induced tunneling, considered by the Keldysh photoionization theory as one of the limiting regimes and one of the pathways of ionization in the presence of a laser field, in this section, we will provide a brief overview of the main results of the early-day research into the theory of quantum tunneling.

In a series of papers, the first of which was submitted to a journal in November 1926, Friedrich Hund [29, 30] examines the properties of molecular spectra related to nonstationary superposition states, in which the system oscillates between two classical equilibrium states, penetrating through a potential barrier V, separating the atoms that form a molecule. Hund's work deals with a potential exhibiting a mirror symmetry, typical of a broad class of molecular systems. In the basis of stationary states, the ground state of such a potential is even, while the first excited state is odd (Fig. 1a). Superposition of these two states is a nonstationary state, in which the system oscillates between two classical equilibrium states. According to the Hund theory, the period of such an oscillation, T, is proportional to $\exp(V/h\nu)$, where $h = 2\pi\hbar$ is the Planck constant and ν is the frequency of oscillations in a harmonic-oscillator potential well — the approximation used to describe each of the atoms in the molecule. The quantity inverse of this period, $w = 1/T$, is proportional to the exponential

$$w \propto \exp(-G)\,, \tag{1}$$

where G is the phase shift controlled by the width of the potential barrier d and the effective wave number

$$\kappa = \frac{(2mV)^{1/2}}{\hbar} \tag{2}$$

of a particle that penetrates under the barrier. It is remarkable that the exponential $\exp(-G)$, archetypical of quantum tunneling, had emerged in the theory of quantum tunneling even before the term 'quantum tunneling' was coined [31, 32].

In his paper that dates back to the same year of 1927, Lothar Nordheim has studied thermal electron emission from a metal surface [33]. His analysis has shown that electrons can penetrate, due to their wave properties, through a classically forbidden region of a potential barrier that keeps these electrons inside the metal. Nordheim's analysis of transmission of electrons through a rectangular potential barrier and reflection of electrons from such a barrier is reproduced in many present-day textbooks on quantum mechanics.

A year later, Fowler and Nordheim [34] have generalized the Nordheim's treatment of quantum tunneling to a triangular potential barrier induced on a metal surface by a uniform dc electric field F applied along the normal to this surface (Fig. 1b). As part of their analysis, Fowler and Nordheim have shown that the argument of the tunneling exponential $\exp(-G)$ in this case is given by

$$G \propto \frac{(2m)^{1/2}(V - E_F)^{3/2}}{\hbar F}\,, \tag{3}$$

where E_F is the Fermi energy of electrons in the conduction band and V is the height of the potential barrier. The difference $V - E_F$ appearing in the argument of the tunneling exponential is thus equal to the work function Φ (Fig. 1b).

The tunneling exponential written in the form of Eqn (3) helps explain many of the key tendencies observed in experiments and sets a physically significant reference for the analysis of more complex regimes of ionization, including ionization by an ac external field. In an important limiting case of small γ and low field frequencies, the Keldysh-theory formula for the ionization rate reproduces the tunneling exponential in the form of Eqn (1), with the argument of the exponential defined by Eqn (3). In Section 11, we will get back to the Fowler–Nordheim result and discuss it in the context of attosecond pulse generation by photoelectrons tunneling from a metal nanotip irradiated by an ultrashort laser pulse.

As an important step in the development of the quantum tunneling theory, Robert Oppenheimer highlighted in his 1928 papers [35, 36] that an external field can distort the Coulomb potential binding electrons in atoms, giving rise to a potential barrier of a finite width and depth, thus allowing electrons to tunnel through this barrier.

The theory of alpha decay, developed by George Gamow [37] and, independently, Gurney and Condon [38, 39], is, perhaps, the most celebrated example of an early-day application of the quantum tunneling theory. These studies not only provided a quantitative theory explaining the key properties of alpha decay (Fig. 1c), but also stimulated a further progress in the theory of quantum tunneling. As a significant accomplishment, the transmission coefficient of a particle with energy E tunneling through a barrier $V(x)$ in these studies takes a more general form:

$$D = \exp\left\{-\frac{2}{\hbar}(2m)^{1/2}\int_{x_1}^{x_2}\left[V(x) - E\right]^{1/2}\mathrm{d}x\right\}, \tag{4}$$

where x_1 and x_2 are the boundaries of the potential barrier (Fig. 1c), defined as classical turning points from the equation $V(x_{1,2}) = E$.

2.3 Tunneling in semiconductors

The earliest studies of quantum tunneling in semiconductors and dielectrics were aimed at understanding optical breakdown of solids by a strong electric field. It is in the context of

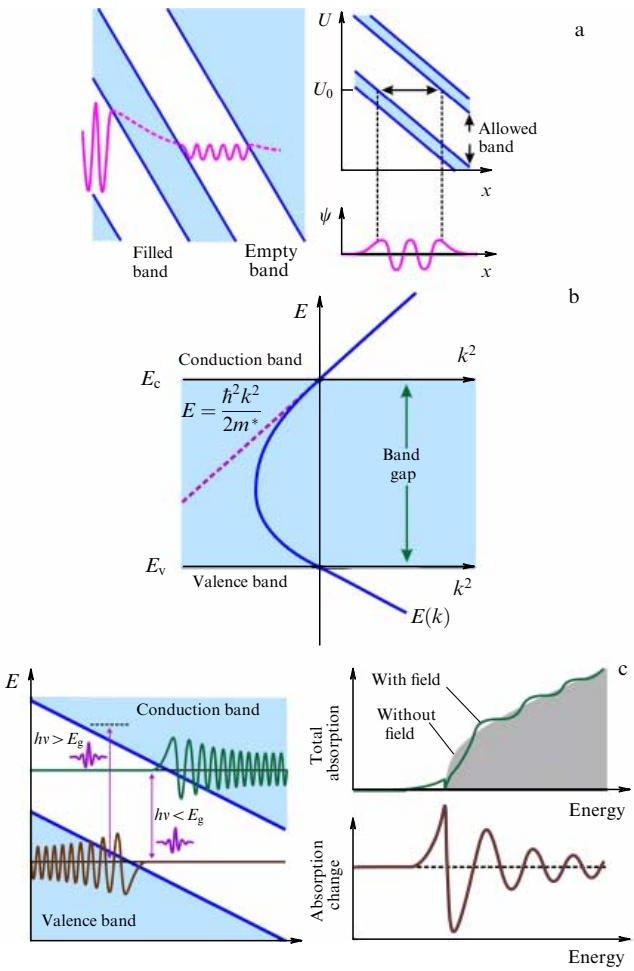

Figure 2. (Color online.) Tunneling in semiconductors and dielectrics. (a) The Zener picture of tunneling between the electron bands of a semiconductor in the presence of an electric field (left) and the electron bands of a semiconductor distorted by an external electric field (right). The electron wave function is also shown. (b) The k-space picture of tunneling in a semiconductor (or dielectric). (c) The Franz–Keldysh effect: (left) electron states modified by an external field and the electron wave function in the valence band and conduction bands; (right) absorption spectrum and a change in the absorption induced by an external field.

this problem that Zener has developed his quasiclassical model of field-induced ionization in semiconductors in his seminal 1934 paper [40]. This model treats field-induced ionization of a semiconductor as a result of field-induced electron transitions from the valence band to the conduction band (Fig. 2a). The right panel in Fig. 2a sketches a diagram of electron bands of a semiconductor distorted by an external dc electric field along with the wave function $\psi(x)$ localized in the allowed electron band. Tunneling in the Zener model is due to the exponentially decaying, evanescent tails of the wave function $\psi(x)$ (Fig. 2a).

The 1950s witnessed an astonishing progress in semiconductor electronics, giving rise to a new wave of interest in quantum tunneling in semiconductors. Similar to the quantum effect in atoms, field-induced electron emission from metal surfaces, and alpha decay of nuclei, tunneling of electrons from the valence band to the conduction band in semiconductors is due to the wave properties of quantum objects. In its simplest form, the theory of quantum tunneling in semiconductors can be developed in close analogy with the theory of electron-emission tunneling from metal surfaces. However, a detailed analysis of tunneling in semiconductors requires a more accurate treatment of a specific dispersion $E(\mathbf{k})$ for all the electron bands involved in the process (Fig. 2b), which makes the problem much more complicated [41–46].

A typical $E - k^2$ plot of a dispersion relation in a semiconductor is sketched in Fig. 2b. Near the top of the valence band, as well as near the bottom of the conduction band, the energy can usually be approximated by a quadratic function of k. In this approximation, the electron energy can be written in the form of a free-electron energy, $E = \hbar^2 k^2/2m^*$, with an effective mass m^*. In the valence band ($E < E_v$), as well as in the conduction band ($E > E_c$), k^2 is positive, corresponding to real k. In the band gap ($E_c < E < E_v$, shown by shading in Fig. 2b), however, k^2 is negative, dictating imaginary k, leading to an exponentially decaying, evanescent wave function.

As one of the fundamental properties of quantum tunneling in semiconductors, an external electric field shifts the absorption band edge of a semiconductor, giving rise to absorption at radiation frequencies nominally still below the band gap (Fig. 2c). This effect, independently predicted by Keldysh [41] and Franz [42] and known as the Franz–Keldysh effect, plays an important role in understanding the optical response of solids. In its dynamic version, the Franz–Keldysh effect enables an ultrafast modulation of the optical response of solid-state semiconductors and dielectrics [47].

In the following sections, we will discuss some of the most important applications of the Keldysh theory of photoionization in solids. As part of this discussion, we will show that the Keldysh-theory analysis helps identify universal properties of the nonlinear-optical response of semiconductors and dielectrics. We will also focus on new applications of ultrashort laser pulses for all-optical diagnostics of solids and ultrafast reversible switching of solid-state dielectrics to the conducting state on the subfemtosecond time scale.

2.4 Multiphoton ionization

Multiphoton ionization is a nonlinear version of the photoelectric effect (Fig. 3a), known since the pioneering work by Hertz and Stoletow [48, 49], one of the first effects consistently explained in terms of quantum concepts [50]. According to the Einstein theory of the photoelectric effect, the kinetic energy of electrons ejected by light with a frequency ω from the surface of a metal with a work function Φ is given by $E_k = \hbar\omega - \Phi$. In the case of N-photon ionization, the kinetic energy of photoelectrons is related to the frequency of the light field by the equation $E_k = N\hbar\omega - \Phi$. Manifestations of multiphoton ionization are numerous, including the multiphoton photoelectric effect on metal surfaces, multiphoton processes in atoms and molecules yielding free electrons, as well as multiphoton interband transitions giving rise to electron–hole pairs in semiconductors. Depending on the context, the quantity Φ in the above expressions for the multiphoton photoelectric effect is understood as the work function in the case of a photoelectric effect on a metal surface, the ionization potential in the case of photoionization of an atom or a molecule, or the width of the band gap separating the valence and conduction bands in semiconductors.

Since N-photon ionization involves absorption of N photons (Fig. 3a), a consistent quantitative theory of this process is in many ways analogous to a perturbative treatment of N-photon absorption, relying on a perturba-

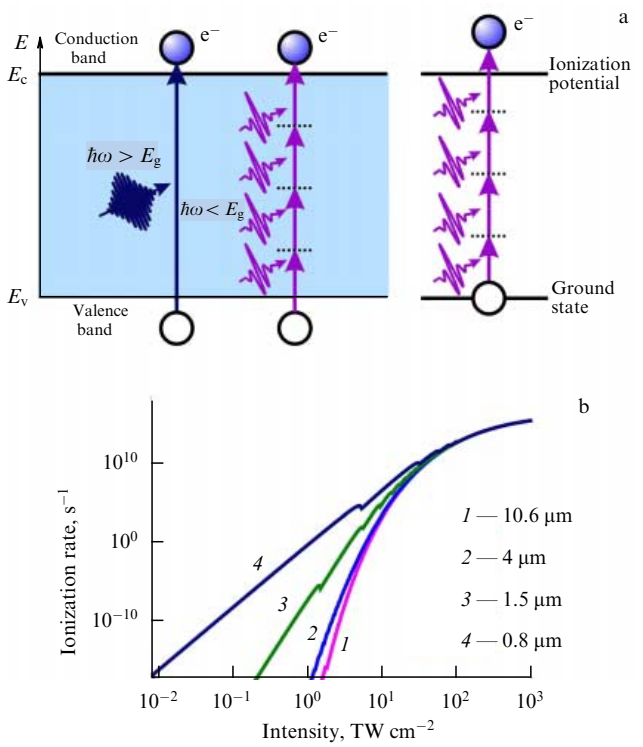

Figure 3. (Color online.) (a) One-photon photoelectric effect and multiphoton processes leading to absorption of radiation and ionization in a semiconductor or dielectric (left) and an atomic system (right). (b) Photoionization rate calculated within the framework of the Keldysh–Popov–Perelomov–Terent'ev formalism as a function of the field intensity.

tion-theory calculation of the Nth order correction in a perturbative series for the electric current, with the external field treated as a small perturbation. In the case of two-photon absorption ($N = 2$), such a theory was developed by Göppert-Mayer back in the 1930s [51]. The first studies into a detailed theory of the quadratic photoelectric effect on metal surfaces also date back to the pre-laser era [52].

The invention of lasers triggered broad-scale research into nonlinear-optical phenomena, providing long-sought tools for an experimental observation of the two-photon photoelectric effect in semiconductors [53] and stimulating deeper theoretical analysis of multiphoton ionization. A comprehensive review of experimental and theoretical studies performed in this area in the early years of laser science is provided in Refs [54, 55]. The ionization potential of atoms (on the order of 10 eV) is much higher than the band-gap energy of a typical semiconductor (on the order of 1 eV). As a consequence, while the multiphoton photoelectric effect in semiconductors is readily observed in the regime of two-photon absorption ($N = 2$), much larger numbers of photons are needed for a multiphoton ionization of atoms (Fig. 3a). A systematic experimental investigation of multiphoton ionization in atoms is thus possible only with much more intense light fields [56–59].

As a characteristic tendency, high-intensity light–matter interactions often lead to an optical breakdown even in a gas medium. In view of this circumstance, multiphoton ionization of gases in the early years of laser physics and nonlinear optics was most often discussed in the context of optical breakdown (see also Section 13 of this review). Fully in line with this tradition is the work by Albert Gold and Barry Bebb [59] submitted to *Physical Review Letters* in November of 1964 and published in January 1965, that is, a few months before the publication of the English translation of the Keldysh paper on the theory of photoionization [1] in May 1965. In this important paper, Gold and Bebb employ an Nth-order semiclassical perturbative treatment to derive an explicit formula for the transition amplitude defining the probability of N-photon ionization of an atom.

This result is then used to provide practically significant realistic estimates for the probabilities of multiphoton ionization for rare gases and to examine the relation between multiphoton ionization and optical breakdown in gases. The Nth-order semiclassical perturbative treatment of multiphoton ionization yields a signature I^N scaling of the probability of N-photon ionization as a function of the laser field intensity. This dependence, typical of any nonlinear-optical process, described in terms of the Nth-order nonlinear-optical susceptibility, provides yet another fundamental reference for a more general photoionization theory. The Keldysh photoionization theory [1] recovers this result in the limit of low field intensities. This theoretical framework, fully developed in a subsequent work by Nikishov, Ritus, Popov, Perelomov, Terentyev, Faisal, Reiss, Delone, and Krainov [60–70], provides a powerful tool for the analysis of laser–matter interactions within a broad range of laser intensities. The basic concepts of this formalism are discussed in the next section.

3. Basic concepts of the Keldysh photoionization theory

The Keldysh theory [1] treats photoionization in an ac field $\mathbf{E}(t)$ as a result of a transition between the initial electron bound state with a wave function $\psi_0(\mathbf{r})$ to a free-electron state modulated by the field $\mathbf{E}(t)$ with a wave function $\psi_{\mathbf{p}}(\mathbf{r}, t)$. The matrix element for such a transition is calculated in the first order of perturbation theory in the interaction, leading to

$$w(\mathbf{p}, t) = \int \psi^*_{\mathbf{p}}(\mathbf{r}, t)\, V(\mathbf{r}, t)\, \psi_0(\mathbf{r})\, \mathrm{d}\mathbf{r}\,, \tag{5}$$

where $V(\mathbf{r}, t)$ is the electron–field interaction part of the Hamiltonian.

The external field $\mathbf{E}(t)$ is assumed to be monochromatic, $\mathbf{E}(t) = \mathbf{E}_0 \cos(\omega t)$, and the interaction Hamiltonian is written in the dipole approximation,

$$V(\mathbf{r}, t) = e\mathbf{r}\mathbf{E}_0 \cos(\omega t)\,. \tag{6}$$

The wave function of the initial electron state is assumed to have the form of the ground-state wave function of a hydrogenlike atom,

$$\psi_0(\mathbf{r}) = (\pi a^3)^{-1/2} \exp\left(-\frac{r}{a}\right), \tag{7}$$

where $a = \hbar^2/(me^2)$ is the Bohr radius.

The field-dressed free-electron wave function is taken in the form of the Volkov-type solution [71],

$$\psi_{\mathbf{p}}(\mathbf{r}, t) = \exp\left\{\frac{\mathrm{i}\mathbf{P}(t)\,\mathbf{r}}{\hbar} - \frac{\mathrm{i}}{2m\hbar}\int_0^t \left[\mathbf{P}(\theta)\right]^2 \mathrm{d}\theta\right\}. \tag{8}$$

Here, in the case of a monochromatic driver field $\mathbf{E}(t) = \mathbf{E}_0 \cos(\omega t)$, the generalized momentum $\mathbf{P}(t)$ is given by $\mathbf{P}(t) = \mathbf{p} + e\omega^{-1}\mathbf{E}_0 \sin(\omega t)$.

With $w(\mathbf{p}, t)$ averaged over the field cycle and integrated over the momentum, the photoionization rate is expressed as a series

$$w_{\mathrm{K}} = \frac{2\pi}{\hbar} \int \left|L(\mathbf{p})\right|^2 \sum_n \delta\left(I_0 + \frac{p^2}{2m} + \frac{e^2 E_0^2}{4m\omega^2} - n\hbar\omega\right) \frac{\mathrm{d}^3 p}{(2\pi\hbar)^3}\,, \tag{9}$$

where

$$L(\mathbf{p}) = \frac{1}{2\pi} \oint \mathrm{d}\xi\, W\left(\mathbf{p} + \frac{e\mathbf{E}_0}{\omega}\,\xi\right) \times \exp\left\{\frac{\mathrm{i}}{\hbar\omega} \int_0^{\xi} \left[I_0 + \frac{1}{2m}\left(\mathbf{p} + \frac{e\mathbf{E}_0}{\omega}\,u\right)^2\right] \frac{\mathrm{d}u}{(1-u^2)^{1/2}}\right\}, \tag{10}$$

I_0 is the ionization potential,

$$W(\mathbf{s}) = e\pi^{-1/2} a^{-3/2} \int \exp\left(-\frac{\mathrm{i}\mathbf{s}\mathbf{r}}{\hbar}\right) \mathbf{E}\mathbf{r} \exp\left(-\frac{r}{a}\right) \mathrm{d}\mathbf{r}\,, \tag{11}$$

and integration is along a closed contour enclosing the $[-1, 1]$ segment.

Since the exponential in $L(\mathbf{p})$ is rapidly oscillating, the integral in Eqn (9) is dominated by the saddle points, defined by the equation

$$I_0 + \frac{1}{2m}\left(\mathbf{p} + \frac{e\mathbf{E}_0}{\omega}\sin(\omega t)\right)^2 = 0\,. \tag{12}$$

As highlighted by Keldysh [1], a pole in Eqn (10), defined by the solution of Eqn (12), reflects the general property of the scattering amplitude, which exhibits poles at momentum values corresponding to electron bound states. With the integral in $L(\mathbf{p})$ calculated using the saddle-point approximation, we arrive at the celebrated Keldysh formula for the rate of photoionization:

$$w_{\mathrm{K}} = Q(\gamma, I_0, \omega) \exp\left[-\xi(\gamma, I_0, \omega)\right], \tag{13}$$

where $Q(\gamma, I_0, \omega)$ is a pre-exponential factor,

$$\xi(\gamma, I_0, \omega) = \frac{2}{\hbar\omega} I_0 \left(1 + \frac{1}{2\gamma^2}\right)\left[\sinh^{-1}\gamma - \gamma\,\frac{(1+\gamma^2)^{1/2}}{1+2\gamma^2}\right], \tag{14}$$

and

$$\gamma = \frac{\omega(2mI_0)^{1/2}}{eE_0} \tag{15}$$

is the Keldysh parameter.

The beauty of this result is that it provides a unified description of multiphoton and tunneling ionization, showing that these processes are two limiting cases of ionization in an ac field (Fig. 3b). Indeed, in the limit of $\gamma \gg 1$, Eqns (13) and (14) recover the signature $w_{\mathrm{K}} \propto I^N$ scaling of the multiphoton ionization rate as a function of the field intensity and the minimum number of photons N needed for photoionization (Fig. 3b). With $\gamma \ll 1$, on the other hand, Eqns (13) and (14) lead to the tunneling exponential, which, in the case of a linearly polarized field, is written as

$$w_{\mathrm{K}} \propto \exp\left[-\frac{4}{3}(2m)^{1/2} I_0^{3/2} (e\hbar E_0)^{-1}\left(1 - \frac{\gamma^2}{10}\right)\right]. \tag{16}$$

For low intensities and/or low frequencies, the γ^2 term in the argument of the exponential can be omitted, yielding a frequency-independent ionization rate (Fig. 3b). The resulting expression recovers, with an accuracy up to the pre-exponential factor (calculation of this factor is beyond the scope of the Keldysh theory), the canonical result for the probability of tunneling in a dc field [Eqns (1) and (3)].

The above analysis highlights the role of the Keldysh γ as a fundamental parameter defining the regime of light–matter interaction. Equations (13) and (14) make it easy to appreciate the role of the Keldysh parameter as a borderline between the high- and weak-field ionization regimes. Remarkably, this parameter also provides a measure of ionization adiabaticity. This insight offered by of the Keldysh theory is discussed in the next section.

4. Keldysh parameter, adiabaticity of photoionization, and tunneling time

Any attempt to understand the Keldysh parameter as a measure of ionization adiabaticity inevitably brings up a question of tunneling time. Keldysh's 1964 paper addresses this question in its opening paragraph, which remains mysterious even now, more than half a century later (see, e.g., the discussion in reviews [72–74]). This important physical argument, which serves as a starting point for the Keldysh analysis, is based on the observation that "virtually no time lag" is a typical feature of quantum tunneling. In other words, as Keldysh articulates in his paper, the tunneling probability remains constant, independent of the field frequency up to the highest frequencies in the radio-frequency range. The reason for this, according to Keldysh, is that the tunneling time is defined by the mean time required for an electron to pass through a barrier with a thickness (in the notation of the Keldysh paper) $l = I/(eF)$, where I is the ionization potential and F is the electric field (Fig. 4a). The mean electron velocity in this argument is on the order of $(I/m)^{1/2}$, where m is the electron mass. Thus, up to a characteristic frequency $\omega_{\mathrm{t}} = eF/(2mI)^{1/2}$, quantum tunneling is governed by the instantaneous field amplitude.

This argument seems to explain why the tunneling-limit photoionization rate ($\gamma \ll 1$) becomes independent of the field frequency ω, interpreting this result in terms of the tunneling time. Indeed, the Keldysh parameter can be represented as $\gamma = 4\pi\tau_{\mathrm{b}}/T_0$, where $T_0 = 2\pi/\omega$ is the cycle of the driver field, and $\tau_{\mathrm{b}} = d/v = (mI_0/2)^{1/2}(eE_0)^{-1}$ is the time it takes for a classical particle with a velocity $v = (2I_0/m)^{1/2}$ to travel a distance $d = I_0/(eE_0)$ equal to the width of the potential barrier formed by a rectangular-step potential barrier with a height I_0 and uniform dc electric field E_0.

The main difficulty of this argument is that the area behind the potential barrier is forbidden for a classical particle. As a consequence, the tunneling time, defined as the time of under-barrier motion of a particle becomes imaginary. When expanded in a small momentum parameter, the solution to Eqn (12) for the time is complex:

$$t_0 \approx \frac{\mathrm{i}}{\omega}\left\{\sinh^{-1}\gamma + \frac{\gamma}{(1+\gamma^2)^{1/2}} \times \left[\mathrm{i}\,\frac{p_{\parallel}}{(2mI_0)^{1/2}} + \frac{1}{4mI_0}\left(\frac{\gamma^2}{1+\gamma^2}\,p_{\parallel}^2 + p_{\perp}^2\right)\right]\right\}, \tag{17}$$

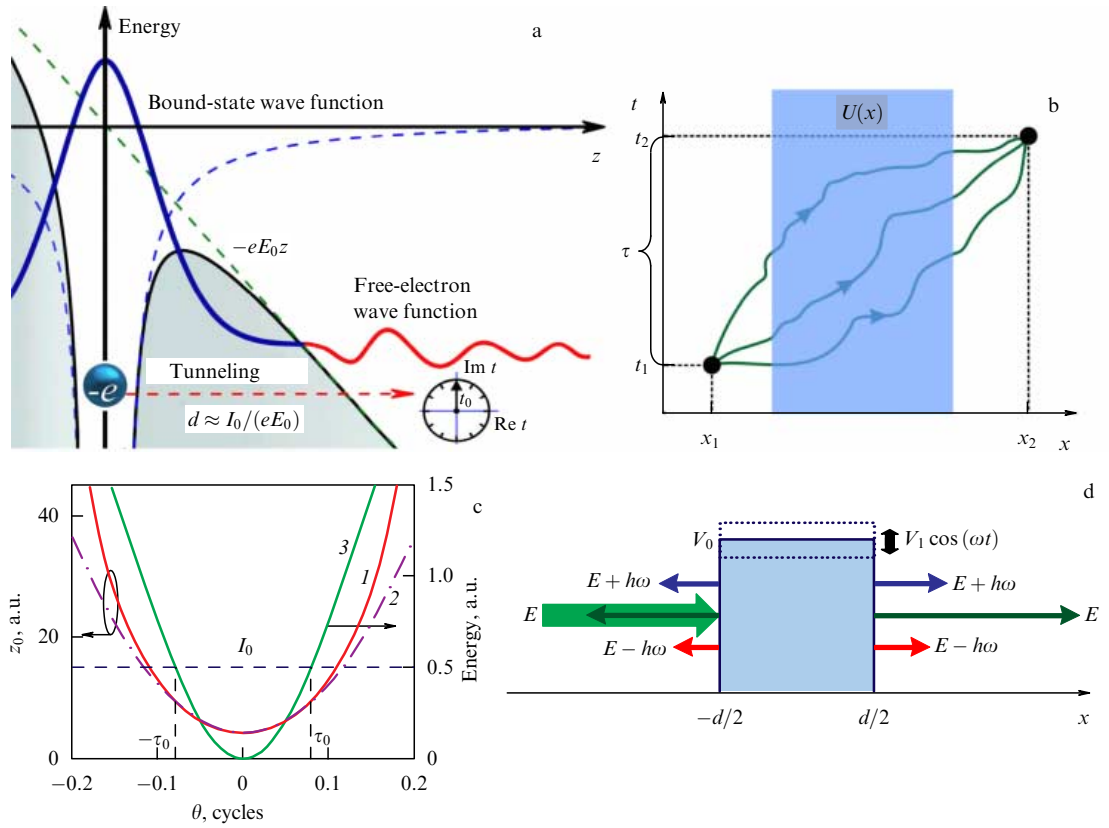

Figure 4. (Color online.) (a) Electron tunneling in atoms in the presence of an external field. The external field distorts the Coulomb potential binding electrons in atoms, giving rise to a potential barrier of finite height and width, allowing electron tunneling. (b) Tunneling and quantum trajectories. (c) Width z_0 of the potential barrier produced by the potential of the atomic core and a laser field with a field intensity of 500 TW cm^{-2} and a wavelength of 800 nm, found by solving the $\Phi(z, \theta) = 0$ equation (red solid line *1*) and calculated with the approximation of Eqn (12) (dash–dotted line *2*). Green solid line *3* shows the electron kinetic energy U_p as a function of time θ expressed in field cycles. Also shown is the time τ_0 required for an electron to acquire the kinetic energy U_p equal to the ionization potential I_0 (shown by the horizontal dashed line). (d) Landauer–Büttiker oscillating potential barrier.

where $p_\parallel$ and $p_\perp$ are the parallel and normal components of the electron momentum.

Thus, the interpretation of the Keldysh parameter as a ratio of the under-barrier passage time $\tau_b = d/v$ to the field cycle $T_0 = 2\pi/\omega$ encounters fundamental difficulties. In a big-picture perspective, these difficulties are inevitable in a canonical quantum theory, which does not provide a clear recipe for the definition of the tunneling time. In this section, we dwell on this important issue following an insightful path-integral analysis of quantum tunneling by Sokolovski and Connor [75–79].

In quantum mechanics, the dynamics of a particle is described by the wave function $\Psi(x, t)$, governed by the quantum evolution equation. The time-dependent Schrödinger equation is the pertinent evolution equation in the case of nonrelativistic photoionization. Quantum mechanics also provides a system of postulates allowing the position of a particle x at the instant of time t to be determined using the wave function $\Psi(x, t)$. To define the time interval τ within which a quantum particle evolves from position x_1 to position x_2, we need to represent the wave function $\Psi(x, t)$ as an integral [75–79],

$$\Psi(x, t) = \int_0^t \Phi(x, t\,|\tau)\,\mathrm{d}\tau\,. \tag{18}$$

Thus, the state of particle found at point x at the instant of time t is a result of interference of an infinite number of 'quantum prehistories' (Fig. 4b), which can be instructively interpreted in terms of quantum trajectories [80]. Similar to the celebrated two-slit diffraction scheme, where the number of quantum prehistories is two, an attempt to find out which individual trajectory is behind the quantum evolution of a particle demolishes the state $\Psi(x, t)$. Thus, the interference of different $\Phi(x, t\,|\tau)$ leads to a loss of information on individual quantum trajectories corresponding to well-defined time intervals τ in the integral for $\Psi(x, t)$ in Eqn (18).

Since $\Phi(x, t\,|\tau)$ is a continuous function of τ, measurement with a finite precision yields an amplitude [75–79]

$$\Psi(x, t\,|\tau) = \int_{-\infty}^{\infty} F(\tau - \tau')\,\Phi(x, t\,|\tau')\,\mathrm{d}\tau'\,, \tag{19}$$

where an apparatus function $F(\tau)$ is centered at $\tau = 0$ and has a characteristic width $\delta\tau$. Thus, the probability to detect τ within an interval between $\tau - \delta\tau$ and $\tau + \delta\tau$ can be written as

$$\rho(x, t\,|\tau) = \left|\Psi(x, t\,|\tau)\right|^2. \tag{20}$$

A measurement aimed at detecting an individual trajectory corresponds to an expansion

$$\Psi(x, t\,|\tau) \approx \Psi(x, t)\left[F(\tau) - F'(\tau)\,\bar{\tau}(x)\right], \tag{21}$$

where

$$\bar{\tau}(x) = \frac{\int_0^t \tau\Phi(x, t\,|\tau)\,\mathrm{d}\tau}{\Psi(x, t)}\,. \tag{22}$$

Following [75–79], we consider a scheme of measurements that detects only those particles that reach the point x at the instant of time $t = T$. By its definition, such a measurement scheme, which is one of the modifications of a weak measurement, requires an extremely large number of measurements. The expectation value of τ in such a scheme of measurements is

$$\langle \tau(x) \rangle = \frac{\int_{-\infty}^{\infty} \tau \left| \Psi(x, T|\tau) \right|^2 \mathrm{d}\tau}{\int_{-\infty}^{\infty} \left| \Psi(x, T|\tau) \right|^2 \mathrm{d}\tau} \,. \tag{23}$$

Since $\int_{-\infty}^{\infty} \tau |F(\tau)|^2 \,\mathrm{d}\tau = 0$, we find $\langle \tau(x) \rangle \approx \mathrm{Re}\,[\bar{\tau}(x)]$.

However, according to Eqn (22), the expectation value $\bar{\tau}(x)$ is calculated with a complex, rapidly oscillating distribution $\Phi(x, t|\tau)$. Therefore, even if no quantum trajectory represents τ beyond the interval between 0 and T, $\mathrm{Re}\,[\bar{\tau}(x)]$ can fall outside this interval. This contradiction indicates a fundamental difficulty of such a definition of time intervals.

This problem can be addressed if the point at which the particle is detected in the scheme of weak measurements is not fixed. The expectation value in such a measurement scheme,

$$\langle \tau \rangle = \int_0^T \mathrm{d}t \int_{x_1}^{x_2} \left| \Psi(x, t) \right|^2 \mathrm{d}x \,, \tag{24}$$

does not encounter the difficulties explained above. When defined as the expectation value in Eqn (24), time τ always falls within the $[0, T]$ interval.

For a quantum particle tunneling through a potential $V(x)$, the distribution $\Phi(x, t|\tau)$ can be represented as [75–79]

$$\Phi(x, t|\tau) = \frac{1}{2\pi\hbar} \int \Psi(x, t|W) \exp\left(\mathrm{i}\, \frac{W}{\hbar}\, \tau \right) \mathrm{d}W \,. \tag{25}$$

In this expression, $\Psi(x, t|W)$ is a result of an evolution of the initial state $\Psi(x, 0)$ in the presence of a potential $V(x) + W\Theta(x)$, where

$$\Theta(x) = \begin{cases} 1 \,, & x_1 \leqslant x \leqslant x_2 \,, \\ 0 \,, & x < x_1 \,, \quad x > x_2 \,. \end{cases} \tag{26}$$

Thus, fixing the parameter τ is equivalent to an effective change in the potential. This result reflects an inevitable backaction of a measuring apparatus on a quantum system. A measuring apparatus with the width of an apparatus function $\delta\tau$ will effectively change the potential by δW in such a way that the uncertainty relation $\delta\tau\,\delta W \geqslant \hbar$ is satisfied. In other words, an apparatus that provides a higher accuracy of τ measurements induces larger changes in the potential.

The wave function of a particle behind the potential barrier $V(x) = V_0\Theta(x)$ is

$$\Psi(x, t) = T(k, V) \exp\left(\mathrm{i}kx - \mathrm{i}\, \frac{E}{\hbar}\, t \right) , \tag{27}$$

where $T(k, V)$ is the transmission coefficient.

In the classical limit, $\xi = k(x_2 - x_1) \gg 1$, analysis of the function $\Phi(x, t|\tau)$ for a free particle, $V = 0$, leads to the equation for the stationary-phase point [75–79],

$$\frac{m(x_2 - x_1)}{\left[2m(E - W)\right]^{1/2}} = \tau \,, \tag{28}$$

identical to the equation of the classical trajectory. The integral over all the other trajectories is vanishingly small because of the destructive interference of these trajectories.

For $V \neq 0$, the stationary-phase point is shifted to the complex plane off the real axis. In the quasiclassical limit, $V \gg E$, the equation for the stationary-phase point gives two purely imaginary solutions for τ [75–79]:

$$\tau(V) = \pm\mathrm{i}\, \frac{m(x_2 - x_1)}{\left[2m(V - E)\right]^{1/2}} \,. \tag{29}$$

It is this situation that one deals with in the case of photoionization by an intense ac field in the $\gamma \ll 1$ regime. The equation for the stationary phase in this case has the form of Eqn (12), dictating a purely imaginary solution for τ. All the trajectories corresponding to the real values of τ are represented by rapidly oscillating terms in the integral for $\Phi(x, t|\tau)$. Destructive interference of individual quantum trajectories leads, in accordance with Eqn (16), to an exponentially small transmission coefficient.

Notably, Eqns (28) and (29) are fully consistent with the Bohmian interpretation of quantum mechanics [81]. This interpretation gives a radically different perspective on tunneling through a quantum barrier, offering a transparent solution [82], as the potential barrier is suppressed by an additional 'quantum' potential [81]. The solution of the tunneling time problem in this picture (see also Ref. [83]) is fully consistent with the insight offered by the opening paragraph in Keldysh's 1964 paper.

5. Photoionization by an ultrashort laser pulse and attosecond electron dynamics

Discussion in Section 4 shows that the role of the Keldysh parameter as a measure of photoionization adiabaticity is difficult to understand from the perspective of the electron under-barrier motion time $\tau_\mathrm{b} = d/v$ and interpretation of the Keldysh parameters in terms of the $4\pi\tau_\mathrm{b}/T_0$ ratio. In the era of modern technologies, a satisfactory solution of this problem in relation to whatever we might like to call the tunneling time goes way beyond purely methodological, interpretational aspects of quantum physics. A clear understanding of extremely fast electron tunneling dynamics would be central to maximizing the speed of semiconductor electronic devices, achieving an ultimate accuracy in attosecond metrology [11], and identifying the fundamental limitations of rapidly emerging petahertz optoelectronics [9, 10, 84].

Unique experimental methods developed within the past few years [85–90] enable the detection of electron tunneling dynamics in photoionization with an unprecedented time resolution. Figure 5 presents a schematic of direct dual-channel detection of the photoelectron yield through above-threshold ionization (ATI). This technique, referred to as stereo-ATI [87], enables direct time characterization of photoelectron currents induced by two adjacent half-cycles of an optical field. Stereo-ATI is a powerful tool of attosecond metrology and a highly accurate method of temporal characterization of single-cycle and subcycle optical field waveforms [91]. However, retrieving the information on characteristic tunneling times from such measurements, as well as from measurements performed with the use of any other technique, no matter how accurate it is, encounters

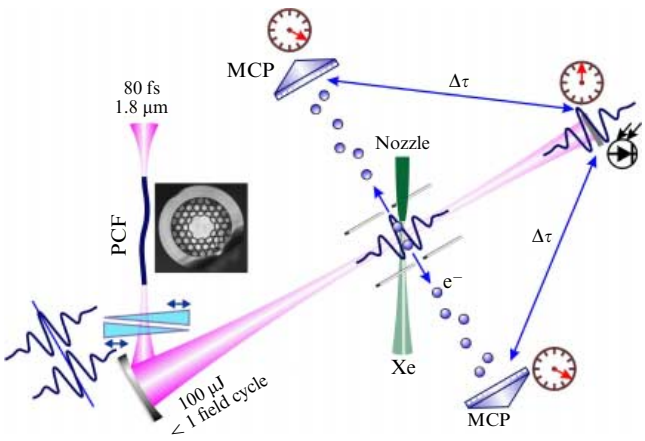

Figure 5. (Color online.) Stereo-ATI detection of attosecond electron dynamics: MCP, microchannel plate, PCF, hollow-core photonic-crystal fiber.

fundamental difficulties related, as emphasized above, to tunneling-time definition and interpretation.

In view of new exciting opportunities offered by attosecond physics and petahertz optoelectronics, the Keldysh tunneling-time intuition offers hope for a clear, physically transparent, albeit not perfectly rigorous perspective on electron tunneling, leading to real-valued predictions for a time scale of electron tunneling in terms of the Keldysh parameter. The main difficulty of such an approach, as explained in detail in the previous section, is that the canonical quantum theory leads to complex tunneling times. Below in this section, we will show that there is a way to achieve a sort of a compromise, if not reconcile, predictions of the canonical quantum theory and an intuitive picture of tunneling in an ac field described in terms of the Keldysh parameter understood as the ratio of the characteristic tunneling time to the field cycle [92]. This compromise can only be achieved, however, at the expense of giving up the interpretation of the γ/ω time as the time of under-barrier motion of an electron. Instead, as will be shown below in this section, the γ/ω parameter relates to the time needed for an electron to acquire a kinetic energy equal to the ionization potential. Such a perspective offers helpful insights into the significance of the Keldysh γ as a universal parameter that not only describes the borderline between the weak- and strong-field regimes of photoionization, but also quantifies the adiabaticity of ionization dynamics in an external ac field.

To this end, we consider the dynamics of photoionization without averaging the probability amplitude $w(\mathbf{p}, t)$ over the field cycle, as it is prescribed in the standard Keldysh-theory formalism. The instantaneous photoelectron yield induced by an external driver field by the time t is then given by

$$J(t) \propto \int_{-\infty}^{t} \mathrm{d}\eta \int \mathrm{d}\mathbf{r}\, \exp\left(-\frac{r}{a_0}\right) \mathbf{E}_0 \mathbf{r} \cos(\omega\eta) \times \exp\left\{\frac{\mathrm{i}}{\hbar}\left[I_0\eta - \mathbf{P}(\theta)\,\mathbf{r} + \frac{1}{2m}\int_0^{\eta}\left[\mathbf{P}(\theta)\right]^2 \mathrm{d}\theta\right]\right\}. \quad (30)$$

Since $w(\mathbf{p}, t)$ is dominated by photoelectrons with small p [1, 62], Eqn (30) applied to a one-dimensional geometry of photoionization induced by a driver field linearly polarized along the z-axis gives

$$J(t) \propto \int_{-\infty}^{t} \mathrm{d}\eta \int_{-\infty}^{\infty} \mathrm{d}z\, \exp\left(-\frac{z}{a_0}\right) E_0 z \cos(\omega t) \times \exp\left[\frac{\mathrm{i}}{\hbar}\int_0^{\eta} \Phi(z,\theta)\,\mathrm{d}\theta\right], \quad (31)$$

where

$$\Phi(z,\theta) = I_0 - eE_0 z\cos(\omega\theta) + \frac{1}{2m}\left(\frac{eE_0}{\omega}\right)^2 \sin^2(\omega\theta). \quad (32)$$

The exponential under the integral in Eqn (31) rapidly oscillates unless $\Phi(z,\theta) \approx 0$. Noting that the strong-field regime criterion $\gamma \ll 1$ is equivalent to the inequality $(eE_0)^2/(2m\omega^2) \gg I_0$, we see that, in this regime, an electron acquires a kinetic energy equal to the ionization potential I_0 within a small time interval $[-\tau_0, \tau_0]$ around the peak of the driver field (Fig. 4c), with τ_0 defined by the equation

$$\sin^2(\omega\tau_0) = \omega^2 \frac{2mI_0}{(eE_0)^2} = \gamma^2 \ll 1. \quad (33)$$

Since within this interval, $\sin^2(\omega\tau_0) \ll 1$ in Eqn (33), we can use Taylor-series expansions $\sin^2(\omega\theta) \approx (\omega\theta)^2$ and $\cos(\omega\theta) \approx 1 - (\omega\theta)^2/2$ in Eqn (32) to write the solution to the $\Phi(z,\theta) = 0$ equation as

$$z_0 \approx \frac{I_0}{eE_0}\left[1 + \left(1 + \frac{2}{\gamma^2}\right)\frac{\omega^2\theta^2}{2}\right]. \quad (34)$$

Plugging this solution into Eqn (31), we arrive at the following estimate for $J(t)$:

$$J(t) \propto \exp\left[-\frac{(2m)^{1/2} I_0^{3/2}}{e\hbar E_0}\right] \times \int_{-\infty}^{t} \exp\left\{-\frac{(2m)^{1/2} I_0^{3/2}}{e\hbar E_0}\left[\left(1 + \frac{2}{\gamma^2}\right)\frac{\omega^2\theta^2}{2}\right]\right\} \mathrm{d}\theta. \quad (35)$$

Despite its approximate character, Eqn (35) correctly reproduces the $\omega \to 0$ limit of the photoionization rate, recovering the probability of dc-field-induced tunneling,

$$w_{\mathrm{dc}} \propto \exp\left[-\frac{4}{3}\frac{(2mI_0^3)^{1/2}}{e\hbar E_0}\right]. \quad (36)$$

This expression can be written in a canonical form of Eqn (1), $w \propto \exp(-\kappa d)$, with $d = I_0/(eE_0)$ and κ being the wave number of the de Broglie wave representing the tunneling electron.

Evaluating the integral in Eqn (35), we find

$$J(t) \propto \exp\left[-\frac{(2m)^{1/2} I_0^{3/2}}{e\hbar E_0}\right]\left[1 + \mathrm{erf}\left(\frac{t}{\tau_{\mathrm{e}}}\right)\right], \quad (37)$$

where $\mathrm{erf}(u) = 2\pi^{-1/2}\int_0^u \exp(-\xi^2)\,\mathrm{d}\xi$ is the error function and

$$\tau_{\mathrm{e}} = 2^{1/4}(e\hbar E_0)^{1/2}(mI_0^3)^{-1/4}\omega^{-1}\left(1 + \frac{2}{\gamma^2}\right)^{-1/2}. \quad (38)$$

It is straightforward to see from Eqn (37) that the temporal profile of $J(t)$ has a shape of a step centered at the

point where the driver field reaches its maximum. Such steps are indeed observed in attosecond time-resolved studies of the photoelectron yield in the strong-field regime. The buildup rate of $J(t)$, that is, the steepness of the $1 + \mathrm{erf}\,(t/\tau_e)$ step in Eqn (14), is controlled by the τ_e time-scale parameter. Due to the $\tau_0 \propto E_0^{-1/2}$ scaling, stronger driver fields give rise to steeper steps in $J(t)$. In the $E_0 \to \infty$ limit, $J(t)$ tends to a Heaviside unit-step function, $J(t) \to \Theta(t)$, whose step is locked to the peak of the field. In this sense, electron tunneling instantly follows the driver field without any time lag with respect to the driver field.

We are now in a position to address the key question as to why the Keldysh parameter serves simultaneously as the adiabaticity parameter and a borderline between weak- and strong-field ionization. When the field intensity is high enough so that the condition

$$\frac{1}{2m}\left(\frac{eE_0}{\omega}\right)^2 \sin^2(\omega\theta) \gg I_0\,, \qquad -\tau_0 < \theta < \tau_0 \tag{39}$$

is satisfied everywhere within the field cycle except for a short time interval $[-\tau_0, \tau_0]$ around the peak of the driver field (Fig. 4c), Eqn (34) for the effective width of the potential barrier is reduced to

$$z_0 \approx I_0(eE_0)^{-1}\left[1 + \left(\frac{\omega}{\gamma}\right)^2 \theta^2\right] = I_0(eE_0)^{-1} + (2m)^{-1} eE_0\theta^2\,. \tag{40}$$

The photoelectron yield $J(t)$ is then frequency-independent, with its buildup time given by

$$\tau_e \approx (e\hbar E_0)^{1/2}(2mI_0^3)^{-1/4}\,\frac{\gamma}{\omega} = \left(\frac{2m}{I_0}\right)^{1/4}\left(\frac{\hbar}{eE_0}\right)^{1/2}. \tag{41}$$

Thus, the analysis of ultrafast photoionization within the field cycle leads us to formulate the criterion of strong-field photoionization in the form of Eqn (39). When written in such a form, this criterion automatically implies, through Eqns (33)–(35), that the photoionization rate is frequency-independent, or, for that matter, adiabatic. Notably, since the Keldysh formula involves integration over the field cycle, the pondermotive energy enters into the Keldysh-theory equations in its averaged form — as the $e^2E_0^2/(4m\omega^2)$ term in Eqn (9) and as the $[1 + 1/(2\gamma^2)]$ factor in Eqn (14). The relation of ω cancellation in the photoionization rate to the subcycle dynamics of photoionization is thus lost.

Equations (30)–(39) clearly show that it is the photoionization dynamics occurring within a small fraction of the driver cycle, that is, within the time interval $[-\tau_0, \tau_0]$ near the peak of the driver field, that makes photoionization frequency-independent. As can be seen from these expressions, photoionization in this regime is a result of ultrafast electron tunneling, which is strongly confined to a very short time gate $[-\tau_0, \tau_0]$. As can be seen from Eqn (40), within this interval, the width of the potential barrier, controling the photoionization rate, remains approximately constant and equal to $d = I_0/(eE_0)$. The expression for the effective width of the potential barrier involves no term that would be linear in time. The first nonvanishing correction grows as $(2m)^{-1}eE_0\theta^2$ as a function of time and is also independent of the frequency of the driver field.

We can now confront the question as to whether the time γ/ω is in any way representative of the beneath-the-barrier electron passage time $\tau_b = d/v$. We note that Eqn (39) leads to $(eE_0)^2/(2m\omega^2) \gg I_0$. This inequality can be rewritten in the form $\gamma^2 \ll 1$ [see also Eqn (33)], which is equivalent to the criterion of both tunneling and adiabaticity in the Keldysh theory of photoionization. Then, solving Eqn (33) for τ_0, we find $\tau_0 = \omega^{-1}\arcsin\gamma$. With $\gamma \ll 1$, this expression reduces to $\tau_0 \approx \gamma/\omega = (2mI_0)^{1/2}/(eE_0)$. We see that the γ/ω ratio does indeed define an important time scale of photoionization. However, this time scale is not related to the time of electron motion beneath the potential barrier, $\tau_b = d/v$, but connects instead to the time needed for an electron to acquire a kinetic energy equal to the ionization potential.

We see now that the considered semiclassical perspective on the adiabaticity of photoionization driven by an ultrashort light pulse leads to an adiabaticity criterion that exactly recovers the Keldysh-theory criterion, but does not require a notion of a real electron under-barrier passage time. An experimentally measurable characteristic tunneling time scale is now defined as $\tau_e \approx (e\hbar E_0)^{1/2}(2mI_0^3)^{-1/4}\tau_0$. For a driver field intensity of 10^{14} W cm^{-2}, this gives $\tau_e \approx 0.14$ fs. Despite its brevity, the buildup time τ_e of the photoelectron yield $J(t)$ can be measured with a reasonable accuracy in experiments through a direct time-resolved photoelectron detection [85, 87] (see Fig. 5) or through the spectral analysis of optical harmonics [16, 17, 93].

6. Photoionization and an oscillating potential barrier

To provide deeper insights into the dynamic aspects of photoionization in the Keldysh theory, we will now focus on the relation between ionization in an external ac field and transmission of a quantum particle through an oscillating rectangular potential barrier in the formulation of Landauer and Büttiker [94]. In its canonical version, this problem treats a free particle with a plane-wave wave function tunneling through a rectangular potential barrier with a height V_0 and width d. Analysis of tunneling through a barrier of such a form is important as it helps understand tunneling processes in semiconductor materials and structures. Büttiker and Landauer have examined tunneling through a time-dependent, oscillating rectangular potential barrier (Fig. 4d)

$$V(x,t) = V_0(x) + V_1(x)\cos(\omega t)\,. \tag{42}$$

The perturbation $V_1(x)$ is assumed to be constant and equal to V_1 within the barrier and equal to zero outside the barrier (Fig. 4d).

With such an oscillating potential barrier, the Hamiltonian of a particle is

$$H = \frac{p^2}{2m} + V_0 + V_1\cos(\omega t)\,. \tag{43}$$

The solution to the Schrödinger equation with such a Hamiltonian is written as

$$\psi(x,t;E) = \varphi_E(x)\exp\left(-\mathrm{i}\,\frac{E}{\hbar}\,t\right)\exp\left[-\mathrm{i}\,\frac{V_1}{\hbar\omega}\sin(\omega t)\right], \tag{44}$$

where $\varphi_E(x)$ is the solution to the Schrödinger equation

$$H_0\varphi_E(x) = E\varphi_E(x) \tag{45}$$

with the Hamiltonian

$$H_0 = \frac{p^2}{2m} + V_0 \,. \tag{46}$$

Representing the solution to Eqn (45) in the region of the rectangular potential barrier as $\varphi_E(x) = \exp(\pm\kappa x)$, with $\kappa = [2m(V_0 - E)]^{1/2}/\hbar$, we find

$$\psi_\pm(x, t; E) = \exp(\pm\kappa x) \exp\left(-\mathrm{i}\,\frac{E}{\hbar}\,t\right) \times \sum_{n=-\infty}^{\infty} J_n\left(\frac{V_1}{\hbar\omega}\right) \exp(-\mathrm{i}n\omega t)\,, \tag{47}$$

where $J_n(x)$ is the Bessel function.

In the Büttiker–Landauer model, the ratio $V_1/\hbar\omega$ is so small that the sum in n in Eqn (47) is fully dominated by its terms with $n = 0, \pm 1$. Analysis of transmission coefficients $T_\pm$ for particles with energies $E \pm \hbar\omega$, corresponding to $n = \pm 1$, shows that, in the limiting case of low frequencies, $T_+ \approx T_-$. As the frequency increases, however, the difference between T_+ and T_- becomes significant, with $(T_+ - T_-)/(T_+ + T_-) \approx \tanh(\omega\tau_{\mathrm{LB}})$, where $\tau_{\mathrm{LB}} = -md/(\hbar\kappa)$. This result is attributed in the Büttiker–Landauer treatment to the difference in the times of under-barrier passage of particles with energies $E \pm \hbar\omega$. Such an interpretation suggests that the time $\tau_{\mathrm{LB}} = md/(\hbar\kappa)$ plays the role of the time of under-barrier passage.

Since the time $\tau_{\mathrm{LB}} = md/(\hbar\kappa)$ can be rewritten as $\tau_{\mathrm{LB}} = d/v$, this interpretation is consistent with the interpretation of the Keldysh-parameter-related time γ/ω as the time $\tau_{\mathrm{b}} = d/v$ of under-barrier passage. In this sense, the 'Keldysh time' is often categorized as a particular case of the Landauer–Büttiker time. Below in this section, we will discuss the relation between these times in greater detail.

We start by articulating that the problem of photoionization by the field of electromagnetic radiation addressed by the Keldysh theory differs in the underlying ionization dynamics and the form of the potential from the problem dealing with a particle tunneling through an oscillating rectangular barrier as defined by Eqn (42). The wave functions of stationary electron states in a Coulomb potential are significantly different from the plane-wave wave function describing the tunneling particle in the Landauer–Büttiker problem. In contrast to the perturbation of a rectangular potential barrier in the Landauer–Büttiker problem, perturbation of the stationary potential by the electromagnetic field in the photoionization problem is not spatially uniform (cf. Figs 4a and 4d). Finally, in the photoionization problem, the potential is modulated in such a way that each flash in the photoelectron current, confined to the interval of time when the potential barrier is partially or completely suppressed by the driver field, is followed by a phase within which the next field half-cycle increases the potential barrier for a given direction in space, thus making some fraction of electrons that have tunneled through the barrier within the previous field half-cycle return to the parent ion.

The finding that both the γ/ω time, related to the Keldysh parameter, and the Landauer–Büttiker time can be interpreted as the under-barrier passage time $\tau_{\mathrm{b}} = d/v$ is an important and in many ways characteristic observation common for various regimes of quantum tunneling. This result highlights once again the heuristic value of the Bohmian notion of velocity [81], which remains in many respects meaningful in the context of quantum tunneling, when the momentum and related velocity defined according to the recipes of canonical quantum mechanics become imaginary. As shown in Section 4 and 5, in the framework of canonical quantum mechanics, interpretation of the time parameter γ/ω in the Keldysh photoionization theory and the τ_{LB} parameter in the Landauer–Büttiker model of an oscillating barrier as under-barrier passage times encounters fundamental difficulties. The standard version of quantum mechanics can give real and measurable tunneling times only in the scheme of weak measurements [75–79, 95, 96] at the expense of modifying the conventional definition of time inherited from classical mechanics, implying that the starting and final points of mechanical motion are fixed in time (Fig. 4b).

Without offering a satisfactory recipe for the measurement of conventionally understood time intervals, a canonical quantum-mechanical analysis of tunneling leads us again and again to a stationary picture of tunneling, expressed by Eqns (1) and (2). In this picture, the tunneling probability is an exponentially decreasing function of the effective depth of the potential barrier d to the de Broglie wavelength. The equation for the stationary point of ionization in an ac field and equations for the transmission coefficients $T_\pm$ in the Landauer–Büttiker model give the same result for the ionization rate or the tunneling probability.

Let us now examine more closely Eqn (47) for the wave function of a particle tunneling through a periodically oscillating barrier (42) and consider the wave function described by Eqn (47) without restricting our analysis to the $n = 0, \pm 1$ terms. We observe that the sum in n on the right-hand side of Eqn (47) represents a superposition of states with energies $E \pm n\hbar\omega$. For small $V_1/\hbar\omega$, the expansion coefficients of the function $\psi_\pm(x, t; E)$ in the eigenfunctions of the stationary states $\exp(\pm\kappa x)\exp(-\mathrm{i}Et/\hbar)$ are given by the first terms in the polynomial expansion for the Bessel functions, $c_n \propto (V_1/\hbar\omega)^n$. If the perturbation of the potential is proportional to an external field, $V_1 \propto E$, we then find that, for a state with energy $E \pm n\hbar\omega$, the probability of transmission through the barrier scales as I^n with the field intensity I. With $n > (V_0 - E)/(\hbar\omega)$, we deal with a particle whose energy, as a result of absorption of n photons, is higher than the potential barrier, $E + n\hbar\omega > V_0$, and whose transmission through the barrier has signatures of multiphoton ionization. Similar to multiphoton ionization, the tunneling probability of such a particle is proportional to I^n. The approximation $c_n \propto (V_1/\hbar\omega)^n$ is applicable only for $V_1/\hbar\omega < 1$. With $V_1 \sim eEa_0$, where $a_0 = \hbar/(2mI_0)^{1/2}$ and I_0 is the ionization potential, this condition is equivalent to the inequality $\gamma > 1$, i.e., the criterion of multiphoton ionization in the Keldysh theory.

7. Gauge invariance and applicability limits of the dipole approximation

One of the main fundamental difficulties of the Keldysh photoionization theory is related [97, 98] to the character of the scalar and vector potentials chosen for the description of the fields in this theory, as well as with the approximations used to introduce the Hamiltonian of interaction between an electron and a light field,

$$V(\mathbf{r}, t) = e\mathbf{r}\mathbf{E}_0 \cos(\omega t)\,. \tag{48}$$

The interaction operator is obviously written in the dipole approximation. The fields defined by a scalar potential $\varphi(t) = -e\mathbf{r}\mathbf{E}(t)$ with zero vector potential, $\mathbf{A} = 0$, belong to the class of longitudinal fields. Such fields can vary in time, but cannot propagate. Electromagnetic fields, on the other hand, belong to the class of propagating fields. The vector potential for such fields, $\mathbf{A}(\mathbf{r}, t) \neq 0$, depends on both time and spatial coordinates. In view of these general properties of electromagnetic fields, the choice of the interaction Hamiltonian in the form of Eqn (48) and the wave function of a photoelectron in the form of the Volkov function (8) raises broadly discussed questions with regard to the applicability of the tunneling limit of the Keldysh theory to the description of ionization in a laser field, which should be described by a nonzero, position-dependent vector potential $\mathbf{A}(\mathbf{r}, t)$.

Indeed, except for the case of a zero-range potential, the photoionization rate calculated in the canonical version of the Keldysh theory generally differs from the ionization rate found with the use of the Coulomb gauge. In other words, this result is not gauge-invariant. However, within the applicability limits of the dipole approximation, when effects related to the magnetic field and the position dependence of the vector potential are negligible, the difference in the photoionization rates calculated with different gauges is purely nominal [25]. Quantitative analysis of photoionization beyond the applicability limits of the dipole approximation obviously falls beyond the scope of the original Keldysh theory developed in the early years of the laser era. However, deeper insights into these problems are certainly useful in the modern age of laser science, when cutting-edge laser sources of high-intensity ultrashort light pulses enable direct experimental studies of photoionization within a broad range of frequencies [99–110].

We start by noting that both the apparent paradox of the physical nonequivalence of different gauges and the general scheme of resolving this paradox have been known for quite a while [51, 111]. An illuminating, in-depth review of this problem has been provided by Bykov [112]. To illustrate the main arguments helping put the issue to rest, we consider an electron with a momentum $\mathbf{p}$ and a potential energy $U(\mathbf{r})$ in an atom or a molecule in the presence of an electromagnetic field with electric and magnetic components $\mathbf{E}$ and $\mathbf{H}$ and a vector potential $\mathbf{A}$. In the Coulomb gauge ($\operatorname{div}\mathbf{A} = 0$), the full Hamiltonian of such a system is written as

$$H = \frac{1}{2m}\left(\mathbf{p} - \frac{e}{c}\mathbf{A}\right)^2 + U(\mathbf{r}) + \frac{1}{8\pi}\int(\mathbf{E}^2 + \mathbf{H}^2)\,\mathrm{d}V\,. \quad (49)$$

The Hamiltonian of interaction of an electron with the field can then be isolated as

$$H_{\mathrm{int}} = -\frac{e}{mc}\,\mathbf{p}\,\mathbf{A} + \frac{e^2}{2mc^2}\,\mathbf{A}^2\,. \quad (50)$$

In the dipole approximation, i.e., in the approximation that the radiation wavelength is much larger than the size of an atom, Eqn (50) is dominated by the first term,

$$H_{\mathrm{int}} \approx -\frac{e}{mc}\,\mathbf{p}\,\mathbf{A}(\mathbf{r} = 0)\,. \quad (51)$$

However, the Hamiltonian of the considered system can also be written as

$$\tilde{H} = \frac{1}{2m}\,\mathbf{p}^2 + U(\mathbf{r}) + \frac{1}{8\pi}\int(\mathbf{E}^2 + \mathbf{H}^2)\,\mathrm{d}V - e\mathbf{r}\mathbf{E}_{\perp} + \ldots\,. \quad (52)$$

In the dipole approximation, the interaction operator is given by

$$\tilde{H}_{\mathrm{int}} = -e\mathbf{r}\mathbf{E}\,. \quad (53)$$

Within the dipole approximation, i.e., when

$$ka \ll 1\,, \quad (54)$$

where k is the wave number of the electromagnetic field and a is a typical spatial scale of electron motion, the Hamiltonian (51) can be transformed to the Hamiltonian with an interaction operator in the form of Eqn (53) by means of a canonical transformation found by Göppert-Mayer [51]. Power and Zienau [111] have considered a quantum problem and found a unitary transformation S_{PZ} such that $\tilde{H} = S_{\mathrm{PZ}}^{-1} H S_{\mathrm{PZ}}$. Willis Lamb, however, has observed [113–115] that the interaction Hamiltonian in the form of Eqn (48) provides a much higher accuracy of quantitative analysis of experimental spectra. Thus, one faces a paradox of physical nonequivalence of H_{int} and $\tilde{H}_{\mathrm{int}}$, suggesting that the gauge with the Hamiltonian with an interaction operator (48) is preferable.

The paradox can be resolved [112] by consistently applying the quantum treatment to both an atom or molecule and the electromagnetic field. To ensure correct calculation of the matrix elements defining the relevant transition probabilities, Hamiltonian transformation $\tilde{H} = S^{-1}HS$ in such a treatment should be performed, in agreement with the general rules of unitary transformations in quantum mechanics, jointly with the pertinent transformation of the state vector $|\psi\rangle$ of the 'atom (molecule) + field' system, $|\tilde{\psi}\rangle = S^{-1}|\psi\rangle$. It is the vortex part of the $|\tilde{\psi}\rangle$ state that accurately removes the time dependence of the initial state of the problem, restoring the correct form of the stationary Coulomb field, identical to the Coulomb field of the initial state prior to the unitary transformation.

Within the applicability limits of the dipole approximation, the $|\tilde{\psi}\rangle = S^{-1}|\psi\rangle$ transformation does not give rise to a dramatic change in the wave function of the system. In this approximation, calculations performed with the interaction Hamiltonian (48) and the initial state $\psi_0(\mathbf{r}) = (\pi a^3)^{-1/2}\exp(-r/a)$ lead to a photoionization rate with an exponential in the form of Eqn (10), whose value at the stationary-phase point (9) is gauge-invariant [25].

We consider now the question regarding the long-wavelength boundary of the applicability of the dipole approximation [97, 98]. As the frequency of the driver field decreases, effects related to the magnetic component of the optical field start to play a noticeable role at lower field intensities. In the presence of the magnetic field $\mathbf{H}$, electrons, when viewed in an appropriate frame of reference, tend to move along signature figure-of-eight trajectories (Fig. 6a) with characteristic amplitudes ξ_E and ξ_H of oscillations along the electric field $\mathbf{E}$ and along the normal to this field. Broadly discussed in the literature is the question as to whether the dipole approximation and, hence, the Keldysh photoionization theory are applicable for magnetic fields H_0 inducing electron oscillations along the normal to the electric field with an amplitude ξ_H comparable with the Bohr radius a_0. This requirement on the magnetic field is usually expressed as $\beta_0 \approx U_{\mathrm{p}}/(2mc\omega)$. The intensity of the driver field I_H needed to fulfill this requirement scales as ω^3 with the driver frequency, growing faster as a function of the driver

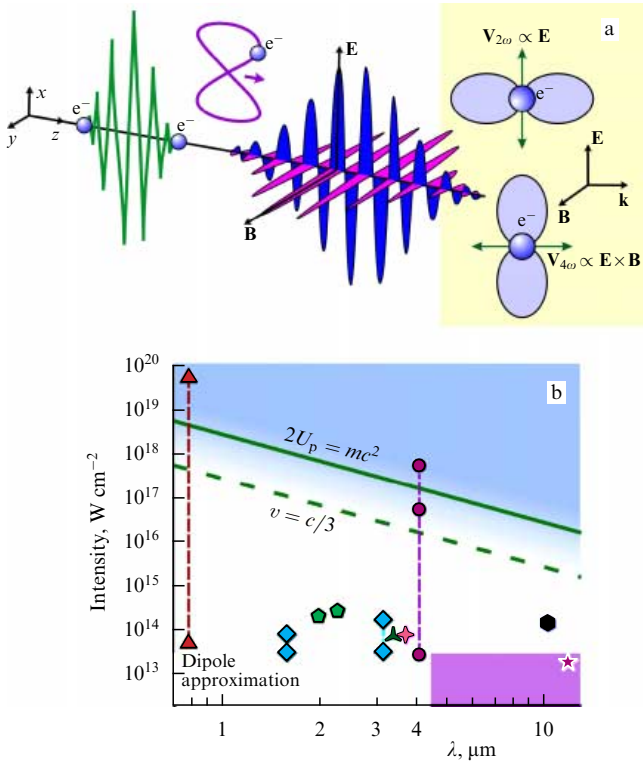

Figure 6. (Color online.) (a) Electron in the field of intense electromagnetic radiation. (b) The long-wavelength boundary of the dipole approximation on the intensity–wavelength plane. The solid line corresponds to $2U_p = mc^2$. Along the dashed line, the field of the electromagnetic wave accelerates electrons up to the velocity $v = c/3$. Also shown are the existing laser sources of high-intensity ultrashort pulses: (▲) titanium sapphire laser systems, (◆) [106], (⬟) [101], (⮝) [103], (✦) [100], (●) [105, 107], (⬢) [99], (★) [104, 109, 110].

frequency than the field frequency $I_{\rm rel}$ required to accelerate electrons to relativistic velocities, $I_{\rm rel} \propto \omega^2$. Viewing the problem from this perspective, one has to conclude that, in the long-wavelength range, the quasistatic tunneling regime, predicted by the Keldysh theory, is possible only within a very limited parameter space or is not possible at all.

Questioning these aspects of laser-induced ionization is indeed timely [97, 98], as high-power laser sources of ultrashort pulses in the mid-infrared developed in the past few years [100–102, 104–110] provide an access to the pertinent parameter space where such unusual regimes of laser–matter interactions can be studied as a function of the driver wavelength (Fig. 6b). With these emerging laser technologies in mind, we will examine in greater detail the condition $\beta_0 \approx a_0$ and its significance for the applicability of the dipole approximation and the feasibility of the quasistationary tunneling regime as predicted by the Keldysh theory.

To this end, we use the following estimate on the ratio ξ_H/ξ_E of electron oscillation amplitudes in the presence of electric and magnetic fields:

$$\frac{\xi_H}{\xi_E} \approx \frac{eE}{m\omega c}\,. \tag{55}$$

This estimate leads us to a natural result: $\xi_H/\xi_E \approx v_E/c$, where $v_E = eE/(m\omega)$.

Now, setting $\xi_H \approx a_0$, we find that the magnetic-dipole term of the multipolar expansion of the interaction Hamiltonian is still much smaller than the electric-dipole term for all the wavelengths $\lambda \gg 8\pi a_0$. Notably, except for a numerical factor, this inequality is no different from the condition of Eqn (54), defining the short-wavelength boundary of the dipole approximation.

The magnetic-dipole term in the multipolar expansion of the interaction Hamiltonian remains small compared to the electric-dipole term as long as $v_E \ll c$. Since $v_E/c \approx \gamma^{-1}(v_{\rm K}/c)$, where $v_{\rm K} = (2I_0/m)^{1/2}$, this condition is equivalent to

$$\gamma \ll \alpha\,, \tag{56}$$

where $\alpha \approx 1/137$ is a fine-structure constant.

The condition of Eqn (56), however, does not necessarily imply the existence of a low-frequency boundary for the applicability of the Keldysh photoionization theory. Indeed, when the condition of Eqn (56) is satisfied, electrons are accelerated up to relativistic speeds within a typical time $\tau_{\rm rel}$ on the order of a quarter of the field cycle, $\tau_{\rm rel} \sim T_0/4$. However, photoionization in this regime, as shown in Sections 4–6 of this review, occurs within a typical time of $\gamma T_0/(2\pi)$. Since the condition of Eqn (56) is assumed to be satisfied, i.e., $\gamma \ll \alpha \ll 1$, we have $\gamma T_0/(2\pi) \ll \tau_{\rm rel}$. Thus, photoionization occurs within an interval of time that is too short for an electron to acquire a relativistic velocity. Thus, inequality (56) does not necessarily imply a limitation on the applicability of the Keldysh theory. An illuminating, in-depth discussion of photoionization in the relativistic regime and methodological questions related to the gauge choice can be found in Refs [24, 116–128].

Recent experimental studies [105, 107, 129–131] reveal unusual properties of the ultrafast nonlinear-optical response of materials in the mid-infrared. However, a satisfactory explanation of these results can be found within the framework of the dipole approximation and Keldysh photoionization theory, perhaps, extended to include the subcycle dynamics of photoionization. These questions will be discussed in the next section of this review.

8. Subcycle dynamics of photoionization and new regimes of nonlinear optics

Analysis of the ultrafast electron dynamics behind photoionization, resolved on a time scale faster than the cycle of the driver field, gives a key to understand a broad class of unusual nonlinear-optical phenomena observed in experiments with ultrashort laser pulses [5, 11, 132–135]. The properties of the nonlinear-optical response become especially intriguing and complex when mid-infrared ultrashort laser pulses are used in laser–matter interaction experiments [100, 101, 136]. The dipole approximation remains valid for the description of the nonlinear-optical response of matter and nonlinear-optical properties of materials in such studies within the range limited by Eqns (54) and (56). In the weak-field regime, the polarization induced in the medium can be expanded as a perturbative power-series expansion [137]. The coefficients of such an expansion define nonlinear-optical susceptibilities, which are usually calculated by summing over the states of the discrete spectrum of the system. In fact, it is this approximation, limiting summation to the discrete states of the system, that often becomes insufficient, as recent experiments show, for an accurate description of the nonlinear-optical response of matter to high-intensity fields in the mid- and long-wavelength-infrared ranges [138].

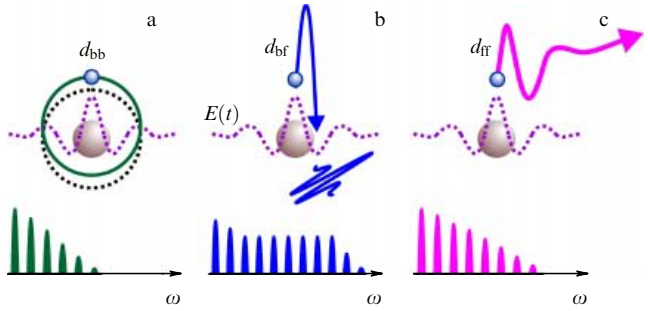

Figure 7. (Color online.) Optical nonlinearity due to the dipole moment related to bound–bound (a), bound–free (b), and free–free (c) electron transitions.

To examine this question, it is convenient to write the wave function of an optical electron as a sum $\psi(\mathbf{r}, t) = \psi_b(\mathbf{r}, t) + \psi_f(\mathbf{r}, t)$ of two terms, $\psi_b(\mathbf{r}, t)$ and $\psi_f(\mathbf{r}, t)$, representing negative- and positive-energy parts of the wave function, respectively. Negative energies correspond to bound electron states. Positive energies, on the other hand, correspond to an infinite motion of an electron. Such states are often referred to as free states, although the wave function $\psi_f(\mathbf{r}, t)$ is certainly different from the wave function of a free electron in the absence of any potential.

The longitudinal component of the dipole moment is then given by a sum of three terms (Fig. 7), $d_z(t) = d_{bb}(t) + d_{ff}(t) + d_{bf}(t)$, which isolate the contributions of bound–bound ($d_{bb}(t)$), free–free ($d_{ff}(t)$), and bound–free ($d_{bf}(t)$) electron transitions, respectively. In the presence of an external mid- or long-wavelength-infrared driver field, the dynamics of these three components of the dipole moment is strikingly different.

In Figs 8 and 9, we present typical radiation spectra and the time dynamics of radiation amplitudes $a_{bb,ff,bf} \propto \partial^2 d_{bb,ff,bf}/\partial t^2$ related to different components of the dipole moment as predicted by the numerical solution of the time-dependent Schrödinger equation for a hydrogen atom. The shape of the radiation spectrum related to the dipole moment d_{bb} is typical of the weak-field, perturbative regime within the entire range of field intensities I_0 and wavelengths λ_0 studied in calculations in Fig. 8. The intensity of low-order harmonics in the spectrum of d_{bb} rapidly decays as a function of the harmonic order (Fig. 7a), indicating that the nonlinear response related to this component of the dipole moment can be accurately described within the framework of perturbation theory, in terms of power-series expansion of the nonlinear polarization in the driver field.

Within the same range of I_0 and λ_0, the spectrum of radiation related to bound–free transitions (the d_{bf} component of the dipole moment) displays an extended plateau (Figs 7b, 8e), which can span over hundreds of harmonics and within which the harmonic intensity remains almost constant. These features in harmonic spectra clearly indicate the nonperturbative character of the nonlinear-optical response. The cutoff of the plateau in harmonic spectra, as shown by Corkum in his seminal work [139], is determined by the ionization potential and the kinetic energy acquired by an electron driven by an external field by the instant of recollision with the parent ion (Figs 7b, 9). This regime of interaction of high-intensity ultrashort pulses with matter is broadly used for the generation of attosecond pulses and

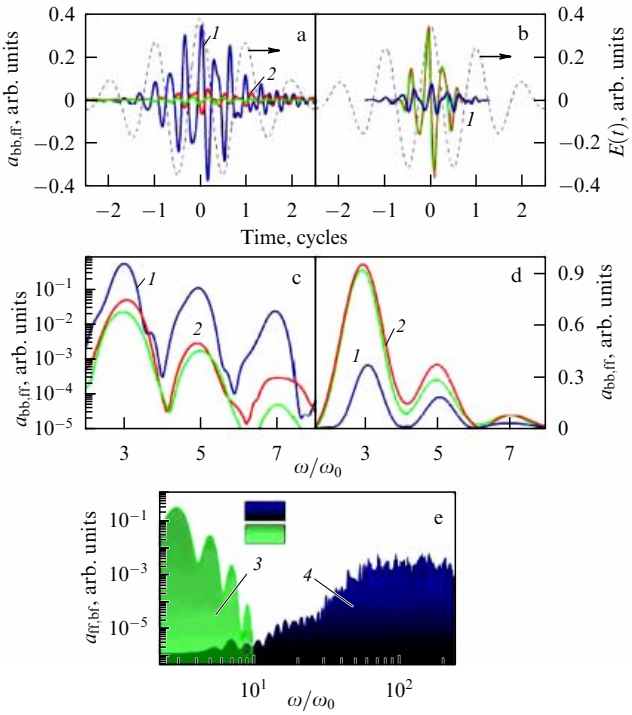

Figure 8. (Color online.) Temporal dynamics (a, b) and spectra (c, d) of radiation amplitudes a_{bb} (blue line *1*) and a_{ff} (red line *2*) for a laser driver (shown by the dashed line) with a field intensity of 110 TW cm^{-2}, a pulse width of $10/\omega_0$, and a central wavelength of 0.8 μm (a, c) and 4.0 μm (b, d). Results of calculations using the semiclassical model are given with a green line. (e) The spectra of a_{ff} (green *3*) and a_{bf} (blue *4*) for a laser driver pulse with a field intensity of 110 TW cm^{-2}, a pulse width of $10/\omega_0$, and a central wavelength of 4.0 μm.

attosecond metrology of ultrafast processes in matter (see Fig. 9) [11, 120].

The properties of the nonlinear-optical response due to free–free electron transitions are strikingly different. For low field intensities I_0 and short wavelengths λ_0, the radiation amplitude a_{ff}, related to free–free transitions, is at least one to two orders of magnitude lower than the a_{bb} amplitude (see Fig. 8). However, as the field intensity I_0 and the wavelength λ_0 increase, the ratio of the a_{ff} and a_{bb} amplitudes radically changes. For high-intensity fields in the mid-infrared range, free–free transitions, as can be seen in Fig. 8, tend to dominate over bound–bound transitions, emitting much more intense optical harmonics.

To understand the physics behind the enhancement of the nonlinear-optical response of free–free electron transitions to low-frequency fields, it is instructive to examine the behavior of the population of continuum states $\rho_f(t) = \int_V |\psi_f(\mathbf{r}, t)|^2 \, d\mathbf{r}$. For low field intensities I_0 and short driver wavelengths λ_0, the electron wave function is strongly localized near the atomic core. The continuum population in this regime displays oscillations, following, as shown in Fig. 9a, the cycles of the driver field. Such oscillations in $\rho_f(t)$ indicate that most of the electrons that undergo ionization within one field half-cycle tend to return to the atomic core, recombining into bound states, within the next field half-cycle (see Figs 8 and 9). Trajectories of such electrons calculated by numerically solving the time-dependent Schrödinger equation [138] are presented in Fig. 9a. In this regime, the continuum population at any moment of time is low compared to bound-state populations, defined by the expansion coeffi-

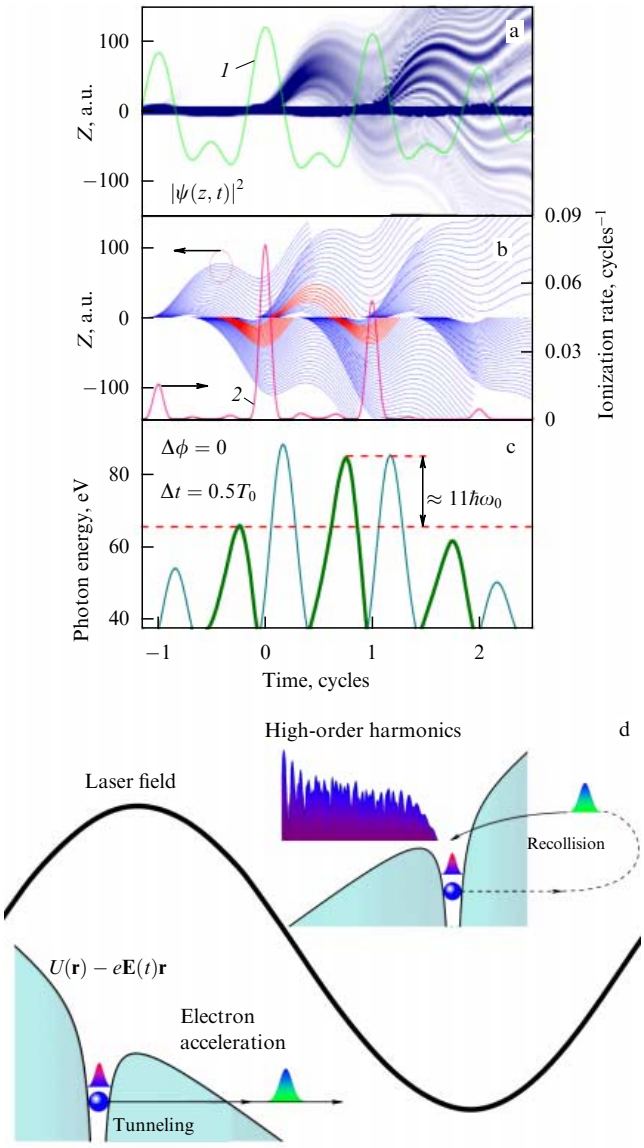

Figure 9. (Color online.) (a–c) Short-wavelength radiation from photoelectrons in the field of a high-intensity ultrashort two-color laser pulse (green line *1*): (a) photoelectron trajectories found by solving the time-dependent Schrödinger equation, (b) photoelectron trajectories found by solving classical equations of motion, along with the related photoionization rate (red line *2*), (c) energy of radiation emitted by the photoelectrons; $\Delta\phi$, phase shift between the driver field and its second harmonic; Δt, delay time of the second-harmonic pulse relative to the driver pulse. (d) High-order optical harmonic generation by photoelectrons in the Corkum model. A high-intensity ultrashort laser pulse induces photoionization of an atom, giving rise to photoelectrons driven by the laser field. Some of these photoelectrons return to the parent ion, generating optical harmonics as they undergo rescattering by the ion.

cients $|\alpha_{n,l}(t)|^2$ of the wave function

$$\psi_{\mathrm{b}}(\mathbf{r},t) = \sum_{n=1}^{N}\sum_{l=0}^{n-1}\alpha_{n,l}(t)\,\psi_{n,l}(\mathbf{r})$$

in the eigenfunctions of electron states with quantum numbers n and l.

Higher field intensities and longer wavelengths λ_0 increase the amplitude of field-driven electron motion (see Fig. 8). In the limit of classical dynamics, the amplitude of field-induced electron oscillations scales as $E_0\lambda_0^2$ with the field E_0 and the driver wavelength. Due to the quasiclassical character of electron dynamics in continuum states, this tendency, typical of classical electron dynamics, tends to show up in quantum electron dynamics as well. In an external field of a higher intensity and longer wavelength, the electron wave function is no longer tightly localized near the atomic core. Instead, it is distributed in an extended area. The energy acquired by electrons accelerated by the external field increases with the growth in the field intensity and the wavelength of the driver field (scaling as $I_0\lambda_0^2$ in the classical limit). In this regime, the intensity of low-order harmonics emitted by the d_{ff} component of the dipole moment becomes much higher than the intensity of low-order harmonics emitted through bound–bound electron transitions (Fig. 8e). Thus, the time-resolved analysis of subcycle electron dynamics of photoionization offers important insights into a broad class of unusual nonlinear-optical phenomena observed in the field of high-intensity ultrashort pulses in the mid- and long-wavelength-infrared ranges.

9. Detection of electron tunneling dynamics

Photoionization is one of the key fundamental processes in laser–matter interactions. Photoelectrons generated as a result of laser-induced ionization on an extremely short time scale launch cascades of diversified, complicated, strongly coupled phenomena in physical, chemical, and biological systems (Figs 10a, b). While the methods for studying these secondary, much slower processes are well developed, methodology and instrumentation for the investigation of ultrafast processes underlying photoionization, including, in the first place, subfemtosecond laser-induced electron tunneling dynamics, are still in their infancy [140].

Rapidly progressing methods of attosecond metrology of ultrafast processes offer means for a direct time-resolved detection of the photoelectron yield [85, 87]. This constantly progressing methodology provides unique information on laser tunneling, helping understand the fundamental physical properties of electron tunneling in the field of high-intensity laser pulses and providing means to employ the photoelectron yield of laser-induced tunneling for the investigation of molecular dynamics with an unprecedented time resolution. The recently developed method of two-channel detection of tunneling photoelectrons [87] enables a parallel measurement of photoelectron currents induced by two adjacent half-cycles of the laser field, offering a unique tool for the investigation of ultrafast dynamics of atoms and molecules (see Fig. 5). Recent experiments demonstrate that this stereo-ATI technique can be successfully combined with fiber sources of single-cycle light pulses [91].

As a natural limitation, however, methods of attosecond spectroscopy and metrology based on direct photoelectron-current detection are difficult to apply for time-resolved studies of ultrafast photoionization processes in the bulk of solids and liquid-phase media. In view of the widespread use of optical methods for the microscopy of biological systems [141–147] and a rapid progress in optical methods of brain research and neurostimulation [148–158], the demand for all-optical methods for photoionization detection in biological systems is constantly growing. Even for electron densities well below the levels creating a risk of optical breakdown, photoionization in biological systems, as a thresholdless process, gives rise to photoelectrons [159–161], some of which become solvated (Fig. 10a) and produce reactive

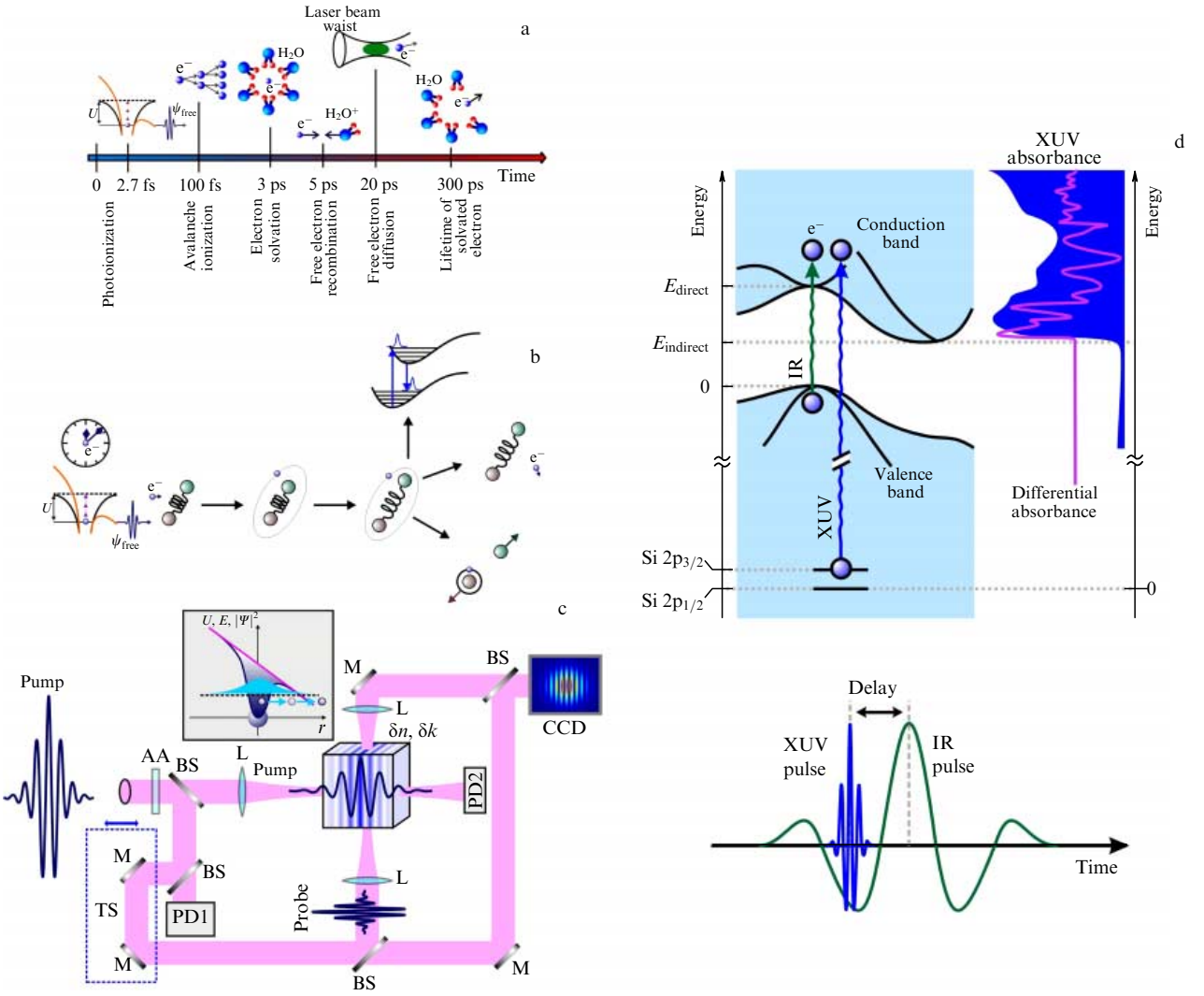

Figure 10. (Color online.) Cascades of photoionization-triggered processes in a liquid phase and biological systems involving photoelectrons, giving rise to solvated electrons (a) and reactive oxygen species (b). (c) Optical detection of ultrafast photoionization in a solid: PD, photodiode; M, mirrors; BS, beam splitters; TS, translation stage; L, lenses; AA, adjustable attenuator. (d) Time-resolved spectroscopy of attosecond electron dynamics in a semiconductor using an ultrashort laser pulse and attosecond XUV pulse [168].

oxygen species (Fig. 10b), causing a death of cells and producing a background signal in optical microscopy and fiber-based detection systems.

All-optical methods for the detection of ultrafast laser-induced ionization (Figs 10c, d) open ways to address these problems. As one of the most promising approaches, nonlinear-optical methods based on optical harmonic generation and multiwave mixing using nano- and picosecond pulses [13, 162–165], as well as cutting-edge femto- [166, 167] and attosecond [168] field waveforms (Figs 10c, d), offer unique tools for the detection of ultrafast photoionization.

Rapidly progressing laser technologies and new methods of characterization of nonlinear-optical signals arising as a result of interaction of optical fields with an ionizing system give rise to novel methods of ultrafast ionization detection in gases [11, 16, 135], solids [17, 169–172], and biological systems [173] (Figs 10c, d). Unique information on subfemtosecond photoionization dynamics can be retrieved from the spectra of optical harmonics [16, 17]. A careful analysis of such spectra enables an all-optical detection of ultrafast ionization phenomena in the gas and condensed phases [17, 169–172]. A small fraction of an optical cycle serves as a subfemtosecond probe in such an experimental scheme, inducing ultrafast electron tunneling (Fig. 10c). The temporal profile of the electron density, rapidly building up near the peak of the field, displays steep steps locked to half-cycles of the laser field. Quantitative information on photoionization dynamics can now be retrieved from the spectra of optical harmonics, viewed as the Fourier transform of the temporal profile of the electron density [17]. Central to this method of photoionization detection is a detailed understanding of the spatiotemporal dynamics of an ultrashort laser pulse in an ionizing medium [174].

Figure 11a presents the results of calculations performed with the use of the Yudin–Ivanov model of tunneling ionization [175]. The solid line in this figure shows a temporal profile of the absolute value of the correction to the refractive index $|\Delta n_p|$ induced by free-electron generation by an ultrashort light pulse with an intensity of 8.5×10^{14} W cm^{-2}, providing the tunneling regime of photoionization. Since the rate of tunneling ionization reaches its maximum values near the peaks of the instantaneous field intensity (shown by the

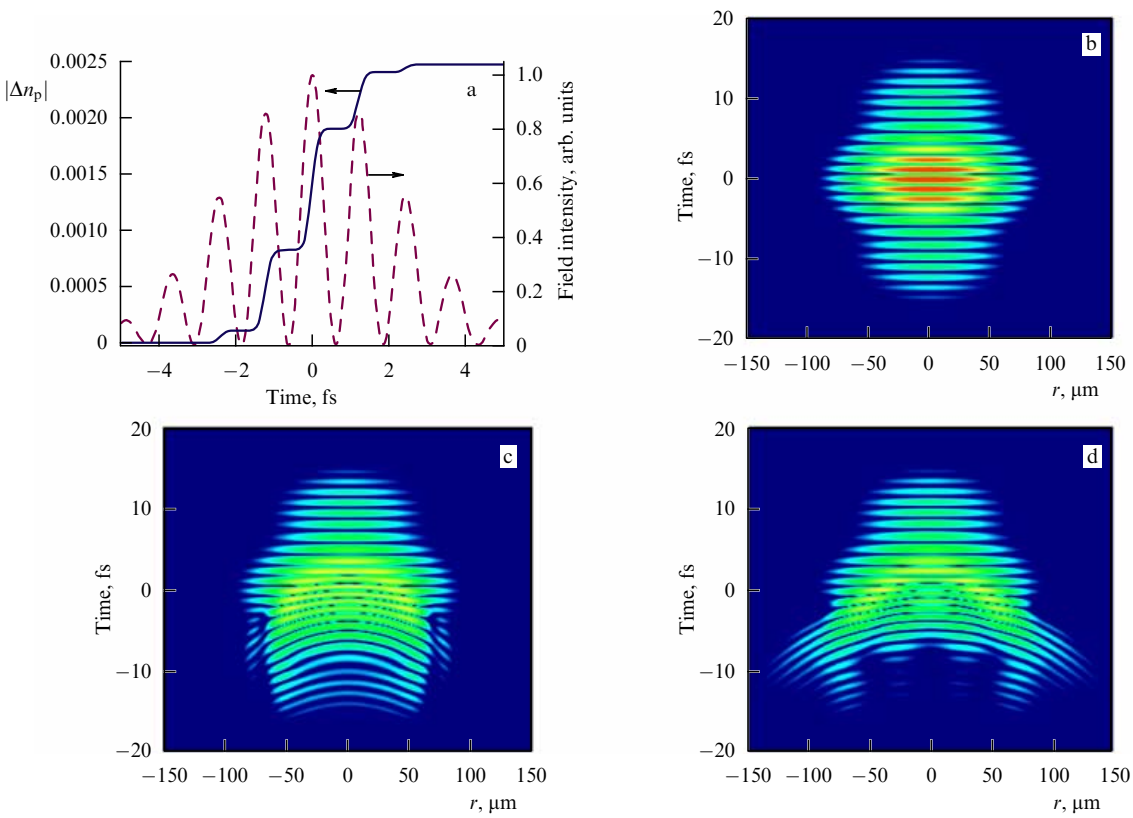

Figure 11. (Color online.) (a) Dynamics of ionization of neon by a few-cycle laser pulse: temporal profiles of the absolute value of the correction to the refractive index induced by free-electron generation (solid line) and field intensity (dashed line). The peak intensity of the light field is 8.5×10^{14} W cm^{-2}. The pressure of neon is 1 atm. (b–d) Spatiotemporal maps of a few-cycle light pulse in a gas medium (neon at a pressure of 20 bar) undergoing photoionization: (b) at a distance of 1.5 mm before the focus, (c) in the focus, and (d) at a distance of 1.5 mm behind the focus.

dashed line in Fig. 11a), the temporal profile of the free-electron density and the related correction Δn_p to the refractive index display well-pronounced steps (visible in the solid line in Fig. 11a).

Such ultrafast changes in the electron density in a gas ionized by an ultrashort pulse have been recently detected experimentally by means of mass spectrometry [85] and optical-harmonic generation [16, 17]. Each step in the temporal profile of Δn_p is locked to the related half-cycle of the laser field (Fig. 11a). A typical buildup time of the electron density within the most intense field half-cycle in Fig. 11a is estimated as approximately 0.5 fs. Such ultrafast variations in the local refractive index can be employed for high-speed switching of optical signals in fiber-optic systems [176, 177] and semiconductor waveguide microcavities [178]. Steep changes in the electron density within each field half-cycle, tightly confined to the peak of the field intensity, translate into radial-coordinate-dependent field-cycle distortions across the laser beam (Figs 11b–d). Information on such distortions and, hence, information on ultrafast ionization processes can be retrieved from the spectrum of an ultrashort laser probe [16, 17, 179, 180].

10. Keldysh formalism and a universal dispersion profile of optical nonlinearity

The Keldysh formalism for the analysis of photoionization and multiphoton absorption in solids offers important insights into the universal properties of dispersion of the nonlinear-optical response related to interband transitions in semiconductors and dielectrics [181, 182]. These properties of dispersion play an important role in the spatiotemporal dynamics of ultrashort light pulses interacting with solid-state semiconductors and dielectrics [183, 184]. The probability of M-photon absorption β_M calculated within the framework of the Keldysh formalism and its generalizations [185] is related to the imaginary part of the nonlinear-optical susceptibility $\chi^{(2M-1)}(\omega, \ldots, \omega)$. The pertinent Kramers–Krönig relation for the nonlinear-optical susceptibility [186] can be written as

$$\chi^{(n)}(\omega_1, \omega_2, \ldots, \omega_n) = \frac{1}{\mathrm{i}\pi}\,\mathrm{p.v.}\int_{-\infty}^{\infty} \frac{\chi^{(n)}(\omega_1, \omega_2, \ldots, \omega_{i-1}, \Omega, \omega_{i+1}, \ldots, \omega_n)}{\Omega - \omega_i}\,\mathrm{d}\Omega\,, \tag{57}$$

where p.v. stands for the principal-value integration by Cauchy.

As can be seen from Eqn (57), to find the real part of the nonlinear-optical susceptibility $\chi^{(2M-1)}(\omega_1, \ldots, \omega_M)$ through the Kramers–Krönig relation, we need to know the imaginary part of the frequency-nondegenerate nonlinear optical susceptibility $\chi^{(2M-1)}(\omega_1, \ldots, \omega_M)$. Causality also dictates the following Kramers–Krönig relation for the changes in the refractive index $\Delta n(\omega, \varepsilon)$ and absorption coefficient $\Delta\alpha(\omega, \varepsilon)$ caused by the same causal factor, described by the variable ε [182, 186]:

$$\Delta n(\omega, \varepsilon) = \frac{c}{\pi}\,\mathrm{p.v.}\int_0^{\infty} \frac{\Delta\alpha(\omega', \varepsilon)}{\omega'^2 - \omega^2}\,\mathrm{d}\omega'\,. \tag{58}$$

In a particular case of two-photon absorption (TPA), Eqn (58) relates the change in the refractive index $\Delta n(\omega, \Omega)$ induced at the frequency ω by a light field with a frequency Ω to the integral of the change in the absorption $\Delta\alpha(\omega, \Omega) = \beta_2(\omega, \Omega) I_\Omega$ at the frequency ω, with $\beta_2(\omega, \Omega)$ being the coefficient characterizing the probability of two-photon absorption of photons with frequencies ω and Ω and I_Ω being the intensity of the field with frequency Ω. In this case, we should take $\varepsilon = \Omega$ in Eqn (58).

The solid-state photoionization formalism leads to the following expression for the S-matrix [182]:

$$S = \frac{\mathrm{i}\pi}{\hbar} \frac{e\mathbf{a}\mathbf{p}_{\mathrm{vc}}}{mc} \sum_{k,l} J_k(\theta_1) J_l(\theta_2) \Big[A_1 \delta\big((k+1)\omega_1 + l\omega_2 + \omega_{\mathrm{vc}}\big) + A_1 \delta\big((k-1)\omega_1 + l\omega_2 + \omega_{\mathrm{vc}}\big) + A_2 \delta\big(k\omega_1 + (l+1)\omega_2 + \omega_{\mathrm{vc}}\big) + A_2 \delta\big(k\omega_1 + (l-1)\omega_2 + \omega_{\mathrm{vc}}\big) \Big], \tag{59}$$

where A_1 and A_2 are the amplitudes of the vector potentials of the fields with frequencies ω_1 and ω_2, $\mathbf{A} = \mathbf{a}[A_1 \cos(\omega_1 t) + A_2 \cos(\omega_2 t)]$, $\mathbf{a}$ is the unit polarization vector,

$$\theta_i = (m_{\mathrm{vc}} c \omega_i)^{-1} e A_i \mathbf{k}\mathbf{a}, \quad m_{\mathrm{vc}}^{-1} = m_{\mathrm{c}}^{-1} - m_{\mathrm{v}}^{-1},$$

m_{c} is the effective mass of an electron in the conduction band and m_{v} is the effective mass of a hole in the valence band, which is taken negative,

$$\mathbf{p}_{\mathrm{vc}} = \frac{\mathrm{i}}{\hbar} \int u_{\mathrm{c}}^*(\mathbf{k}, \mathbf{r}) \nabla u_{\mathrm{v}}(\mathbf{k}, \mathbf{r}) \, \mathrm{d}\mathbf{r}, \tag{60}$$

$$\hbar\omega_{\mathrm{vc}} = E_{\mathrm{g}} - \Delta E_{\mathrm{vc}} + \Delta E_{\mathrm{cv}} + \frac{\hbar^2 k^2}{2m_{\mathrm{vc}}}, \tag{61}$$

E_{g} is the band-gap width, and ΔE_{vc} and ΔE_{cv} are the quadratic Stark shifts of the valence and conduction bands.

It is straightforward to see from Eqn (59) that, even in the case of the simplest multiphoton process, viz., two-photon absorption, different frequency mixing schemes contribute to the S-matrix and need to be taken into account. In its general form, this expression includes both frequency-nondegenerate multiphoton absorption and Raman-type processes. The change in absorption $\Delta\alpha(\omega_1, \omega_2)$ due to these processes is given by [182]

$$\Delta\alpha(\omega_1, \omega_2) = \frac{2^{10}\pi}{5} \frac{e^4}{m^{1/2} c^2} \frac{E_{\mathrm{p}}^{1/2}}{n(\omega_1) n(\omega_2) E_{\mathrm{g}}^3} F_2\left(\frac{\hbar\omega_1}{E_{\mathrm{g}}}, \frac{\hbar\omega_2}{E_{\mathrm{g}}}\right) I_2, \tag{62}$$

where $E_{\mathrm{p}} = 2|\mathbf{p}_{\mathrm{vc}}|^2/m$, I_2 is the intensity of the field at the frequency ω_2, and the function $F_2(x_1, x_2)$ is

$$F_2(x_1, x_2) = \frac{(x_1 + x_2 - 1)^{3/2}}{2^7 x_1 x_2^2} \left(\frac{1}{x_1} + \frac{1}{x_2}\right)^2, \quad x_1 + x_2 \geqslant 1 \tag{63}$$

for two-photon absorption and

$$F_2(x_1, x_2) = \frac{(x_1 - x_2 - 1)^{3/2} - (x_2 - x_1 - 1)^{3/2}}{2^7 x_1 x_2^2} \left(\frac{1}{x_1} - \frac{1}{x_2}\right)^2 \tag{64}$$

for the Raman-type process.

Equation (58), jointly with Eqns (62)–(64), gives the I-intensity-dependent change in the refractive index $\Delta n = n_2 I$. The nonlinear refractive index n_2 in Δn includes both TPA and Raman-type parts. The TPA part of this coefficient is defined by the real part of the third-order nonlinear-optical susceptibility $\chi_{\mathrm{TPA}}^{(3)} = \chi^{(3)}(\omega_1, -\omega_2, \omega_2, \omega_1)$ and contributes to Δn through the transformation of Eqn. (58) performed with $\Delta\alpha(\omega_1, \omega_2)$ related to two-photon absorption. The electronic Raman part of n_2 is defined by the real part of the nonlinear-optical susceptibility $\chi_{\mathrm{Ram}}^{(3)} = \chi^{(3)}(\omega_1, \omega_2, -\omega_2, \omega_1)$ and contributes to Δn through the transformation of Eqn (58) performed with $\Delta\alpha(\omega_1, \omega_2)$ corresponding to the Raman-type process.

When used jointly with Eqn (62) for $\Delta\alpha(\omega_1, \omega_2)$, Eqn (58) dictates the following frequency dependence of the nonlinear refractive index:

$$n_2(\omega) = K \frac{E_{\mathrm{p}}^{1/2}}{n_0 E_{\mathrm{g}}^4} G_2\left(\frac{\hbar\omega}{E_{\mathrm{g}}}\right), \tag{65}$$

where

$$G_2(x) = \frac{2}{\pi} \, \mathrm{p.v.} \int_0^\infty \frac{F_2(\xi, x)}{\xi^2 - x^2} \, \mathrm{d}\xi, \tag{66}$$

and K is a material-nonspecific constant.

Equation (65) describes a universal dispersion profile of the nonlinear refractive index for a broad class of dielectric materials [182, 186] (Fig. 12a). In a typical situation of laser–semiconductor interaction, when the frequency of the laser field ω is on the order of half the minimum two-photon absorption frequency, $\omega_{\mathrm{TPA}} = E_{\mathrm{g}}/(2\hbar)$ (with the Franz–Keldysh effect neglected), that is

$$2\omega \sim \frac{E_{\mathrm{g}}}{\hbar}, \qquad \omega \ll \frac{E_{\mathrm{g}}}{\hbar}, \tag{67}$$

the nonlinear-optical susceptibility $\chi_{\mathrm{TPA}}^{(3)}$ is much larger than the $\chi_{\mathrm{Ram}}^{(3)}$ susceptibility, which does not involve any terms close to a TPA or any other resonance. In this regime, the Kerr-type optical nonlinearity of a solid is mainly determined by two-photon absorption (Fig. 12a).

When conditions of Eqn (67) are satisfied, the exact Kramers–Krönig relation can be replaced with an approximate relation [181], which is identical in its form to Eqn (58), but where the replacement

$$\Delta\alpha(\omega, \Omega) \to \beta_2\left(\frac{\omega + \Omega}{2}\right) I_\Omega \tag{68}$$

has been made. Equation (68) implies that the function $\Delta\alpha(\omega, \Omega)$ used in the exact Kramers–Krönig relation of Eqn (58) is replaced by the product $\beta_2((\omega + \Omega)/2) I_\Omega$, involving the β_2 TPA probability calculated using the Keldysh formalism or one of its generalizations and the radiation intensity at the frequency Ω. Rigorously, with such a replacement made, Eqn (58) is no longer consistent with causality [182]. To verify this, we can write the Kramers–Krönig relation for a nonlinear-optical susceptibility of the form of Eqn (57). Since $n - 1$ frequency arguments of the nonlinear susceptibility in this relation are free parameters, which can take arbitrary values within the entire spectral range where the nonlinear susceptibility is still defined, there is, clearly, no way to find a relation that would express the multiphoton-absorption probability functions $\beta_{q+1}(\omega)$, which depend on only one frequency argument, through the nonlinear refractive index $n_{2q}(\omega)$, where q is an integer.

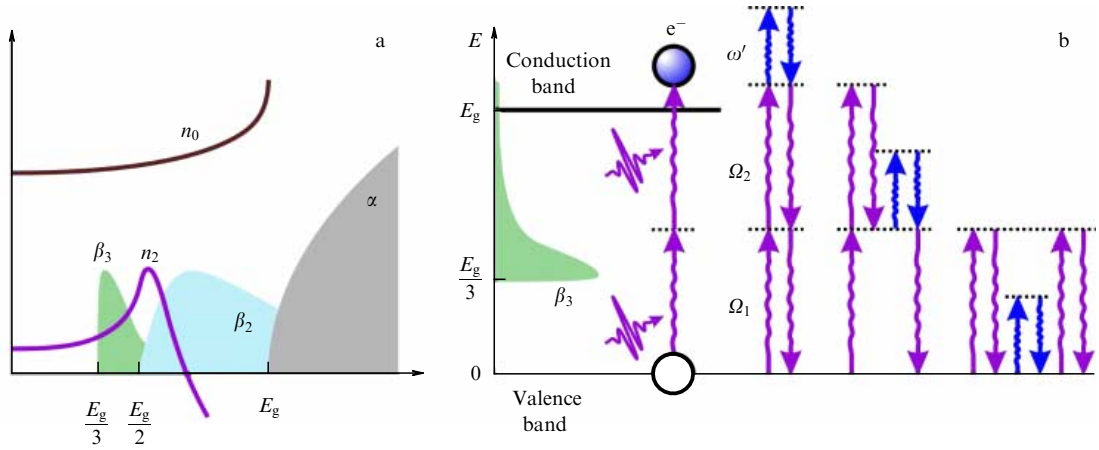

Figure 12. (Color online.) (a) Universal dispersion profiles of the absorption coefficient α, refractive index n_0, two- and three-photon absorption coefficients β_2 and β_3, and the nonlinear refractive index n_2; E_g is the band gap. (b) A two-photon absorption process related to one of the terms in the third-order nonlinear-optical susceptibility responsible for the Kerr-type nonlinearity along with a few (out of many) higher-order processes contributing to the fifth-order nonlinear-optical susceptibility.

It is also clear from this causality-based argument that, in a particular case of two-photon absorption with the conditions of Eqn (67) satisfied, the transformation of Eqn (58) with a replacement $\Delta\alpha(\omega,\Omega) \to \beta_2((\omega+\Omega)/2)I_\Omega$ can provide a reasonably accurate description of the dispersion profile of $n_2(\omega)$ for a broad class of dielectrics [181]. Predictably, the error of this approximation grows as the radiation frequency approaches the edge of the band gap [182].

However, an extension of this approximation to higher-order Kerr-type optical nonlinearities, described in terms of nonlinear coefficients n_{2q} with $q > 1$, encounters fundamental difficulties related to the causality issue as explained above. To have a better feeling of this problem, it is instructive to examine the simplest case of a higher-order Kerr effect (HOKE) and explore an attempt to use the replacement of Eqn (68) for a simplified calculation of the first HOKE term in the expansion $\Delta n = n_2 I + n_4 I^2$ of the intensity-dependent correction to the refractive index. Using Eqn (58), we can express the field-induced change in the refractive index $\Delta n(\omega,\Omega) = n_2(\omega,\Omega)I_\Omega$ through the nonlinear correction to the absorption coefficient $\Delta\alpha(\omega',\Omega)$. Then, setting $\omega = \Omega$, we find the nonlinear refractive index n_2, which is manifested in many nonlinear-optical experiments and can be measured by nonlinear-optical methods.

The HOKE coefficient n_4 meets the Kramers–Krönig relation that extends Eqn (58) to the higher-order, quadratic in the field intensity correction to the refractive index

$$\Delta n(\omega,\Omega_1,\Omega_2) = n_4(\omega,\Omega_1,\Omega_2)I_{\Omega_1}I_{\Omega_2},$$

expressing it through the pertinent field-induced absorption change

$$\Delta\alpha(\omega',\Omega_1,\Omega_2) = \beta_3(\omega',\Omega_1,\Omega_2)I_{\Omega_1}I_{\Omega_2},$$

where $\beta_3(\omega',\Omega_1,\Omega_2)$ is a coefficient that characterizes the probability of absorption of three photons with frequencies ω', Ω_1, and Ω_2. The generalized Keldysh formalism [185, 187, 188] leads to the following general expression for the coefficient β_M, characterizing the probability of M-photon absorption [185] (Fig. 12a):

$$\beta_M \propto \left(\frac{e^2}{\hbar c}\right)^M \hbar^{M-1} \frac{P^{2M-3}}{n_0^M E_g^{4M-5}} F_M\left(\frac{M\hbar\omega}{E_g}\right), \tag{69}$$

where $P \propto \hbar p_{cv}/m$, $F_M = (M\hbar\omega/E_g - 1)^{\sigma/2}(M\hbar\omega/E_g)^{4M-3}$, and $\sigma = 3$ for even M and 1 for odd M.

The full procedure of $n_4(\omega,\Omega_1,\Omega_2)$ calculation using the Kramers–Krönig relation between $\Delta n(\omega,\Omega_1,\Omega_2)$ and $\beta_3(\omega',\Omega_1,\Omega_2)I_{\Omega_1}I_{\Omega_2}$ is perfectly legitimate. Such a procedure gives an expression for $n_4(\omega,\Omega_1,\Omega_2)$, which can be used to define the nonlinear coefficient $n_4(\omega) = n_4(\omega,\omega,\omega)$ degenerate in its frequency arguments, which shows up in a broad class of nonlinear-optical experiments. We start facing fundamental difficulties with causality, however, if we attempt to further simplify this procedure by adopting a replacement

$$\Delta\alpha(\omega,\Omega_1,\Omega_2) \to \beta_3\left(\frac{\omega+\Omega_1+\Omega_2}{3}\right)I_{\Omega_1}I_{\Omega_2} \tag{70}$$

or

$$\Delta\alpha(\omega,\Omega,\Omega) \to \beta_3\left(\frac{\omega+2\Omega}{3}\right)I_\Omega^2. \tag{71}$$

With such a replacement, Δn and $\Delta\alpha$, as explained above, no longer satisfy the Kramers–Krönig relation. We encounter another serious difficulty if the frequency ω_0 of the driver field is chosen in such a way as to satisfy the conditions of Eqn (67), which is often the case in laser–semiconductor interaction experiments. Integration in the variable ω' in the Kramers–Krönig relation then probes only the tail of the three-photon absorption coefficient stretching from $2\omega_0 \sim E_g/\hbar$ to infinity (Fig. 12a). However, with the replacement of Eqn (68), this integration probes the entire frequency profile of the three-photon absorption coefficient $\beta_3(\omega)$, including its peak near $\omega \sim E_g/3\hbar$ (Fig. 12b). In its correct version, the Kramers–Krönig relation does not involve integration around this peak, as $2\omega_0 \sim E_g/\hbar > E_g/3\hbar$ (Fig. 12b). The HOKE coefficient n_4 calculated with such a replacement (unjustified from the causality standpoint) corresponds to a completely different frequency range (Fig. 12b) and is not applicable to an analysis of Kerr-nonlinearity saturation at the frequency ω_0. Because of these issues, the above-specified simplifications may result in unnecessarily inaccurate predictions for the HOKE coefficients and may even lead to n_4 values of the same sign as n_2, offering no explanation for the saturation of optical nonlinearity.

In search for a more consistent method for the analysis of higher-order optical nonlinearities, we resort to Eqn (59) for the S-matrix. We emphasize once again that, in its general form, this expression includes all the pertinent multiphoton-absorption and Raman-type nonlinear-optical processes of different orders with all possible combinations of laser frequencies (Fig. 12b). We will show now that, for each perturbative nonlinear-optical process described by a nonlinear-optical susceptibility $\chi^{(3)}$, giving rise to a Kerr-effect correction to the refractive index, we can isolate a higher-order, $\chi^{(5)}$ nonlinear-optical process that saturates the $\chi^{(3)}$-related Kerr nonlinearity.

To this end, we consider the S-matrix term that describes absorption of two photons with the frequency ω_1 ($k=-1$, $l=0$),

$$S_{-1,0}^{\mathrm{TPA}} = \frac{\mathrm{i}\pi}{\hbar}\,\frac{e\mathbf{a}\mathbf{p}_{\mathrm{vc}}}{mc}\,A_1 J_{-1}(\theta_1) J_0(\theta_2)\delta(\omega_{\mathrm{vc}} - 2\omega_1)\,. \tag{72}$$

In a weak-field regime, $\theta_{1,2} \ll 1$, this process corresponds to the $\chi^{(3)}$-related Kerr-type nonlinearity characterized by the nonlinear coefficient n_2 with a dispersion profile as described by Eqn (65). It is straightforward to see that the $k=-2$, $l=0$ term,

$$S_{-2,0}^{\mathrm{HOKE}} = \frac{\mathrm{i}\pi}{\hbar}\,\frac{e\mathbf{a}\mathbf{p}_{\mathrm{vc}}}{mc}\,A_1 J_{-2}(\theta_1) J_0(\theta_2)\delta(\omega_{\mathrm{vc}} - 3\omega_1)\,, \tag{73}$$

and the $k=-1$, $l=-1$ term,

$$S_{-1,-1}^{\mathrm{HOKE}} = \frac{\mathrm{i}\pi}{\hbar}\,\frac{e\mathbf{a}\mathbf{p}_{\mathrm{vc}}}{mc}\,A_1 J_{-1}(\theta_1) J_{-1}(\theta_2)\delta(\omega_{\mathrm{vc}} - 2\omega_1 - \omega_2)\,, \tag{74}$$

in Eqn (59) correspond to a higher-order, $\chi^{(5)}$ nonlinear susceptibility, giving rise to a higher-order Kerr effect.

Since the field is assumed to be weak in this consideration, $\theta_{1,2} \ll 1$, we have $J_n(x) \approx x^n/(2^n n!)$. Then, using the identity $J_{-n}(x) = (-1)^n J_n(x)$, we find that each of the terms (73) and (74) gives rise to a quadratic in the field intensity nonlinearity with n_4 whose sign is opposite to the sign of the n_2 coefficient. Thus, for each n_2 Kerr-nonlinearity term in the expression for the S-matrix, we can always isolate the terms corresponding to a higher-order, quadratic in the field intensity optical nonlinearity that saturate the n_2 nonlinearity.

In the weak-field regime, $\theta_{1,2} \ll 1$, Eqns (73) and (74) give

$$\zeta = \frac{|S_{-2,0}^{\mathrm{HOKE}}|^2}{|S_{-1,0}^{\mathrm{TPA}}|^2} \approx \eta I\,, \tag{75}$$

where

$$\eta \approx \frac{16\pi e^2}{mc\hbar^2 n_0}\,\frac{E_{\mathrm{g}}}{\omega^4}\left|\frac{3\hbar\omega}{E_{\mathrm{g}}} - 1\right| \tag{76}$$

is an order-of-magnitude estimate for the ratio of the $\chi^{(5)}$ nonlinearity to the $\chi^{(3)}$ Kerr-type nonlinearity.

Notably, the maximum of η is achieved at $\omega_{\mathrm{m}} \approx 4E_{\mathrm{g}}/(9\hbar)$. This point makes the dominant contribution to the sum in k in Eqn (59). When the laser frequency is roughly half the band-gap frequency, $2\hbar\omega \approx E_{\mathrm{g}}$ — a relation typical of laser–semiconductor interaction experiments — the frequency ω is close to ω_{m}. Equation (76) then leads to

$$\eta \approx \frac{128\pi e^2\hbar^2}{mcn_0}\,\frac{1}{E_{\mathrm{g}}^3}\,. \tag{77}$$

The saturation intensity can then be estimated from $\zeta \approx 1$ as

$$I_{\mathrm{s}} \propto \frac{mcn_0}{e^2\hbar^2}\,E_{\mathrm{g}}^3\,. \tag{78}$$

It is instructive to compare Eqn (78) with an estimate on the saturation intensity for the TPA coefficient that can be found from Eqn (69),

$$I_{\mathrm{s}}' \propto \frac{n_0 c E_{\mathrm{g}}^4}{e^2 P^2}\,, \tag{79}$$

where $P \approx p_{\mathrm{cv}}\hbar/m$.

With $m_{\mathrm{vc}} \sim m$ and, hence, $p_{\mathrm{cv}}^2 = E_{\mathrm{g}} m/2$, we find from Eqn (79)

$$I_{\mathrm{s}}' \propto \frac{2n_0 cm}{e^2\hbar^2}\,E_{\mathrm{g}}^3\,, \tag{80}$$

which fully agrees with Eqn (78) for I_{s}.

In the opposite limiting case of $\omega \ll E_{\mathrm{g}}/\hbar$, which is typical of the interaction of laser radiation in the visible, near-, and mid-infrared ranges with wide-gap dielectrics, Eqn (76) yields

$$\eta \approx \frac{16\pi e^2}{mc\hbar^2 n_0}\,\frac{E_{\mathrm{g}}}{\omega^4}\,. \tag{81}$$

In this regime, the saturation intensity is estimated as

$$I_{\mathrm{s}} \propto \frac{mc\hbar^2 n_0}{e^2}\,\frac{\omega^4}{E_{\mathrm{g}}}\,. \tag{82}$$

The saturation intensity defined by Eqn (82) exhibits an ω^4 scaling, which is archetypical of nonresonant light scattering. Such a scaling offers an important insight into the enhancement of higher-order nonlinear-optical effects observed in the interaction of mid-infrared radiation with wide-band dielectrics. It is instructive to compare the ratio of η estimates for two characteristic laser wavelengths — $\lambda_1 \approx 0.8$ μm and $\lambda_2 \approx 4$ μm. The former is chosen as a typical wavelength of titanium sapphire lasers, widely used in ultrafast optics. The latter wavelength, on the other hand, is a typical wavelength of recently developed sources of mid-infrared radiation based on optical parametric chirped-pulse amplification. Due to a unique combination of the output wavelength, a high peak power, and a short output pulse width, such sources help reveal new regimes of nonlinear-optical interactions. Using Eqn (82), we find $\eta(\lambda_2)/\eta(\lambda_1) \approx 625$. Thus, in experiments performed in the mid-infrared range, e.g., at $\lambda_2 \approx 4$ μm, much stronger higher-order nonlinear-optical effects should be expected. This tendency is clearly observed in experiments on soliton self-compression and laser-induced filamentation of ultrashort high-peak-power mid-infrared pulses propagating in wide-gap dielectrics [189–192]. Experiments of this class are discussed in Section 15 of this review.

11. Photoelectric effect in an intense laser field and attosecond pulses of electron current

The discovery of the photoelectric effect [48, 49] is one of the milestone achievements of natural sciences in the 19th century [50]. The photoelectric effect is widely used in present-day experiments as a powerful spectroscopic technique and a

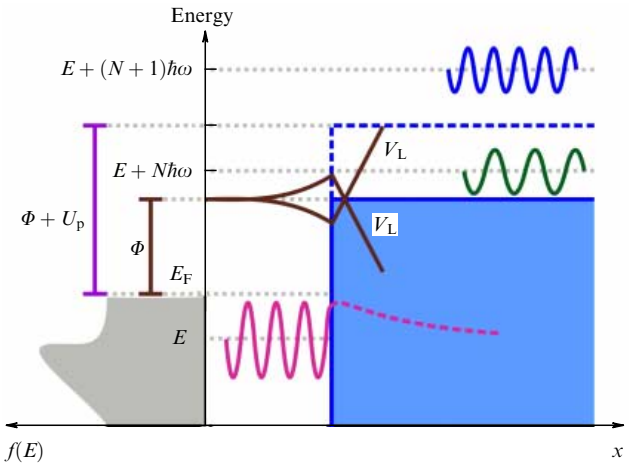

Figure 13. (Color online.) The photoelectric effect in the field of a high-intensity ultrashort laser pulse: E_F, electron Fermi energy in the conduction band of a metal; Φ, work function; U_p, electron pondermotive energy; $f(E)$, electron density of states in the metal; and V_L, potential induced by the laser field.

method for the detection of electromagnetic radiation, providing a principle of operation for a vast arsenal of physical measuring instruments. When combined with cutting-edge laser sources of ultrashort pulses, the photoelectric effect enables new methods of time-resolved studies of ultrafast processes in matter [193, 194]. The photoelectric effect is at the heart of the rapidly growing area of time-resolved structure analysis of complex molecular systems with ultrashort photoelectron pulses [195–199]. One of the promising directions of attosecond technologies involves time-resolved photoelectron spectroscopy and microscopy for the investigation of ultrafast electron dynamics and attosecond tomography of wave functions in atoms and molecules [199]. Local field enhancement provided by metal nanostructures helps observe new regimes of the photoelectric effect accompanied by enhanced nonlinear-optical interactions [200, 201 (Fig. 13).

We consider a generic experimental arrangement with a metal tip irradiated by an intense few-cycle laser pulse. A bias voltage U is applied to the metal tip to induce a tunneling current through a gap between the tip and a sample in a standard tunneling or atomic-force microscopy scheme. With image charge effects included in accordance with the Fowler–Nordheim treatment (see Section 2.2), the density of the tunneling electron current is given by

$$j = \frac{e^3 F^2}{16\pi^2 \hbar \Phi \theta^2(\xi)} \exp\left[-\frac{4(2m)^{1/2}\Phi^{3/2} v(\xi)}{3\hbar e F}\right], \tag{83}$$

where e and m are the electron charge and mass, F is the electric field across the tip–sample gap, Φ is the work function (see Fig. 13), $\theta(\xi)$ and $v(\xi)$ are the Nordheim elliptical functions of $\xi = e^{3/2}\Phi^{-1}(F/4\pi)^{1/2}$.

We represent the electric field in Eqn (83) as a sum

$$F(t) = E_0 + \tilde{E}(t), \tag{84}$$

where E_0 is the dc component related to the bias voltage U and $\tilde{E}(t) = E(t)\exp(-\mathrm{i}\omega t) + \text{c.c.}$ is the ac field of the laser pulse, $E(t) = \mathbf{E}(t)\mathbf{n}$, $\mathbf{E}(t)$ is the field envelope, $\mathbf{n}$ is the unit vector along the normal to the metal surface, and ω is the carrier frequency of the laser field.

In the case of an ideally periodic laser field, the current density given by Eqn (83) is also periodic. The Fourier-series expansion of this function yields

$$j(t) = \sum_n j_n \exp(\mathrm{i}n\omega t), \tag{85}$$

where j_n is the amplitude of the nth Fourier harmonic.

The harmonic modulation of the tunneling current translates into the harmonics in the spectrum of a laser pulse interacting with the metal tip. Since the function $j(t)$ is a periodic function whose period is defined by the field cycle $T_0 = 2\pi/\omega$, the current density j and, hence, the spectrum of the optical field transmitted through the tip–sample gap feature both odd- and even-order harmonics of ω. This is in stark contrast with the case of optical harmonic generation in a gas medium, where the tunneling ionization rate is controlled by the field intensity, rather than the field itself. Physically, this important difference in the spectra of optical harmonics is due to the symmetry of field–target interaction geometry. In a gas medium, the interaction of the light field with a gas target is centrosymmetric, suppressing even-order harmonics. When a light field interacts with a metal tip, however, the central symmetry is broken, lifting the prohibition on even-harmonic generation.

For a typical laser intensity of 0.1 MW cm^{-2} used to illuminate a gold tip ($\Phi \approx 5$ eV) with a bias field $E_0 \approx 1$ kV μm$^{-1} \approx 10^7$ V cm^{-1}, we find $\kappa = 4(2m)^{1/2}\Phi^{3/2} v(\xi_0)(3\hbar e E_0)^{-1} \approx 70$, with $\xi_0 = \xi(E=0)$. Thus, the ratio $\kappa E/E_0 \ll 1$ is a small parameter. We can therefore us a power-series expansion in this parameter in Eqn (83) to find for a laser field $\tilde{E}(t) = E(t)\cos(\omega t)$

$$j = \frac{e^3 E_0^2}{16\pi^2 \hbar \Phi \theta^2(\xi_0)} \exp(-\kappa)\left[1 - \frac{\kappa E}{E_0}\cos(\omega t) + \frac{1}{2}\left(\frac{\kappa E}{E_0}\right)^2 \cos^2(\omega t) - \frac{1}{6}\left(\frac{\kappa E}{E_0}\right)^3 \cos^3(\omega t) + \ldots\right]. \tag{86}$$

As can be seen from Eqn (86), the amplitude of the second-harmonic response scales as E^2 with the amplitude of the laser field. Since $E = \mathbf{E}\mathbf{n}$, the $I_{SH} \propto I^2$ scaling of the second-harmonic intensity translates into the $I_{SH} \propto \cos^4\alpha$ dependence of the second-harmonic intensity on the angle α between the polarization vector of the laser field and the normal to the metal surface, which agrees well with experiments [201].

We will now demonstrate that an ultrafast modulation of the current of photoelectrons tunneling from a metal nanostructure induced by an ultrashort light pulse provides a means to generate attosecond electron pulses. To this end, we use Eqn (83) with $|E_0| \ll |E|$ and $\tilde{E}(t) = E(t)\cos(\omega t)$ to derive the following equation for the photoelectron pulse width at the $1/e$ level:

$$\cos(\omega\tau_{el}) = \frac{1}{1+\delta}, \tag{87}$$

where $\delta = (3/4)\hbar e(2m)^{-1/2}\Phi^{-3/2}[v(\bar{\xi})]^{-1} f E$, $\bar{\xi} = \xi(t=0)$, and f is the local field enhancement factor provided by the metal nanostructure.

Under typical experimental conditions, a laser field on the order of 10^4 V cm^{-1} induces a sufficiently strong photoelectron current from a metal tip (in excess of 10^6 electrons per second for a laser pulse repetition rate of 80 MHz) and is still

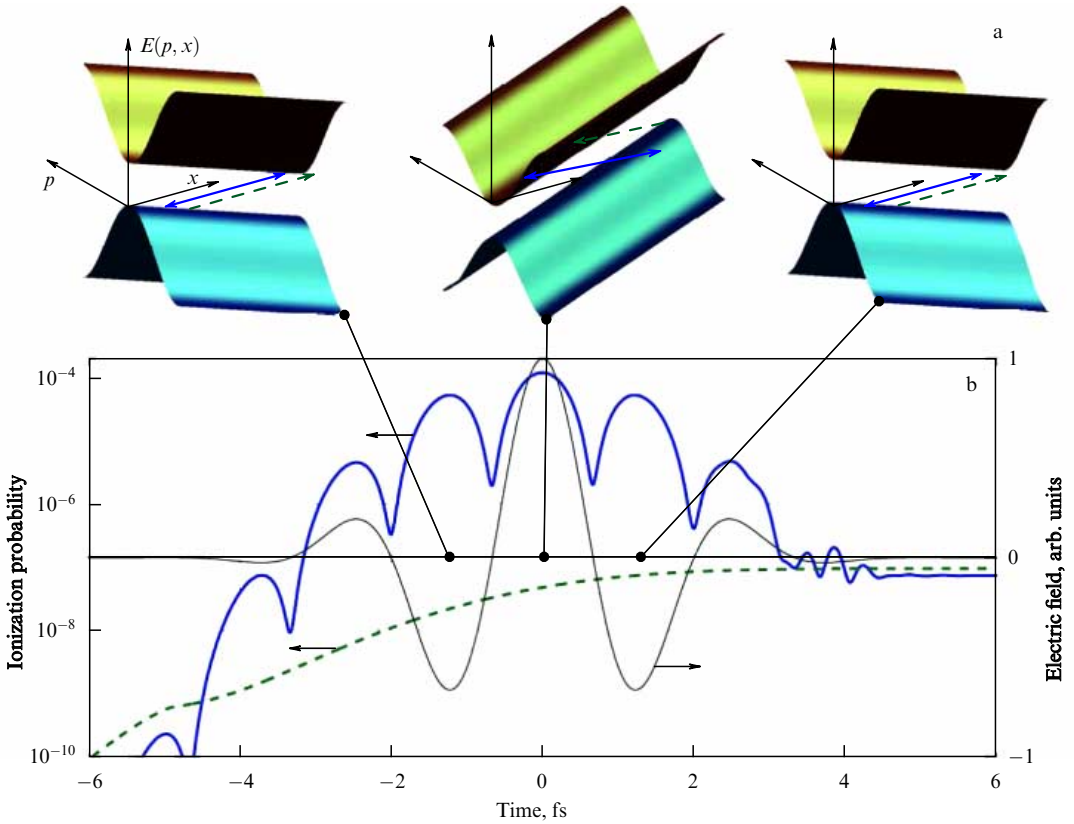

Figure 14. (Color online.) (a) Electron bands of a semiconductor (dielectric) modified by a laser field. (b) Population of the conduction band in the presence of an ultrashort laser pulse (shown by the thin line) as a function of time calculated using the canonical Keldysh theory with averaging over the field cycle (green dashed line) and the generalized Keldysh formalism without time averaging (blue bold solid line).

safe from the viewpoint of a laser-induced damage of a metal tip. With $f \approx 1000$, such laser field corresponds to $\delta \approx 5 \times 10^{-3}$. With a power-series expansion in the small parameter δ, Eqn (87) gives

$$\tau_{\rm el} \approx \frac{1}{\pi}\left(\frac{\delta}{2}\right)^{1/2} T_0 \,. \tag{88}$$

Using the above estimate for δ, we find $\tau_{\rm el} \approx 1.7 \times 10^{-2} T_0$. With $T_0 \approx 2.7$ fs for 0.8-μm Ti: sapphire laser pulses, this gives electron pulses with a pulse width $\tau_{\rm el} \sim 0.1$ fs.

12. Ultrafast photoionization dynamics in solids

The physical picture of ultrafast photoionization of solids resolved on an ultrafast time scale without averaging over the field cycle is of special interest from the fundamental point of view and from the standpoint of numerous applications. Understanding of photoionization dynamics resolved within the field cycle would help achieve an ultimate time resolution in attosecond time-resolved studies, provide important insights into the fundamental aspects of quantum tunneling, allow solid dielectrics to be switched to the conducting state on the subfemtosecond time scale, and enable a high-speed control of optical signals in fiber-optic systems [176, 177] and semiconductor waveguide microcavities [178], opening routes toward petahertz optoelectronics [9, 10, 84, 169, 202].

For solid-state dielectrics, a field-cycle-resolved photoionization theory applicable to laser pulses of an arbitrary pulse shape and pulse width has been developed in Ref. [203]. The theory of photoionization developed in this work is not limited to electron bands with a parabolic dispersion — the assumption used in the canonical version of the Keldysh photoionization theory — but can be applied to more complicated and more realistic dispersion profiles of electron bands. Analysis of a periodic dispersion profile, as a particular case, provides important insights into the properties of photoionization in high-intensity laser fields, where effects related to Brillouin-zone edges start to play a significant role. For sufficiently long laser pulses, this generalized model of photoionization recovers the results of the canonical Keldysh theory for multiphoton and tunneling ionization.

The generalized model of laser-induced ionization shows that the subcycle dynamics of photoionization may drastically differ from the predictions of the standard, cycle-averaging photoionization theory (Fig. 14). Specifically, in the weak-field regime, the subcycle dynamics of the electron conduction-band population displays well-resolved oscillations, which follow the cycles of the driver field (Fig. 14b). After each field half-cycle, most of the electron population returns from the conduction band to the valence band. For long pulses, the generalized photoionization theory recovers the signature $w \propto I^N$ scaling of the photoionization rate w as a function of the laser intensity I, with N defined as the minimum number of photons required to transfer an electron from the valence band to the conduction band. In the case of very short pulses, on the other hand, the photon number N becomes uncertain even in the weak-field regime with $\gamma \gg 1$. Manifestations of the Franz–Keldysh effect are also drastically different in this regime.

13. Optical breakdown of solids

Laser-induced breakdown of solid materials has been a subject of in-depth research since the early days of the laser era (see Refs [2] and [3] for review). This effect is one of the key physical factors limiting radiation fluence in laser experiments. Understanding photoionization is central to an adequate description of optical breakdown. This problem is discussed extensively in the literature, starting from the classical texts of the founders of laser technologies and nonlinear-optical physics [2–4, 204].

The criterion of optical breakdown is often defined in terms of the ratio of the electron density ρ to the critical electron density ρ_{cr} for a given radiation wavelength, $\rho = k\rho_{cr}$, where the numerical coefficient k is usually taken at a level of 0.1. However, in the case of few-cycle laser pulses, such a criterion encounters serious difficulties. As can be seen in Fig. 14, such laser pulses can give rise to subcycle oscillations of the electron conduction-band population. The peak values of the conduction-band population in these oscillations can be orders of magnitude higher than the conduction-band population in the wake of the laser pulse. In this regime, the $\rho = k\rho_{cr}$ condition clearly fails, as it ceases to provide a physically meaningful criterion of optical breakdown.

As laser sources of ultrashort pulses are rapidly progressing, this regime of laser–matter interactions is quickly becoming less and less exotic. To define a physically meaningful criterion of optical breakdown in this parameter space, we need to examine [205] the entire hierarchy of energy transfer processes, occurring on drastically different time scales, whereby the energy of an ultrashort laser pulse is eventually coupled to the crystal lattice (Fig. 15a). Photoionization, which tends to occur on the fastest, femtosecond time scale (Fig. 15a) triggers the entire sequence of processes transferring the energy of the laser field to the crystal lattice. Photoionization itself, as a physical process, is defined by the dynamics of photoelectrons on an even faster — attosecond — time scale (Fig. 15a). An accurate analysis of ultrafast photoionization dynamics (Fig. 15b) examined jointly with much slower processes involving energy dissipation and relaxation accompanying the transfer of laser energy to the crystal lattice yields a reasonably accurate fit for the available experimental data for the optical breakdown threshold of fused silica measured as a function of the laser pulse width (Fig. 15c).

14. Photoionization and nonlinear-optical diagnostics of solids

The electron band structure is a map of fundamental properties of solids, providing a key to understanding complex physical phenomena in new materials, such as high-temperature superconductors [206], graphenes [207], and topological isolators [208]. Widely used methods of X-ray diffraction analysis [209, 210] allow direct-space crystal-lattice parameters to be determined with a high accuracy and can be employed in the bulk of solids. In contrast to X-ray analysis, angle-resolved photoemission spectroscopy [211] enables analysis of the electron band structure. However, this technique can only be used for surface studies, as it relies on the detection of photoelectron emission.

Since experimental characterization of the electron band structure in the bulk of solids is so challenging, all-optical analysis of the band structure of solids using high-order harmonic generation (HOHG) in the field of ultrashort laser pulses in the mid-infrared (mid-IR) range is of considerable interest for numerous applications. Practical implementation of this approach becomes possible [170–172, 212–216] due to recently developed sources of high-power ultrashort pulses in the mid-IR. The first experiments demonstrating this new approach to the studies of solids were performed with the use

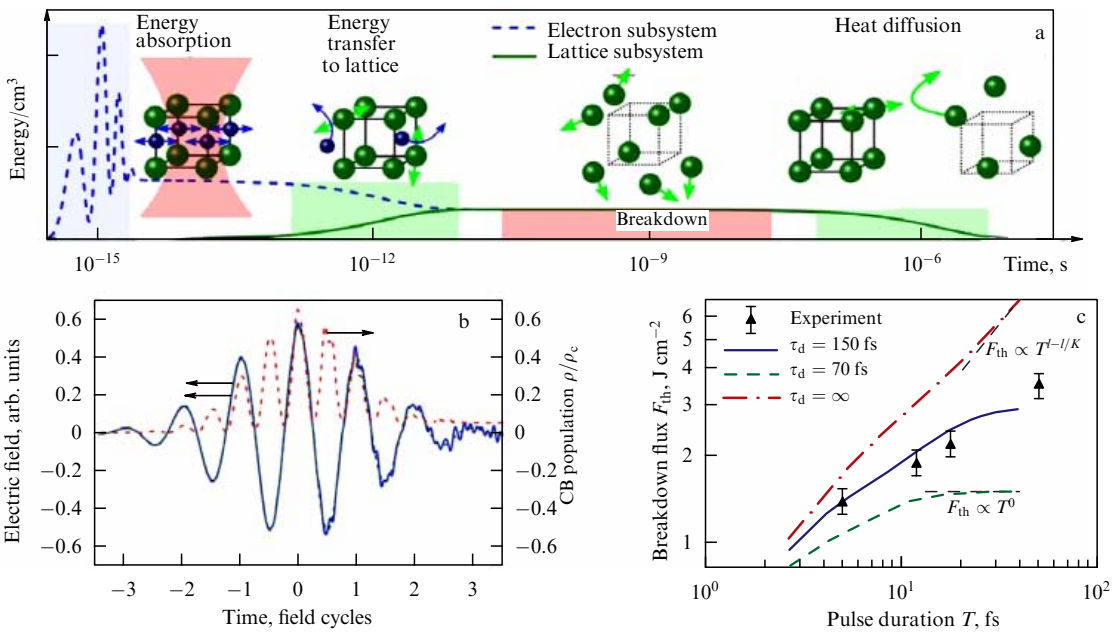

Figure 15. (Color online.) (a) The time scale of laser energy transfer to a crystal lattice leading to laser-induced breakdown. (b) The electric field inside a semiconductor/dielectric near its surface (solid line) and the conduction-band population expressed in units of the critical plasma density (dashed line). The propagation of an ultrashort pulse is analyzed by means of finite-difference time-domain (FDTD) simulations. (c) The laser fluence corresponding to the optical breakdown threshold of fused silica without decoherence processes (red dash–dotted line) and with a decoherence time τ_d equal to 70 fs (green dashed line) and 150 fs (blue solid line).

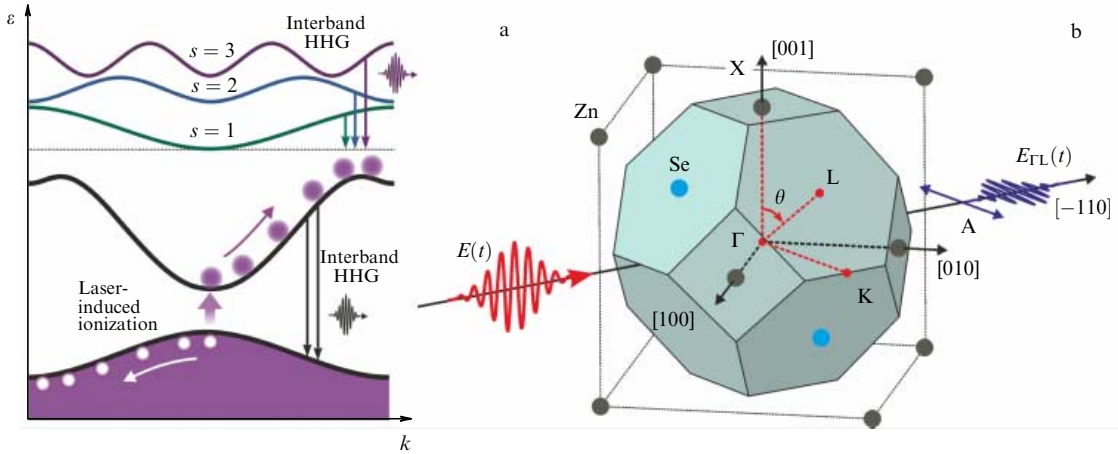

Figure 16. (Color online.) (a) High-order harmonic generation due to interband and intraband processes in a solid. Expansion of the conduction band as a sum of its Fourier harmonics is shown in the upper part. (b) Face-centered cubic crystal lattice of ZnSe (Zn and Se atoms are shown as grey and blue spheres) and its Brillouin zone. The driver laser pulse and the high-order harmonic pulse behind the polarization analyzer (A) are also shown. The angle θ characterizes polarization of the laser driver field.

of ultrashort laser pulses with a central wavelength of 3.66 μm [171, 172]. High-order harmonic generation in solids driven by an intense laser field with such a wavelength is mainly due to interband processes in solids. The frequencies of the most informative harmonics in this regime are higher than the frequency of the energy gap in the band structure of solids, giving rise to a strong attenuation of harmonic radiation and limiting the depth at which the analysis of the band structure of solids is still possible.

As the central wavelength of the laser driver increases, the ratio between the contributions of intraband currents and interband transitions to HOHG changes [217]. Recent experiments [170] have shown that HOHG driven by ultrashort laser pulses with a central wavelength of 5–7 μm is mainly due to intraband processes. With a large group of high-order harmonics generated through intraband mechanisms falling within the transparency range of a solid material, this regime of HOHG is ideally suited for an all-optical metrology of the electron band structure, enabling electron-band analysis in the bulk of solids. Polarization analysis of intraband HOHG allows a full reconstruction of the electron band structure based on the results of measurements performed within the transparency range of a solid-state material [218].

High-order harmonic generation in gas media is one of the key phenomena in strong-field optical physics [5], serving as a cornerstone for the technology of attosecond pulse generation [11]. The physical picture of HOHG in solids is much more complicated and diverse [170–172, 212–217] compared to HOHG in gases. Similar to a standard classification of perturbative mechanisms behind optical nonlinearity in solids [219], it is physically meaningful to distinguish between intra- and interband mechanisms of HOHG (Fig. 16a). Interband HOHG is related to field-induced transitions of electrons from the valence band to the conduction band, leaving holes in the valence band. The subsequent recombination of electrons and holes accelerated by the driver field is accompanied by the emission of harmonics of the driver field. Intraband HOHG (Figs 16a, 17) is due to the nonlinear dependence of the energy of electrons and holes, driven by the laser field along the conduction and valence bands, on their momenta (Figs 17d, e), a strongly nonlinear dependence of the probability of electron transitions from the valence band to the conduction band on the laser intensity, as well as electron–hole scattering effects (Figs. 16a, 17a).

The group velocity of a wave packet generated in an electron band of a solid with a dispersion $\varepsilon(\mathbf{k})$ is

$$\mathbf{v}(\mathbf{k}, t) = \frac{1}{\hbar}\frac{\mathrm{d}\varepsilon(\mathbf{k})}{\mathrm{d}\mathbf{k}} . \tag{89}$$

The momentum $\mathbf{k}(t)$ of the electron wave packet is given by

$$\mathbf{k}(t) = -\frac{e}{\hbar}\int_{-\infty}^{t} \mathbf{E}(\theta)\,\mathrm{d}\theta , \tag{90}$$

where $\mathbf{E}(t)$ is the field of an ultrashort driver laser pulse. The field-driven intraband oscillations of electron wave packets are thus ideally suited to probe the $\varepsilon(k)$ profile, offering a means to map the electron band structure (Fig. 17e).

To identify the properties of this map, we expand $\varepsilon(k)$ as a Fourier series,

$$\varepsilon(k) = \varepsilon_0 + \sum_s \varepsilon_s \cos(ska) . \tag{91}$$

The group velocity of an intraband electron wave packet driven by a field $E(t) = E_0 \cos(\omega_0 t)$ is written, in a scalar form, as

$$v(t) = -\sum_{s=1} s\varepsilon_s a \sin\left[\frac{s\omega_\mathrm{B}}{\omega_0}\sin(\omega_0 t)\right] , \tag{92}$$

where $\omega_\mathrm{B} = eEa/\hbar$ is the Bloch frequency. Such a wave packet driven by a laser field within an electron or hole band of a solid (Fig. 17d) radiates odd harmonics of the driver field (Figs 16a, 17e) with the intensity of the Nth harmonic given by

$$I_N \propto (N\omega_0)^2 \left|\sum_s s\varepsilon_s a J_N\left(\frac{s\omega_\mathrm{B}}{\omega_0}\right)\right|^2 . \tag{93}$$

In the case of low driver intensities, when $J_N(\xi) \approx (\xi/2)^N/N!$, Eqn (93) recovers the I_0^N signature scaling of the Nth harmonic intensity as a function of the driver intensity I_0, characteristic of the perturbative regime of HHG. Since this asymptotic expression is valid as long as $\xi < (N+1)^{1/2}$, the field-intensity borderline between the perturbative and

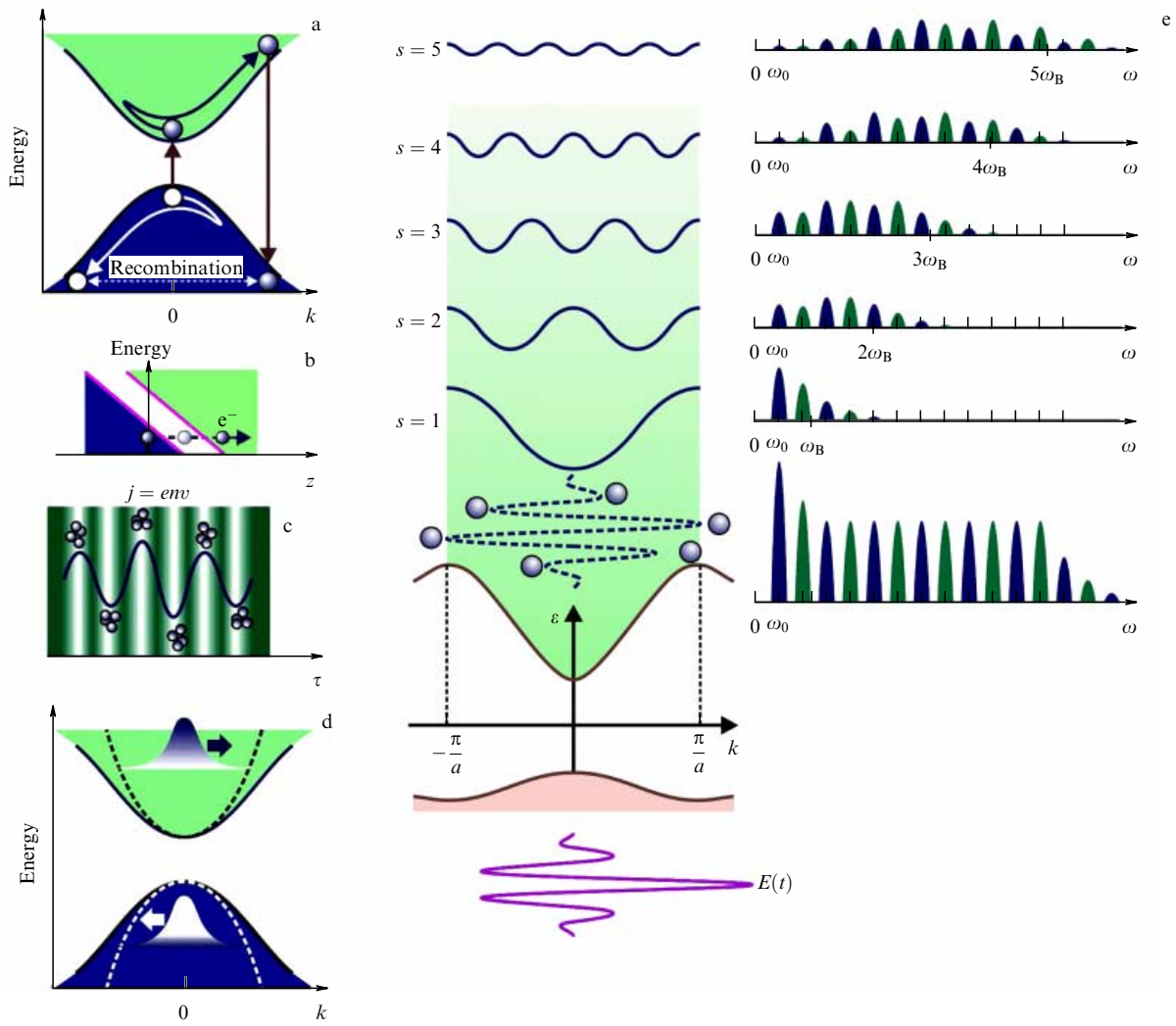

Figure 17. (Color online.) (a–d) Inter- and intraband electron dynamics in a solid semiconductor driven by an ultrashort laser pulse: (a) interband transitions creating electrons and holes, followed by electron–hole recombination, providing a source of optical nonlinearity; (b) interband transitions with electron tunneling across the band gap; (c) modulation of the photoelectron current by inter- and intraband transitions; and (d) dynamics of electron and hole wave packets driven within the bands of a semiconductor/dielectric by an ultrashort laser pulse. (e) Reconstruction of the electron band structure of a solid using intraband high-order harmonic generation.

nonperturbative regimes of HHG scales as $(N+1)\lambda_0^{-2} \propto 1/U_\mathrm{p}$. Thus, similar to gas media, the pondermotive electron energy, $U_\mathrm{p} \propto \lambda_0^2$, is a key parameter that controls the regime of laser–solid interaction.

To understand the key properties of optical harmonics emitted by electron wave packets driven by a laser field within an electron or hole band of a solid, it is instructive to represent the argument of the Bessel functions in Eqn (93) as a ratio $\xi_s = s\omega_\mathrm{B}/\omega_0 = k_\mathrm{e}/K_s$ of the momentum $k_\mathrm{e} = eE_0/\hbar\omega_0$ of the field-driven electron wave-packet oscillatory motion to the reciprocal lattice vector, $K_s = (sa)^{-1}$, of the sth Fourier harmonic in the Fourier expansion of the dispersion $\varepsilon(k)$ of the pertinent band (Fig. 17e). The properties of the Bessel functions suggest a physically transparent qualitative criterion $N_s \approx s\omega_\mathrm{B}/\omega_0$ for the cutoff in the spectrum of harmonics. Optical harmonics near the cutoff region thus represent electrons whose field-induced momenta are large enough to reach the band edges $\pm(sa)^{-1}$ of the sth harmonic of the dispersion $\varepsilon(k)$ of the relevant band (Fig. 17e). This relation allows the dispersion profiles of electron bands in solids to be reconstructed from high-order harmonic spectra through a successive determination of the Fourier harmonics of the dispersion profiles of these bands.

The full electron band structure of solids can thus be determined by means of high-order harmonic generation using ultrashort laser pulses in the mid-infrared range. Electron and hole wave packets whose direction of motion is controlled by the polarization of a laser pulse relative to the symmetry axes of the Brillouin zone provide an effective probe for the electron bands along well-defined directions within the Brillouin zone.

The most informative part of the spectrum of interband harmonics lies above the band gap of solids and experiences absorption in the material. It is, therefore, HOHG due to the nonlinearity of the dispersion of electrons and holes in solids that becomes a focus of interest as a promising method of electron band structure analysis in the bulk of solids. A considerable part of the spectrum of harmonics generated through this nonlinearity mechanism is below the band gap, falling within the transparency range of a solid. Analysis of the properties of high-order harmonics emitted in this regime gives an access to important information on the dispersion

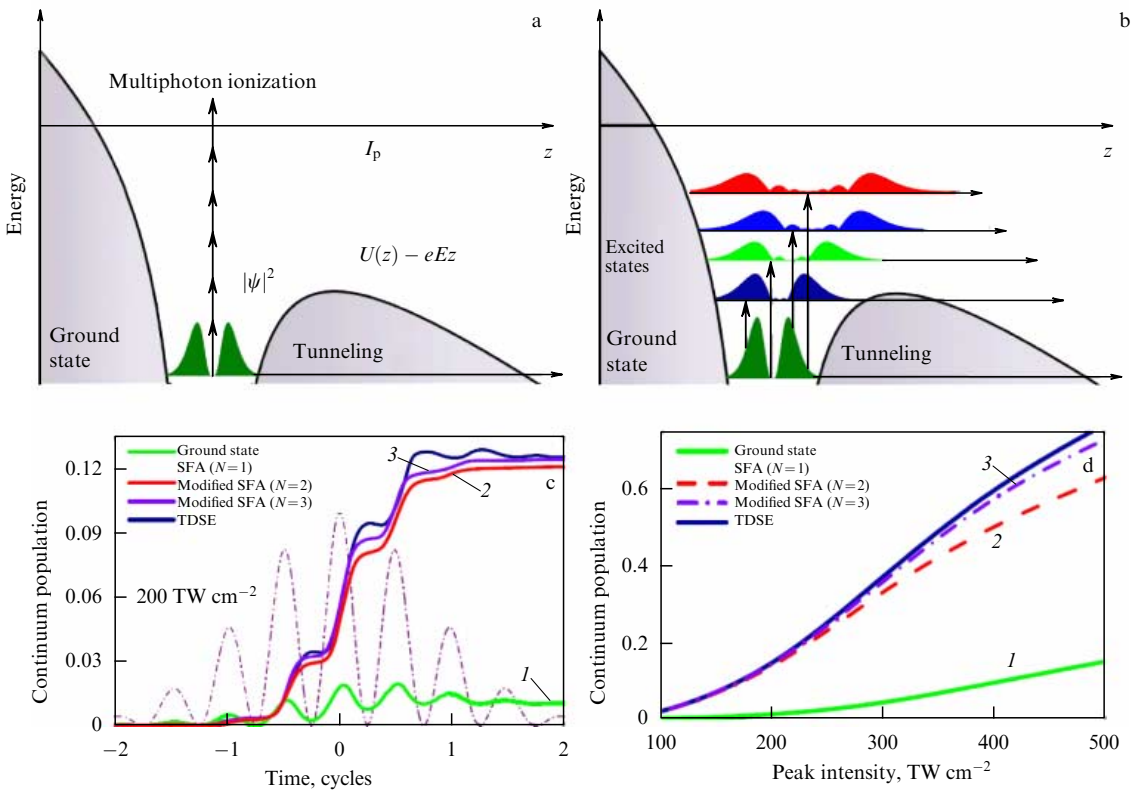

Figure 18. (Color online.) (a) Multiphoton and tunneling ionization from the ground electron state. (b) Photoionization as a result of tunneling from excited electron states. (c) Population dynamics of continuum states and (d) continuum population as a function of the peak intensity of an ultrashort laser pulse (shown by the dash–dotted line in Fig. 18c) calculated with the use of Eqns (94)–(97) including only the ground state ($N = 1$, green line *1*), the ground and the first excited states ($N = 2$, red line *2*), and the ground and the first two excited states ($N = 3$, purple line *3*). Numerical solution of the time-dependent Schrödinger equation (TDSE) is also shown for comparison; SFA, strong-field approximation.

$\varepsilon = \varepsilon(\mathbf{k})$, i.e., on the band structure of a solid. Implementation of this regime of HOHG requires sources of ultrashort pulses with a sufficiently high peak power and a central wavelength much longer than the wavelength of drivers enabling interband HOHG studies. Laser sources meeting these requirements have been developed only recently [104, 109, 110], opening ways toward the practical implementation of all-optical metrology of the band structure in solids.

With a separate detection of HOHG signals due to intraband currents along different directions within the Brillouin zone, selected by a polarizer and an analyzer (Fig. 16b), electron band profiles near this direction within the Brillouin zone can be determined from the spectra of high-order harmonics. The entire band structure of a solid can then be reconstructed section by section using polarization HOHG measurements for $\varepsilon = \varepsilon(\mathbf{k})$ profiles of certain band sections near specific directions of the Brillouin zone, defined by the geometry of polarization HOHG measurements.

15. Electron tunneling from excited states

The canonical version of the Keldysh photoionization theory for atoms and molecules treats laser-induced ionization as a direct transition from the ground electron state to a free-electron state dressed by the external field. The 1964 paper by Keldysh also develops a formalism for the calculation of the photoionization rate, including transitions into resonant intermediate electronic states. Both the formulation of the original version of the Keldysh photoionization theory and the method whereby intermediate electronic states are included in the analysis are based on the assumption of a monochromatic external field, which is a natural first step from the methodological point of view and fully justifiable in the context of the state of the art in laser technologies in the early years of laser science. For a monochromatic external field, photoionization effects related to transitions into intermediate electronic states can be adequately described by a pertinent sum over allowed one-photon and multiphoton transitions into excited bound electronic states.

An attempt to extend this approach to photoionization by ultrashort laser pulses encounters fundamental difficulties related to the broadband character of the external field. For such a field, the sums over intermediate states of the discrete spectrum of the system become poorly defined. An accurate analysis of photoionization effects related to the excited states of an atomic or molecular system has to take into consideration electron dynamics on the subcycle time scale (Figs 18a, b). To make this analysis more physically transparent, we represent the full electron wave function as a sum of positive- and negative-energy terms:

$$\psi(\mathbf{r}, t) = \psi_{\mathrm{b}}(\mathbf{r}, t) + \psi_{\mathrm{f}}(\mathbf{r}, t) = \sum_{n=1}^{N} \sum_{l=0}^{n-1} \alpha_{nl}(t) \psi_{nl}(\mathbf{r}) + \psi_{\mathrm{f}}(\mathbf{r}, t)\,. \tag{94}$$

The probability to find an electron in a bound state with quantum numbers n and l is then given by $|\alpha_{nl}(t)|^2 = |\int_V \psi_{nl}(\mathbf{r}) \psi(\mathbf{r}, t)\, \mathrm{d}\mathbf{r}|^2$. The photoionization rate can now be calculated as the population of continuum states, with all the intermediate bound states included through appropriate

sums:

$$C(t) = \int \mathrm{d}\mathbf{p} \left| \frac{\mathrm{i}}{\hbar} \int_{-\infty}^{t} \mathrm{d}\theta \int_V \mathrm{d}\mathbf{r}\, \psi_{\mathbf{p}}^*(\mathbf{r}, t) eE(\theta) \times \sum_{n=1}^{N} \sum_{l=0}^{n-1} \alpha_{nl}(\theta) \left(z\psi_{nl} - \sum_{s=1}^{N} \sum_{q=0}^{s-1} Z_{sq}^{nl} \psi_{sq} \right) \right|^2, \quad (95)$$

where

$$Z_{sq}^{nl} = \int_V \psi_{nl}(\mathbf{r}) z \psi_{sq}(\mathbf{r})\, \mathrm{d}\mathbf{r}\,, \quad (96)$$

and the coefficients α_{nl} can be found from the equation

$$\mathrm{i}\hbar \frac{\partial \alpha_{nl}}{\partial t} = E_n \alpha_{nl} - eE(t) \sum_{s=1}^{N} \sum_{q=0}^{s-1} Z_{sq}^{nl} \alpha_{sq} - \int_V \psi_{nl}(\mathbf{r}) ezE(t) \psi_{\mathrm{f}}(\mathbf{r}, t)\, \mathrm{d}\mathbf{r}. \quad (97)$$

Figures 18c and 18d present the results of calculations [220] using Eqns (95)–(97) for a quantum system with a hydrogenlike ground state and a Volkov-type wave functions (8) for the continuum states. As can be seen from these calculations, for low field intensities, photoionization is adequately described even when only one term $(N = 1)$, corresponding to the ground state of a hydrogenlike atom, is included in the sum under the integral in Eqn (95). However, as the field intensity grows, calculations in a model including only one electronic state become increasingly inaccurate. Moreover, in the strong-field regime, the photoionization process starts to display qualitatively new features. Transitions to the continuum states via excited bound states open a new ionization channel. The potential barrier height for such states is much lower than the potential barrier height for ground-state electrons (Figs 18a, b). This effect plays an important role for high field intensities. Tunneling of electrons from excited states, which occurs within a small fraction of the laser field cycle, becomes a dominant mechanism of photoionization [220].

16. Photoionization and laser filamentation

16.1 Spatiotemporal dynamics of a high-intensity ultrashort laser pulse in a medium with photoionization

The rapid progress of laser technologies gives rise to new unique sources of high-power ultrashort pulses of electromagnetic radiation, opening a new chapter in photoionization studies. Propagation of high-power ultrashort laser pulses in a medium with photoionization is accompanied by a complex nonlinear evolution [7, 8, 221, 222], where various spectral–temporal field transformations are strongly coupled to spatial beam dynamics, which, in turn, is nonuniform within the laser pulse. Such regimes of pulse propagation are of special interest in the context of long-distance transmission of high-power ultrashort laser pulses [223], efficient white-light supercontinuum generation [12, 14, 15, 224, 225], and temporal compression of high-power ultrashort laser pulses [226–228] in the laser filamentation regime. Lasing in laser-induced filaments [229] offers unique opportunities for a highly sensitive remote sensing of the atmosphere [230, 231]. Analysis of these new phenomena and physical scenarios is impossible without a detailed understanding of photoionization within the extended framework of the Keldysh photoionization theory.

As a universal property of intense laser fields, light beams with peak powers well above the self-focusing threshold become intrinsically unstable with respect to a breakup into multiple filaments [232]. Since such beam instabilities are seeded by random intensity fluctuations across a laser beam or optical inhomogeneities of a medium, a laser beam undergoing multiple filamentation usually loses its axial symmetry. Photoionization is one of the key effects in this complex regime of nonlinear dynamics [233]. In each of the filaments arising as a part of this process, diffraction is suppressed due to the joint action of nonlinear polarization induced in the medium and the radial profile of electron density. Within a limited parameter space, as recent studies have shown, high-power single-cycle and subcycle optical pulses can be generated in laser filaments, giving rise to ultrashort bursts of electromagnetic fields less than a field cycle in duration. Correct analysis of this intriguing regime of pulse evolution is not possible within the standard slowly varying envelope approximation (SVEA) and requires the inclusion of all the relevant non-SVEA effects in nonlinear spatiotemporal dynamics of high-power ultrashort light pulses.

The diversity of physical phenomena involved in this regime of nonlinear spatiotemporal field evolution and the related physical scenarios that may lead to the formation of single-cycle and subcycle pulses can only be understood in the framework of a full model of spatiotemporal field dynamics including all the relevant non-SVEA effects. Since single-cycle and subcycle pulses need to be adequately described, numerical analysis has to be performed with a high resolution in spatial and temporal coordinates within the entire path of nonlinear interaction, which is often very long in the regime of laser filamentation. Such an analysis requires exaflop computations and is usually performed with the use of supercomputers [122, 234, 235]. Exaflop computer simulations reveal new unique phenomena of the spatiotemporal dynamics of high-peak-power ultrashort light pulses, including the generation of single-cycle and subcycle field waveforms. In special regimes of nonlinear dynamics, such field waveforms have been shown to evolve into multiple light bullets.

16.2 Physical model

The spatiotemporal dynamics of high-peak-power ultrashort pulses is analyzed using the generalized nonlinear Schrödinger equation (GNSE) for the complex field amplitude including ultrafast field-induced ionization processes [7, 8, 122, 236]:

$$\begin{aligned} \frac{\partial}{\partial z} A(\omega, x, y, z) &= \left[\frac{\mathrm{i}c}{2\omega} \Delta_\perp + \mathrm{i}\tilde{D}(\omega) \right] A(\omega, x, y, z) \\ &+ \tilde{F} \left\{ \mathrm{i}\, \frac{\omega_0 \tilde{T}}{c} \left[n_2 (1 - f_{\mathrm{R}})\, I(\eta, x, y, z) \right.\right. \\ &+ \left. \sum_{q=2}^{4} n_{2q} I^{2q}(\eta, x, y, z) \right] A(\eta, x, y, z) \\ &+ n_2 f_{\mathrm{R}} \int_{-\infty}^{\infty} R(\eta - \eta')\, I(\eta', x, y, z)\, \mathrm{d}\eta'\, A(\eta, x, y, z) \\ &+ \sum_{s=2}^{5} \frac{\chi^{(2s-1)}}{2^s c^{s-1} \varepsilon_0^{s-1}} A^2(\eta, r, z)\, A(\eta, x, y, z) \\ &- \left. \left(\frac{\mathrm{i}\omega_0}{2cn_0^2 \rho_{\mathrm{cr}} \tilde{T}} \rho + \frac{U_{\mathrm{i}} W(\rho_0 - \rho)}{2I} + \frac{\sigma}{2} \rho \right) A(\eta, x, y, z) \right\}. \end{aligned} \quad (98)$$

Here, $A(\eta, x, y, z)$ is the complex field amplitude, $A(\omega, x, y, z)$ is its Fourier transform, $I(\eta, x, y, z) = |A(\eta, x, y, z)|^2$ is the field intensity, η is the time in the retarded frame of reference, x and y are the transverse coordinates, z is the coordinate along the propagation axis, ω is the radiation frequency, $\Delta_\perp = \partial^2/\partial x^2 + \partial^2/\partial y^2$ is the transverse part of the Laplacian, $\tilde{D} = k(\omega) - k(\omega_0) - \partial k/\partial\omega|_{\omega_0}(\omega - \omega_0)$ is the dispersion operator, ω_0 is the central frequency of the laser pulse, $k(\omega) = \omega n(\omega)/c$ is the wave number, $n(\omega)$ is the refractive index, $n_0 = n(\omega_0)$, $\tilde{F}$ is the Fourier transform operator in the time variable, $\chi^{(3)}$, $\chi^{(5)}$, $\chi^{(7)}$, and $\chi^{(9)}$ are the third-, fifth-, seventh, and ninth-order nonlinear-optical susceptibilities, n_2, n_4, n_6, and n_8 are the Kerr nonlinearity coefficients, $\tilde{T} = 1 + \mathrm{i}\omega_0^{-1}\,\partial/\partial\eta$, $R(\eta)$ is the Raman response function, f_R is the fraction of the Raman (delayed) nonlinearity in the overall nonlinear response of the medium, ρ is the electron density, $U_\mathrm{i} = U_0 + U_\mathrm{osc}$, U_0 is the ionization potential, U_osc is the pondermotive energy of field-induced electron oscillations, $W(I)$ is the photoionization rate, σ is the avalanche ionization cross section, $\rho_\mathrm{cr} = \omega_0^2 m_\mathrm{e}\varepsilon_0/e^2$ is the critical electron density, ρ_0 is the neutral gas density, m_e is the electron mass, e is the electron charge, and ε_0 is the dielectric permittivity of a vacuum.

The field evolution equation (98) is solved jointly with the equation for the electron density, which includes field-induced ionization, as well as avalanche ionization and recombination:

$$\frac{\partial\rho}{\partial\eta} = W(I) + \sigma(\omega_0)U_\mathrm{i}^{-1}\rho I - \frac{\rho}{\tau_\mathrm{r}}\,. \tag{99}$$

The photoionization rate W in Eqns (98) and (99) is calculated using the Keldysh–Popov–Perelomov–Terent'ev formalism. The avalanche ionization cross section σ is calculated with the use of the Drude formula

$$\sigma(\omega) = e^2\tau_\mathrm{c}\left[m_\mathrm{e}\varepsilon_0 n_0 c(1 + \omega^2\tau_\mathrm{c}^2)\right]^{-1}, \tag{100}$$

where τ_c is the collision time and τ_r is the recombination time.

The model based on Eqns (98) and (99) includes all the key physical effects that show up in the evolution of high-peak-power ultrashort pulses in a nonlinear dispersive medium [7, 8, 237]. The spectral representation of the dispersion operator $\tilde{D}$ allows the material dispersion to be described exactly rather than through its polynomial expansion about the central frequency ω_0. An accurate description of material dispersion is of crucial importance for the analysis of a broad class of nonlinear optical processes, including multioctave supercontinuum generation, as well as single-cycle and subcycle pulse generation, where the models based on a series expansion of the frequency dispersion profile in $\omega - \omega_0$ fail. This physical model also includes linear loss and diffraction effects, the field-induced change in the refractive index due to the third-, fifth-, and, whenever necessary, higher-order Kerr-type optical nonlinearities, pulse self-steepening, spatiotemporal self-action phenomena [7, 8, 238], as well as plasma loss, dispersion, scattering, and defocusing due to an ultrafast ionization of the medium by the laser field.

Importantly, the assumption of an axially symmetric beam, which substantially simplifies the solution of Eqn (98), fails in the regime of multiple filamentation. In this regime, a laser beam tends to break up into multiple filaments due to spatial modulation instabilities, arising from random hot spots across the beam seeded by noise-induced intensity fluctuations and random optical inhomogeneities in the medium. In its fully three-dimensional version, the field evolution equation (98), which also involves the time variable and is, hence, often referred to as a $(3+1)$-dimensional model, leads to calculations of high computational complexity [122].

16.3 Multiple filamentation dynamics

A typical picture of the spatiotemporal dynamics of an ultrashort laser pulse with a peak power P two orders of magnitude higher than the self-focusing threshold P_cr is shown in Fig. 19. Here, calculations have been performed for ultrashort mid-infrared pulses with a central wavelength $\lambda_0 = 3.9$ μm and an input pulse width $\tau_0 = 80$ fs. High-peak-power femtosecond pulses at this wavelength are delivered by recently developed mid-infrared sources of generation based on optical parametric chirped-pulse amplification [105, 107, 108]. The dynamics of such pulses in the regime of multiple filamentation is of considerable interest as a way toward the generation of high-power single-cycle and subcycle pulses in the mid-infrared and in the context of interesting new phenomena that may be expected since the central wavelength of such pulses falls within the range of anomalous dispersion of many solid materials. Numerical analysis of single-filamentation dynamics [239, 240], which takes place for much lower ratios of the laser peak power to the critical power of self-focusing, suggests that unique propagation regimes, including formation of light bullets, may become possible for ultrashort laser pulses in the regime of anomalous dispersion.

A light beam with a peak power several orders of magnitude higher than the critical power of self-focusing ($P = 100P_\mathrm{cr}$ for the propagation regime illustrated in Fig. 19) exhibits a complex temporal, spatial, and spectral dynamics (see Fig. 19). The field structure is inhomogeneous across the beam and within the pulse, constantly changing as the beam propagates through the medium, displaying significant variations from the leading edge to the trailing edge of the pulse (see Fig. 19). Such variations in the beam structure are due to a dynamic interplay between the Kerr and ionization nonlinearities [7, 8, 237], which changes from the leading edge of the pulse to its tail. The temporal structure of the field is, in turn, nonuniform across the beam.

A laser field with a peak power $P \gg P_\mathrm{cr}$ is unstable with respect to beam breakup into multiple filaments, seeded by random field intensity fluctuations within the beam. The resulting spatial modulation instabilities give rise to field hot spots across the beam and eventually lead to the loss of coherence within the laser beam (see Fig. 19). As a result of joint action of the Kerr and ionization nonlinearities, the beam breaks up into multiple filaments. This effect is accompanied by efficient spectral broadening (see Fig. 19), which is typical of laser-induced filamentation and which is often referred to as supercontinuum generation.

In the Bespalov–Talanov theory [232], the typical length within which spatial modulation instabilities tend to build up is on the order of the nonlinear length, $L_\mathrm{nl} = (\omega n_2 I_0)^{-1}$, where I_0 is the field intensity. For the propagation regime illustrated in Fig. 19, the buildup of modulational instabilities closely follows the $\exp(z/l_\mathrm{nl})$ growth rate, predicted by the Bespalov–Talanov theory. In this regime, for beam instabilities seeded by noise intensity fluctuations, a 100 gain is achieved within a propagation length of about 1 m. Within a broad range of input laser beam parameters, the length within which multiple filamentation was observed in numerical simulations

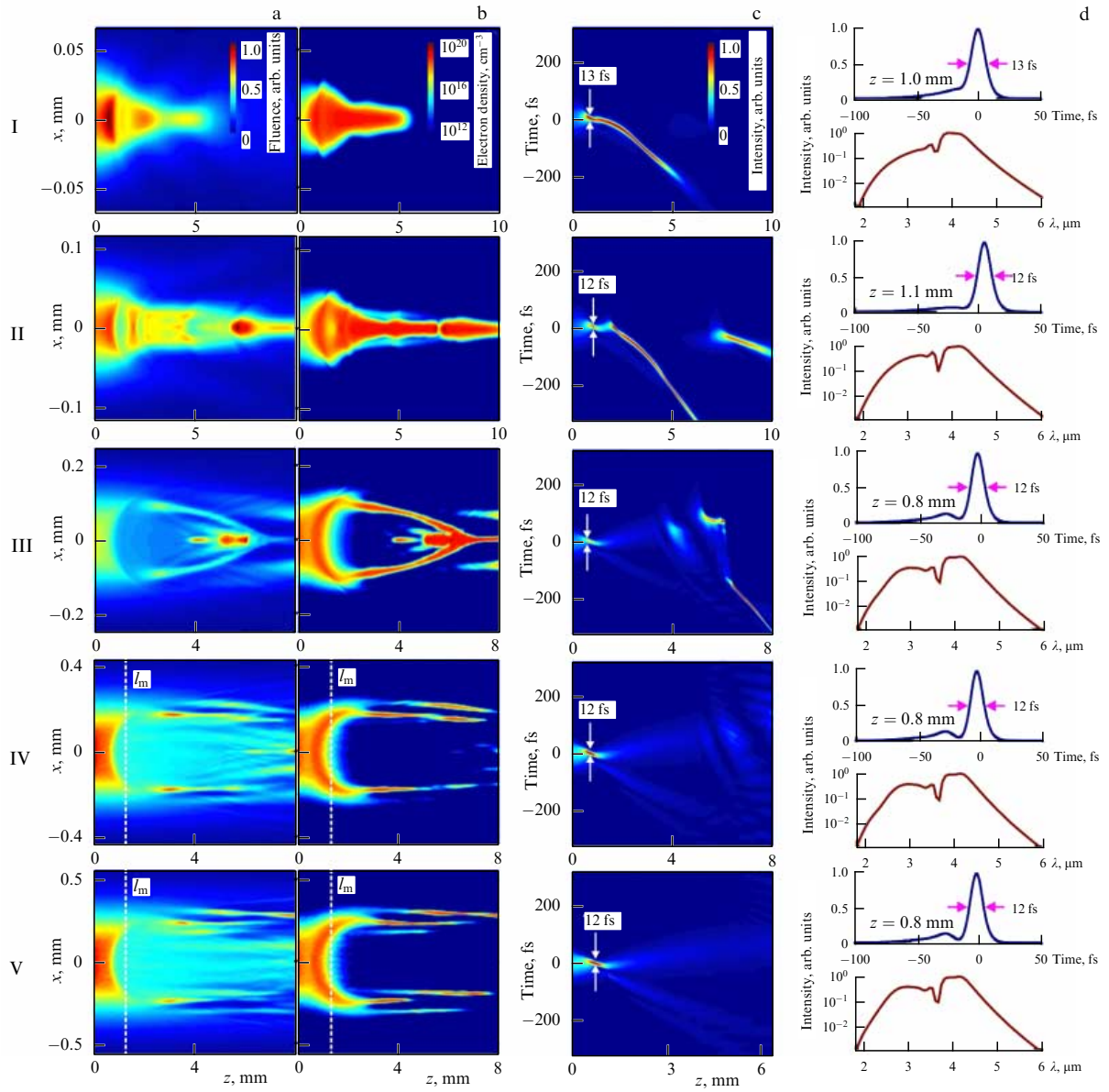

Figure 19. Full $(3+1)$-dimensional dynamics of an ultrashort laser pulse with a central wavelength of 3.9 μm and a pulse width of 80 fs propagating in an anomalously dispersive material under conditions of photoionization: (a) the radial distribution of the field intensity integrated over the pulse along the propagation direction, (b) the electron density induced by the laser pulse, (c) spatiotemporal evolution of the field intensity, and (d) temporal envelope (top) and the spectrum (bottom) of the pulse on the beam axis at the point of maximum pulse compression. The input laser pulse peak power P, energy W, and beam diameter d are (I) $P = 5P_{cr}$, $W = 13$ μJ, $d = 70$ μm; (II) $P = 15P_{cr}$, $W = 40$ μJ, $d = 120$ μm, (III) $P = 100P_{cr}$, $W = 0.25$ mJ, $d = 260$ μm, (IV) $P = 300P_{cr}$, $W = 0.75$ mJ, $d = 450$ μm, and (V) $P = 500P_{cr}$, $W = 1.25$ mJ, $d = 590$ μm.

agrees well with the predictions of the Bespalov–Talanov theory for the modulation instability buildup length. This finding allows complex strongly coupled processes involved in nonlinear spatiotemporal field dynamics observed in numerical simulations to be interpreted in a clear, physically transparent way.

16.4 Self-compression of high-peak-power laser pulses

Soliton self-compression of laser pulses in the anomalous dispersion regime is widely used for the generation of ultrashort optical waveforms in optical fibers [241, 242]. The $(3+1)$-dimensional spatiotemporal dynamics of freely propagating laser beams with a peak power well above the critical power of self-focusing is, however, much more complicated than the dynamics of light pulses in optical fibers, which can be accurately described within the framework of the thoroughly developed model of the generalized nonlinear Schrödinger equation with one temporal and one spatial coordinate. The spatiotemporal evolution of optical fields with peak powers $P \gg P_{cr}$ in the regime of anomalous dispersion can often involve beam breakup into multiple filaments, leading to the loss of beam connectedness and, eventually, spatial coherence (see Fig. 19). Effects of spatial instability in this regime are strongly coupled with the temporal modulation instability of laser pulses [243]. Remarkably, despite all the complexity of their spatiotemporal dynamics, efficient self-compression of high-peak-power ultrashort light pulses is still possible, as shown in Fig. 19, without the loss of beam connectedness and spatial coherence through beam breakup into multiple filaments.

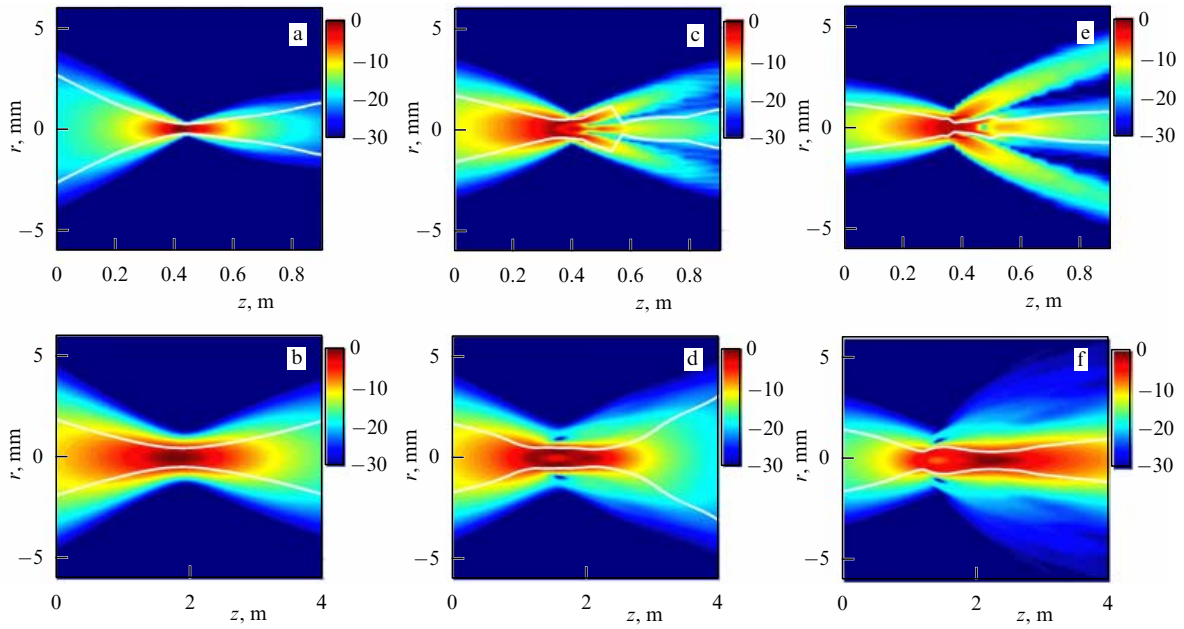

Figure 20. Spatiotemporal maps of field intensity in a subterawatt ultrashort mid-IR pulse propagating in the atmosphere in the leading edge (a, b), in the central part (c, d), and in the trailing edge (e, f) of the pulse. The beam is focused by a lens with a focal length of 45 cm (a, c, e) and 200 cm (b, d, f). The initial driver energy is 20 mJ. The initial pulse width of the driver is 100 fs. The solid line shows the beam diameter defined as its full width at half-maximum.

Of key significance for this regime of nonlinear dynamics is that the typical lengths of self-compression and modulation instability, l_c and l_m, should meet the inequality $l_c < l_m$. When this condition is satisfied, a light pulse experiences self-compression to its minimum pulse width, as a result of the joint action of anomalous dispersion and nonlinearity, before the beam breaks up into multiple filaments. As can be seen from simulations presented in Fig. 19, self-compression yields a subcycle field waveform. Within the propagation length needed to achieve such pulse compression, the beam does not lose its connectedness, with its angular spectrum showing virtually no features that would be indicative of spatial modulation instabilities.

Within longer propagation paths ($z > l_m$), modulation instabilities become noticeable, with field hot spots appearing across the beam. The angular spectra corresponding to this phase of beam dynamics display noticeable distortions, indicating off-axial field components. Beam breakup due to modulation instability is accompanied by multiple filamentation (see Fig. 19), caused by the joint action of the Kerr and ionization nonlinearities.

Thus, our numerical simulations confirm that, when the spatial length of self-compression is kept shorter than the length required for the buildup of modulational instabilities, $l_c < l_m$, high-peak-power light pulses can undergo efficient self-compression without the loss of beam coherence. This effect is of key significance for identifying the physical scenarios whereby single-cycle and subcycle light bullets can be generated in the regime of anomalous dispersion.

16.5 Subterawatt ultrashort mid-infrared pulses in the atmosphere

To gain deeper insights into the physical scenario of filamentation of ultrashort pulses in the mid-IR, we plot in Fig. 20 the maps of field intensity distribution in the filament calculated for the leading edge (Figs 20a, b), the central part (Figs 20c, d), and the trailing edge (Figs 20e, f) of the pulse. As can be seen from these simulations, with the electron density increasing from the leading edge of the pulse to its trailing edge, different sections of the beam undergo different dynamics. This difference is due to the buildup of the electron density within the laser pulse [244, 245]. The leading edge of the pulse induces ionization of the air, giving rise to a transverse profile of the electron density, falling off from the center of the beam to its periphery. Such a profile of the electron density defocuses the central part and especially the trailing edge of the pulse. This dynamics is clearly seen in the maps of field intensity presented in Fig. 20. Scattering of mid-IR radiation off the field-induced plasma also becomes especially strong in the trailing edge of the pulse, leading, in the case of long filaments, to a noticeable pump depletion along a filament.

The white solid line in Fig. 20 shows the beam diameter d defined as the beam full width at half-maximum (FWHM) of the field intensity. The evolution of the beam diameter along the optical path of the mid-IR driver provides a convenient measure of the filament length as the distance between two points along the beam path where the beam diameter is equal to twice the minimum beam diameter d within a filament. When the beam focusing is too tight (Figs 20a, c, e), strong scattering of the central part (Fig. 20c) and the trailing edge (Fig. 20e) of the pulse off the electron-density profile induced by the leading edge of the pulse limits the length of the filament. An appropriate choice of beam-focusing conditions (Figs 20b, d, f) can help achieve a precise balance between beam self-focusing and defocusing by the transverse profile of the electron density. In this regime, the filament length, as can be seen from Fig. 20f, can reach several meters, offering unique options for the remote sensing of the atmosphere and long-range transmission of high-power laser pulses.

17. Conclusion

The Keldysh photoionization theory is a conceptual cornerstone and a universal framework for the description of a broad class of fundamental effects in light–matter interaction. Developed in the early years of the laser era, when the entire area of research focused on laser–matter interactions was still in its infancy, the Keldysh photoionization theory is an extraordinary example of outstanding scientific vision and a researcher's courage.

As one of its central results, the Keldysh photoionization theory offers a fundamental insight into multiphoton and tunneling ionization as two limiting regimes of the same physical phenomenon — ionization induced by an ac electromagnetic radiation field. The photoionization rate calculated within the framework of this theory is one of the key parameters for the analysis of a broad class of laser–matter interaction processes, including laser-induced breakdown, high-order harmonic generation, and laser filamentation. The Keldysh photoionization theory is broadly used for the description of laser–matter interactions occurring on the attosecond time scale and provides a universal framework for a quantitative analysis of complex physical processes enabling the generation of attosecond pulses of electromagnetic radiation and ultrashort light-controlled flashes of photoelectric currents in solids. Keldysh-theory closed form expressions for multiphoton absorption in solids provide a key to understand the universal dispersion properties of the nonlinear-optical response of semiconductors and dielectrics.

Acknowledgments
I keep the warmest memories of numerous discussions that I had the privilege to have with L V Keldysh and am deeply grateful to L V Keldysh for his in-depth comments and useful suggestions on various aspects of research. I am also deeply grateful to A A Voronin, A B Fedotov, D A Sidorov-Biryukov, A V Mitrofanov, A A Lanin, E E Serebryannikov, A Baltuška, A Pugžlys, V Ya Panchenko, P A Zhokhov, and I V Fedotov for long-standing fruitful collaboration.

This research was supported in part by the Russian Foundation for Basic Research (project Nos 16-02-00843 and 17-52-53092) and the Welch Foundation (grant No. A-1801). Research into quantum optical physics and quantum technologies is supported by the Government of the Russian Federation (project No. 14.Z50.31.0040, Feb. 17, 2017). Research into attosecond spectrochronography has been supported by the Russian Science Foundation (project No. 17-12-01533).

Afterword

Great scientists stay in history through their scientific work. Great people remain in our memories and souls. Leonid Veniaminovich Keldysh will be remembered as a great scientist, whose work transformed optical physics and gave rise to new research areas, and as a great human, whose light will stay in the memory of those who had the privilege to know him.

A rare scientific paper is celebrated by special issues of the leading scientific journal devoted to the 50th anniversary of its publication. The 1964 *ZhETF* paper by L V Keldysh, which laid the foundations of photoionization theory in a strong laser field is an outstanding example of such a rare recognition.[1] A rare scientist has a chance to witness how his/her ideas, his/her theories define the development of the entire area of research. Such a remarkable destiny needs to be earned in some unknown high realms. "Glad that my equations still work," Leonid Veniaminovich concluded, with archetypical modesty, one of the seminars celebrating the 50th anniversary of his photoionization theory.

Leonid Veniaminovich Keldysh and Paul Corkum in Red Square, following the RAS Gold Medal award ceremony, March 22, 2016.

The rapid progress of laser technologies and the advent of high-power sources of ultrashort laser pulses called for the extension of the Keldysh photoionization formalism to the case of ultrashort laser pulses. Leonid Veniaminovich spent much of his time thinking about this problem, developed an approach to solve it, found several important equations, but ... never published this work. The only reason why this work has never been published within Keldysh's lifetime is that Leonid Veniaminovich was doubtful as to whether the review of the rapidly growing literature in this field that he put together for the introductory part of the manuscript was complete enough. Even for the leading experts in ultrafast science, it was an utter surprise to hear of the very existence of this work by Keldysh. Over many years, this writing was available only as a carefully formatted and proofread author's manuscript [246]. Interestingly, the easiest way to receive these notes has always been to send a request to the author himself. His reply would always come within a day ... As a proper journal paper, this work first sees the light of day

[1] See the special issue of the *Journal of Physics B: Atomic, Molecular and Optical Physics* **47** October (2014).

in this memorial issue of *Physics–Uspekhi* [247], the journal that Leonid Veniaminovich has put so much effort into as its Editor-in-Chief.

In 2015, Leonid Veniaminovich and Paul Corkum, one of the founders and pioneers of attosecond physics, were awarded the highest prize of the Russian Academy of Sciences — M V Lomonosov Gold Medal. The celebration ceremony took place during a special session of the general meeting of the Russian Academy of Sciences in March 2016. Both laureates delivered remarkably insightful, thoughtful, and moving lectures [248, 249]. In the opening of his talk, Paul Corkum praised Keldysh by saying: "It is a great honor for me to be receiving the RAS Gold Medal jointly with Professor Keldysh, whose discoveries have inspired and continue to inspire generations of researchers, including myself and many of my students today."

In the evening following the ceremony, the author of these lines had the privilege of joining Leonid Veniaminovich and Paul for dinner in a quiet restaurant on Petrovka. By the end of the dinner, Leonid Veniaminovich looked tired, but, having learnt of a car tour of nighttime Moscow that has been promised to Paul, said he would gladly join us. In Red Square, Paul, who had his camera ready, asked me to take a picture. "I will remember this evening forever," Paul wrote in an email accompanying the picture... .

References

1. Keldysh L V *Sov. Phys. JETP* **20** 1307 (1965); *Zh. Eksp. Teor. Fiz.* **47** 1945 (1964)
2. Bloembergen N *IEEE J. Quantum Electron.* **10** 375 (1974)
3. Manenkov A A, Prokhorov A M *Sov. Phys. Usp.* **29** 104 (1986); *Usp. Fiz. Nauk* **148** 179 (1986)
4. Lenzner M et al. *Phys. Rev. Lett.* **80** 4076 (1998)
5. Brabec T, Krausz F *Rev. Mod. Phys.* **72** 545 (2000)
6. Gibson E A et al. *Science* **302** 95 (2003)
7. Couairon A, Mysyrowicz A *Phys. Rep.* **441** 47 (2007)
8. Bergé L et al. *Rep. Prog. Phys.* **70** 1633 (2007)
9. Schultze M et al. *Nature* **493** 75 (2013)
10. Sommer A et al. *Nature* **534** 86 (2016)
11. Corkum P B, Krausz F *Nature Phys.* **3** 381 (2007)
12. Zheltikov A M *Phys. Usp.* **49** 605 (2006); *Usp. Fiz. Nauk* **176** 623 (2006)
13. Zheltikov A M, Koroteev N I *Phys. Usp.* **42** 321 (1999); *Usp. Fiz. Nauk* **169** 385 (1999)
14. Chekalin S V, Kandidov V P *Phys. Usp.* **56** 123 (2013); *Usp. Fiz. Nauk* **183** 133 (2013)
15. Zheltikov A M *J. Phys. B* **50** 092001 (2017)
16. Verhoef A J et al. *Phys. Rev. Lett.* **104** 163904 (2010)
17. Mitrofanov A V et al. *Phys. Rev. Lett.* **106** 147401 (2011)
18. Gattass R R, Mazur E *Nature Photon.* **2** 219 (2008)
19. Hauri C P et al. *Appl. Phys. B* **79** 673 (2004)
20. Goulielmakis E et al. *Opt. Lett.* **33** 1407 (2008)
21. Tirlapur U K, König K *Nature* **418** 290 (2002)
22. Vogel A et al. *Appl. Phys. B* **81** 1015 (2005)
23. Lanin A A et al. *Appl. Phys. Lett.* **100** 101104 (2012)
24. Popov V S *Phys. Usp.* **47** 855 (2004); *Usp. Fiz. Nauk* **174** 921 (2004)
25. Popruzhenko S V *J. Phys. B* **47** 204001 (2014)
26. Karnakov B M et al. *Phys. Usp.* **58** 3 (2015); *Usp. Fiz. Nauk* **185** 3 (2015)
27. Fedorov M V *JETP* **122** 449 (2016); *Zh. Eksp. Teor. Fiz.* **149** 522 (2016)
28. Merzbacher E *Phys. Today* **55** (8) 44 (2002)
29. Hund F *Z. Phys.* **40** 742 (1927)
30. Hund F *Z. Phys.* **43** 805 (1927)
31. Schottky W *Phys. Z.* **32** 833 (1931)
32. Frenkel J *Wave Mechanics; Elementary Theory* (Oxford: The Clarendon Press, 1932)
33. Nordheim L *Z. Phys.* **46** 833 (1928)
34. Fowler R H, Nordheim L *Proc. R. Soc. London A* **119** 173 (1928)
35. Oppenheimer J R *Phys. Rev.* **31** 66 (1928)
36. Oppenheimer J R *Proc. Natl. Acad. Sci. USA* **14** 363 (1928)
37. Gamow G *Z. Phys.* **51** 204 (1928)
38. Gurney R W, Condon E U *Nature* **122** 439 (1928)
39. Gurney R W, Condon E U *Phys. Rev.* **33** 127 (1929)
40. Zener C *Proc. R. Soc. London A* **145** 523 (1934)
41. Keldysh L V *Sov. Phys. JETP* **6** 763 (1958); *Zh. Eksp. Teor. Fiz.* **33** 994 (1957)
42. Franz W *Z. Naturforsch. A* **13** 484 (1958)
43. Kane E O *J. Phys. Chem. Solids* **12** 181 (1960)
44. Kane E O *J. Appl. Phys.* **32** 83 (1961)
45. Bardeen J *Phys. Rev. Lett.* **6** 57 (1961)
46. Il'inskii Yu A, Keldysh L V *Electromagnetic Response of Material Media* (New York: Plenum Press, 1994); Translated from Russian: *Vzaimodeistvie Elektromagnitnogo Izlucheniya s Veshchestvom* (Moscow: Izd. MGU, 1989)
47. Ghimire S et al. *Phys. Rev. Lett.* **107** 167407 (2011)
48. Hertz H *Ann. Physik* **267** 983 (1887)
49. Stoletow M A *Comptes Rendus* **106** 1149 (1888); *Phil. Mag. 5* **26** 317 (1888)
50. Einstein A *Ann. Physik* **322** 132 (1905)
51. Göppert-Mayer M *Ann. Physik* **401** 273 (1931)
52. Makinson R E B, Buckingham M J *Proc. Phys. Soc. London A* **64** 135 (1951)
53. Braunstein R, Ockman N *Phys. Rev.* **134** A499 (1964)
54. Bonch-Bruevich A M, Khodovoi V A *Sov. Phys. Usp.* **8** 1 (1965); *Usp. Fiz. Nauk* **85** 5 (1965)
55. Gladun A D, Barashev P P *Sov. Phys. Usp.* **12** 490 (1970); *Usp. Fiz. Nauk* **98** 493 (1969)
56. Voronov G S, Delone N B *JETP Lett.* **1** 66 (1965); *Pis'ma Zh. Eksp. Teor. Fiz.* **1** (2) 42 (1965)
57. Delone N B *Sov. Phys. Usp.* **18** 169 (1975); *Usp. Fiz. Nauk* **115** 361 (1975)
58. Delone N B *Usp. Fiz. Nauk* **148** 551 (1986)
59. Gold A, Bebb H B *Phys. Rev. Lett.* **14** 60 (1965)
60. Nikishov A I, Ritus V I *Sov. Phys. JETP* **23** 168 (1966); *Zh. Eksp. Teor. Fiz.* **50** 255 (1966)
61. Nikishov A I, Ritus V I *Sov. Phys. JETP* **25** 145 (1967); *Zh. Eksp. Teor. Fiz.* **52** 223 (1967)
62. Perelomov A M, Popov V S, Terent'ev M V *Sov. Phys. JETP* **23** 924 (1966); *Zh. Eksp. Teor. Fiz.* **50** 1393 (1966)
63. Perelomov A M, Popov V S, Terent'ev M V *Sov. Phys. JETP* **24** 207 (1967); *Zh. Eksp. Teor. Fiz.* **51** 309 (1966)
64. Perelomov A M, Popov V S *Sov. Phys. JETP* **25** 336 (1967); *Zh. Eksp. Teor. Fiz.* **52** 514 (1967)
65. Faisal F H M *J. Phys. B* **6** L89 (1973)
66. Reiss H R *Phys. Rev. A* **22** 1786 (1980)
67. Reiss H R *Prog. Quantum Electron.* **16** 1 (1992)
68. Delone N B, Krainov V P *Phys. Usp.* **41** 469 (1998); *Usp. Fiz. Nauk* **168** 531 (1998)
69. Delone N B, Krainov V P *Atoms in Strong Light Fields* (Berlin: Springer-Verlag, 1995); Translated from Russian: *Atom v Sil'nom Svetovom Pole* 2nd ed. (Moscow: Energoatomizdat, 1984)
70. Delone N B, Krainov V P *Multiphoton Processes in Atoms* (Berlin: Springer-Verlag, 1994)
71. Wolkow D M *Z. Phys.* **94** 250 (1935)
72. Hauge E H, Støvneng J A *Rev. Mod. Phys.* **61** 917 (1989)
73. Landauer R, Martin Th *Rev. Mod. Phys.* **66** 217 (1994)
74. Landsman A S, Keller U *Phys. Rep.* **547** 1 (2015)
75. Sokolovski D, Connor J N L *Phys. Rev. A* **42** 6512 (1990)
76. Sokolovski D, Connor J N L *Phys. Rev. A* **44** 1500 (1991)
77. Sokolovski D, Connor J N L *Phys. Rev. A* **47** 4677 (1993)
78. Sokolovski D *Phys. Rev. Lett.* **79** 4946 (1997)
79. Sokolovski D *Phys. Rev. A* **59** 1003 (1999)
80. Feynman R P, Hibbs A R *Quantum Mechanics and Path Integrals* (New York: McGraw-Hill, 1965)
81. Bohm D *Phys. Rev.* **85** 166 (1952)
82. Ivanov I A, Nam C H, Kim K T *Sci. Rep.* **7** 39919 (2017)
83. Leavens C R *Found. Phys.* **25** 229 (1995)
84. Krausz F, Stockman M I *Nature Photon.* **8** 205 (2014)
85. Uiberacker M et al. *Nature* **446** 627 (2007)
86. Eckle P et al. *Science* **322** 1525 (2008)
87. Wittmann T et al. *Nature Phys.* **5** 357 (2009)

88. Pfeiffer A N et al. *Nature Phys.* **8** 76 (2012)
89. Shafir D et al. *Nature* **485** 343 (2012)
90. Landsman A S et al. *Optica* **1** 343 (2014)
91. Balciunas T et al. *Nature Commun.* **6** 6117 (2015)
92. Zheltikov A M *Phys. Rev. A* **94** 043412 (2016)
93. Balciunas T et al. *Chem. Phys.* **414** 92 (2013)
94. Büttiker M, Landauer R *Phys. Rev. Lett.* **49** 1739 (1982)
95. Steinberg A M *Phys. Rev. A* **52** 32 (1995)
96. Hallaji M et al. *Nature Phys.* **13** 540 (2017)
97. Reiss H R *Phys. Rev. Lett.* **101** 043002 (2008)
98. Reiss H R *J. Phys. B* **47** 204006 (2014)
99. Xiong W et al. *J. Phys. B* **21** L159 (1988)
100. Colosimo P et al. *Nature Phys.* **4** 386 (2008)
101. Blaga C I et al. *Nature Phys.* **5** 335 (2009)
102. Popmintchev T et al. *Science* **336** 1287 (2012)
103. Ludwig A et al. *Phys. Rev. Lett.* **113** 243001 (2014)
104. Lanin A A et al. *Opt. Lett.* **39** 6430 (2014)
105. Mitrofanov A V et al. *Sci. Rep.* **5** 8368 (2015)
106. Wolter B et al. *Phys. Rev. X* **5** 021034 (2015)
107. Mitrofanov A V et al. *Phys. Usp.* **58** 89 (2015); *Usp. Fiz. Nauk* **185** 97 (2015)
108. Mitrofanov A V et al. *Opt. Lett.* **40** 2068 (2015)
109. Lanin A A et al. *Opt. Lett.* **40** 974 (2015)
110. Stepanov E A et al. *Phys. Rev. Lett.* **117** 043901 (2016)
111. Power E A, Zienau S *Phil. Trans. R. Soc. A* **251** 427 (1959)
112. Bykov V P *Sov. Phys. Usp.* **27** 631 (1984); *Usp. Fiz. Nauk* **143** 657 (1984)
113. Lamb W E (Jr.), Retherford R C *Phys. Rev.* **72** 241 (1947)
114. Lamb W E (Jr.), Retherford R C *Phys. Rev.* **79** 549 (1950)
115. Lamb W E (Jr.) *Phys. Rev.* **85** 259 (1952)
116. Reiss H R *J. Opt. Soc. Am. B* **7** 574 (1990)
117. Mur V D, Karnakov B M, Popov V S *JETP* **87** 433 (1998); *Zh. Eksp. Teor. Fiz.* **114** 798 (1998)
118. Popov V S, Mur V D, Karnakov B M *JETP Lett.* **66** 229 (1997); *Pis'ma Zh. Eksp. Teor. Fiz.* **66** 213 (1997)
119. Gladkov S M et al. *Opt. Spectrosc.* **65** 149 (1988); *Opt. Spektrosk.* **65** 249 (1988)
120. Karnakov B M, Mur V D, Popov V S *Phys. At. Nucl.* **62** 1363 (1999); *Yad. Fiz.* **62** 1444 (1999)
121. Milosevic N, Krainov V P, Brabec T *Phys. Rev. Lett.* **89** 193001 (2002)
122. Milosevic N, Krainov V P, Brabec T *J. Phys. B* **35** 3515 (2002)
123. Bauer D, Milošević D B, Becker W *Phys. Rev. A* **72** 023415 (2005)
124. Becker W et al. *Adv. At. Mol. Opt. Phys.* **48** 35 (2002)
125. Popov V S, Karnakov B M, Mur V D *JETP Lett.* **79** 262 (2004); *Pis'ma Zh. Eksp. Teor. Fiz.* **79** 320 (2004)
126. Di Piazza A et al. *Rev. Mod. Phys.* **84** 1177 (2012)
127. Crawford D P, Reiss H R *Phys. Rev. A* **50** 1844 (1994)
128. Protopapas M, Keitel C H, Knight P L *J. Phys. B* **29** L591 (1996)
129. Kartashov D et al. *Opt. Lett.* **37** 2268 (2012)
130. Kartashov D et al. *Opt. Lett.* **37** 3456 (2012)
131. Kartashov D et al. *Opt. Lett.* **38** 3194 (2013)
132. Zheltikov A M et al. *Phys. Rev. Lett.* **103** 033901 (2009)
133. Krausz F, Ivanov M *Rev. Mod. Phys.* **81** 163 (2009)
134. Hassan M Th et al. *Nature* **530** 66 (2016)
135. Reiter F et al. *Phys. Rev. Lett.* **105** 243902 (2010)
136. Zheltikov A M *Phys. Usp.* **54** 29 (2011); *Usp. Fiz. Nauk* **181** 33 (2011)
137. Bloembergen N *Nonlinear Optics* (New York: W.A. Benjamin, 1965)
138. Serebryannikov E E, Zheltikov A M *Phys. Rev. Lett.* **113** 043901 (2014)
139. Corkum P B *Phys. Rev. Lett.* **71** 1994 (1993)
140. Zheltikov A *IEEE Photon. J.* **3** 255 (2011)
141. Denk W, Strickler J H, Webb W W *Science* **248** 73 (1990)
142. Helmchen F, Denk W *Nature Meth.* **2** 932 (2005)
143. Kerr J N D, Denk W *Nature Rev. Neurosci.* **9** 195 (2008)
144. Min W et al. *Annu. Rev. Phys. Chem.* **62** 507 (2011)
145. Saar B G et al. *Science* **330** 1368 (2010)
146. Brown C T A, Deckert V, Sergeev A M, Zheltikov A M *J. Biophoton.* **3** 639 (2010)
147. Doronina-Amitonova L V et al. *Appl. Phys. Lett.* **99** 231109 (2011)
148. Boyden E S et al. *Nature Neurosci.* **8** 1263 (2005)
149. Zhang F et al. *Nature Meth.* **3** 785 (2006)
150. Cardin J A et al. *Nature Protocols* **5** 247 (2010)
151. Gradinaru V et al. *Science* **324** 354 (2009)
152. Doronina L V et al. *Opt. Lett.* **34** 3373 (2009)
153. Diester I et al. *Nature Neurosci.* **14** 387 (2011)
154. Deisseroth K *Nature Meth.* **8** 26 (2011)
155. Doronina-Amitonova L V et al. *Sci. Rep.* **3** 3265 (2013)
156. Doronina-Amitonova L V et al. *Phys. Usp.* **58** 345 (2015); *Usp. Fiz. Nauk* **185** 371 (2015)
157. Fedotov I V et al. *Sci. Rep.* **5** 15737 (2015)
158. Ermakova Y G et al. *Nature Commun.* **8** 15362 (2017)
159. Vogel A et al. *Appl. Phys. B* **81** 1015 (2005)
160. Voronin A A, Zheltikov A M *Phys. Rev. E* **81** 051918 (2010)
161. Voronin A A, Zheltikov A M *J. Appl. Phys.* **112** 053101 (2012)
162. Gladkov S M et al. *Sov. Tech. Phys. Lett.* **14** 610 (1988); *Pis'ma Zh. Tekh. Fiz.* **14** 1399 (1988)
163. Fedotov A B et al. *J. Opt. Soc. Am. B* **8** 363 (1991)
164. Zheltikov A M, Koroteev N I, Fedotov A B *Opt. Spectrosc.* **72** 527 (1992); *Opt. Spektrosk.* **72** 971 (1992)
165. Akimov D A et al. *Opt. Lett.* **24** 478 (1999)
166. Fedotov A B et al. *Opt. Commun.* **133** 587 (1997)
167. Fedotov A B et al. *Phys. Lett. A* **271** 407 (2000)
168. Schultze M et al. *Science* **346** 1348 (2014)
169. Cavalieri A L et al. *Nature* **449** 1029 (2007)
170. Lanin A A, Stepanov E A, Fedotov A B, Zheltikov A M *Optica* **4** 516 (2017)
171. Ghimire S et al. *Nature Phys.* **7** 138 (2011)
172. Vampa G et al. *Nature* **522** 462 (2015)
173. Voronin A A et al. *Opt. Lett.* **36** 508 (2011)
174. Zheltikov A M *JETP Lett.* **90** 90 (2009); *Pis'ma Zh. Eksp. Teor. Fiz.* **90** 98 (2009)
175. Yudin G L, Ivanov M Yu *Phys. Rev. A* **64** 013409 (2001)
176. Serebryannikov E E, Zheltikov A M *Phys. Rev. A* **76** 013820 (2007)
177. Fedotov A B, Serebryannikov E E, Zheltikov A M *Phys. Rev. A* **76** 053811 (2007)
178. Savvin A D et al. *Opt. Commun.* **284** 1652 (2011)
179. Fuji T, Suzuki T, Serebryannikov E E, Zheltikov A *Phys. Rev. A* **80** 063822 (2009)
180. Serebryannikov E E et al. *Phys. Rev. A* **80** 053809 (2009)
181. Sheik-Bahae M, Hagan D J, Van Stryland E W *Phys. Rev. Lett.* **65** 96 (1990)
182. Sheik-Bahae M et al. *IEEE J. Quantum Electron.* **27** 1296 (1991)
183. Zheltikov A M *Phys. Rev. A* **79** 023823 (2009)
184. Zheltikov A M *Opt. Commun.* **282** 985 (2009)
185. Wherrett B S *J. Opt. Soc. Am. B* **1** 67 (1984)
186. Hutchings D C et al. *Opt. Quantum Electron.* **24** 1 (1992)
187. Brandi H S, de Araujos C B *J. Phys. C* **16** 5929 (1983)
188. Brandi H S, Jalbert G, Malta O L *Phys. Status Solidi B* **124** 147 (1984)
189. Voronin A A, Zheltikov A M *Phys. Rev. A* **94** 023824 (2016)
190. Shumakova V et al. *Nature Commun.* **7** 12877 (2016)
191. Voronin A A, Zheltikov A M *Sci. Rep.* **7** 36263 (2017)
192. Voronin A A, Zheltikov A M *J. Opt.* **18** 115501 (2016)
193. Baltuška A et al. *J. Phys. Chem. A* **103** 10065 (1999)
194. Suzuki T *Annu. Rev. Phys. Chem.* **57** 555 (2006)
195. Ihee H et al. *Science* **291** 458 (2001)
196. Ruan C-Y et al. *Science* **304** 80 (2004)
197. Baum P, Zewail A H *Proc. Natl. Acad. Sci. USA* **104** 18409 (2007)
198. Zewail A H *Science* **328** 187 (2010)
199. Goulielmakis E et al. *Nature* **466** 739 (2010)
200. Bormann R et al. *Phys. Rev. Lett.* **105** 147601 (2010)
201. Ropers C et al. *New J. Phys.* **9** 397 (2007)
202. Schiffrin A et al. *Nature* **493** 70 (2013)
203. Zhokhov P A, Zheltikov A M *Phys. Rev. Lett.* **113** 133903 (2014)
204. Yablonovitch E, Bloembergen N *Phys. Rev. Lett.* **29** 907 (1972)
205. Zhokhov P, Zheltikov A, in *Proc. of the Conf. on Physics of Quantum Electronics (PQE-2015), January 4–9, 2015, Snowbird, Utah, USA*
206. Lanzara A et al. *Nature* **412** 510 (2001)
207. Bostwick A et al. *Nature Phys.* **3** 36 (2007)
208. Chen Y L et al. *Science* **325** 178 (2009)
209. von Laue M "Concerning the detection of X-ray interferences", in *Nobel Lectures, Physics 1901–1921* (Amsterdam: Elsevier, 1967) p. 347; https://www.nobelprize.org/nobel_prizes/physics/laureates/1914/laue-lecture.html

210. Bragg W L *Proc. Cambridge Phil. Soc.* **17** 43 (1913)
211. Damascelli A, Hussain Z, Shen Z-X *Rev. Mod. Phys.* **75** 473 (2003)
212. Schubert O et al. *Nature Photon.* **8** 119 (2014)
213. Hohenleutner M et al. *Nature* **523** 572 (2015)
214. Luu T T et al. *Nature* **521** 498 (2015)
215. Vampa G et al. *Phys. Rev. Lett.* **115** 193603 (2015)
216. Garg M et al. *Nature* **538** 359 (2016)
217. Vampa G et al. *Phys. Rev. B* **91** 064302 (2015)
218. Lanin A A, Zheltikov A M *JETP Lett.* **104** 449 (2016); *Pis'ma Zh. Eksp. Teor. Fiz.* **104** 475 (2016)
219. Butcher P N, Cotter D *The Elements of Nonlinear Optics* (Cambridge: Cambridge Univ. Press, 1990)
220. Serebryannikov E E, Zheltikov A M *Phys. Rev. Lett.* **116** 123901 (2016)
221. Serebryannikov E E, Goulielmakis E, Zheltikov A M *New J. Phys.* **10** 093001 (2008)
222. Voronin A A, Zheltikov A M *Phys. Usp.* **59** 869 (2016); *Usp. Fiz. Nauk* **186** 957 (2016)
223. Chin S L *Femtosecond Laser Filamentation* (New York: Springer, 2010)
224. Zheltikov A *Appl. Phys. B* **77** 143 (2003)
225. Kasparian J et al. *Science* **301** 61 (2003)
226. Hauri C P et al. *Appl. Phys. B* **79** 673 (2004)
227. Couairon A et al. *Opt. Lett.* **30** 2657 (2005)
228. Skupin S et al. *Phys. Rev. E* **74** 056604 (2006)
229. Kartashov D et al. *Phys. Rev. A* **86** 033831 (2012)
230. Malevich P N et al. *Opt. Express* **20** 18784 (2012)
231. Malevich P N et al. *Opt. Lett.* **40** 2469 (2015)
232. Bespalov V I, Talanov V I *JETP Lett.* **3** 307 (1966); *Pis'ma Zh. Eksp. Teor. Fiz.* **3** 471 (1966)
233. Voronin A A et al. *Opt. Commun.* **291** 299 (2013)
234. Zhokhov P A, Zheltikov A M *Phys. Rev. A* **86** 013816 (2012)
235. Voronin A A, Panchenko V Ya, Zheltikov A M *Laser Phys. Lett.* **13** 065403 (2016)
236. Voronin A A, Zheltikov A M *Phys. Rev. A* **90** 043807 (2014)
237. Zhokhov P A, Zheltikov A M *Phys. Rev. A* **89** 043816 (2014)
238. Zhokhov P A, Zheltikov A M *Phys. Rev. Lett.* **110** 183903 (2013)
239. Durand M et al. *Phys. Rev. Lett.* **110** 115003 (2013)
240. Majus D et al. *Phys. Rev. Lett.* **112** 193901 (2014)
241. Agrawal G P *Nonlinear Fiber Optics* (San Diego: Academic Press, 2001)
242. Zheltikov A M *Phys. Usp.* **50** 705 (2007); *Usp. Fiz. Nauk* **177** 737 (2007)
243. Zheltikov A *Opt. Express* **24** 20716 (2016)
244. Mitrofanov A V et al. *Optica* **3** 299 (2016)
245. Mitrofanov A V et al. *Opt. Lett.* **41** 3479 (2016)
246. Keldysh L "Multiphoton ionization by a very short pulse", private communication
247. Keldysh L V *Phys. Usp.* **60** (11) (2017); https://doi.org/10.3367/UFNe.2017.10.038229; *Usp. Fiz. Nauk* **187** 1280 (2017)
248. Keldysh L V *Herald Russ. Acad. Sci.* **86** 413 (2017); *Vestn. Ross. Akad. Nauk* **86** 1059 (2016)
249. Corkum P *Herald Russ. Acad. Sci.* **86** 426 (2017); *Vestn. Ross. Akad. Nauk* **86** 1073 (2016)